AERODYNAMIC STUDIES IN THE SHOCK TUBE

Thesis by

Josef Rabinowicz

In Partial Fulfillment of the Requirements

For the Degree of

Doctor of Philosophy

California Institute of Technology

Pasadena, California

1957

ACKNOWLEDGMENTS

The author wishes to express his indebtedness to Professor L. Lees for his guidance and encouragement throughout the progress of this work.

To Drs. H. T. Nagamatsu and Y. Yoler are expressed a special word of thanks for initiating and encouraging the author into the shock tube work as well as to Dr. A. Roshko for many helpful discussions and to Mr. R. Evans for much help in the performance of the experiments.

The cooperation of Mr. M. E. Jessey and C. A. Bartsch in the development of the resistance thermometer gage is gratefully acknowledged.

The author wishes to thank Mrs. T. van Harreveld for performing the computations, Mrs. B. Wood for preparing the figures and the GALCIT secretarial staff for preparing the manuscript.

ABSTRACT

In order to utilize the shock tube for quantitative investigations of some aerodynamic problems a thin platinum film resistance thermometer was developed for heat transfer rate measurements. The present report describes the construction and calibration of the heat transfer gage. Since the experimental technique presents a major problem this investigation has been carried out in the straight section of the shock tube where the flow conditions are well defined and readily measured. These flow conditions were calculated utilizing the most recent NBS data on air properties at high temperatures. The flow conditions were also measured utilizing the heat transfer gage and several independent experimental techniques, and good agreement was found with the equilibrium flow calculations after an initial period of 30 - 50 μ sec. Measurements of the heat transfer rate at the forward stagnation point and on the circumference of a circular cylinder are reported and compared with the theoretical calculations of L. Lees. A method for deduction of surface pressure distribution from the laminar boundary-layer heat transfer data is also presented.

TABLE OF CONTENTS

LIST OF FIGURES

LIST OF FIGURES (cont'd)

LIST OF FIGURES (cont'd)

I. INTRODUCTION

Even a very crude estimate of the stagnation temperature at high flight Mach numbers gives values well above the melting points of known structural materials. Thus a need exists for detailed theoretical and experimental investigations of the heat transfer and flow problems encountered in high speed flight. High Mach number flows have been successfully achieved in many hypersonic wind tunnels. However, these tunnels have so far been limited to comparatively low stagnation temperatures, with the maximum value of the order of 2500°F. The search for methods of simulating hypersonic flight conditions led to the development of a number of facilities producing a high temperature flow for a very short time, such as the ballistic range, shock tube, shock tunnel, etc. But the short flow time, in some cases as low as 50 - 100 μsec, means that new experimental techniques must be developed for measuring flow quantities before quantitative studies of the phenomena are possible. For this reason a considerable part of the present work was devoted to the development of a thin platinum film resistance thermometer for accurate heat transfer measurements. Some work was done also on fast-response pressure pickups. Section III contains a detailed discussion of the heat transfer gage and associated electronic equipment, and the second part of this section gives a short account of the development of a piezoelectric pressure gage.

Since the experimental technique presents a major obstacle it was felt that the initial stages of research should be done in a section of a shock tube where the flow conditions are well defined and readily measured. For this reason the flow studies were carried out in the

straight section of the shock tube at flow Mach numbers of 1.8 - 2.0. Although this flow Mach number is low the stagnation enthalpy conditions experienced correspond to free flight Mach numbers of 8 to 10, so that some of the features of hypersonic flight are reproduced. The shock tube and accompanying experimental apparatus is described in Section II.

In order to interpret the experimental results properly the flow conditions must be accurately known or measured. The first part of Section IV presents the calculation of the equilibrium conditions behind a normal shock wave traveling into stationary air. These calculations are based on the most recent NBS data on air properties at high temperatures. Conditions behind a bow wave at the stagnation region of a blunt-nosed body are also calculated for later use in the heat transfer studies.

Bart B of Section IV presents the actual performance of the shock tube as determined by schlieren studies of the flow history over 45^{o} cones and by measurements of the shock detachment distance for a circular cylinder. Measurements of the heat transfer rate at the stagnation region of a circular cylinder and on the shock tube wall are also used to determine the shock tube performance. The boundary layer thickness on the shock tube wall is determined by schlieren studies of boundary layer-shock wave interaction. All of these various independent measurements taken together present a complete picture of the environment produced in the shock tube.

The heat transfer measurement technique is best evaluated on a body of simple geometry, where a theoretical analysis is also available. In this study heat transfer rates were measured at the stagnation point

and over the circumference of a circular cylinder, as a function of shock velocity and initial pressure. This study is discussed in Section V. The measurements were compared with the results of laminar boundary layer calculations based on the approximation of local similarity as developed by L. Lees (Ref. 28).

The main results and conclusions of this investigation are summarized in Section VI, which also contains a discussion of possible extensions of this work and various problems for future development.

II. DESCRIPTION OF EXPERIMENTAL APPARATUS

A. Shock Tube

The design and construction of shock tubes is described in many reports (for example References 1 to 7, particularly Reference 4). Accordingly this section is limited to the description of the GALCIT shock tube, without including detailed design considerations which can be found in the references cited.

The present shock tube (figs. 1 and 2) is a conventional one utilizing a compressed gas driver. It is essentially a modification of the shock tube built by Y. Yoler (Ref. 5). The shock tube can be operated by high pressure helium or nitrogen gas. Air has been used exclusively in the low pressure section. Driver gas pressure up to 800 psi is used, and the low pressure tube can be evacuated to less than 1 mm Hg. Thus, the maximum diaphragm pressure ratio is about 20,000, which gives a maximum shock Mach number of about 7.5 when operating with the He - Air combination initially at room temperature. This shock tube has an additional feature in the 2-dimensional nozzle, which permits the flow Mach number to be increased from the limiting value of about 2 in the straight section to approximately 6 in the nozzle test section. At the present time this nozzle is a wedge type with facilities for bleeding off the boundary layer on top and bottom walls. However, the present work was confined to the straight section to facilitate the interpretation of data obtained by the new techniques.

The shock tube structure is divided into four parts: (1) compression chamber; (2) diaphragm section; (3) low pressure uniform tube; (4) divergent nozzle.

(1) The compression chamber consists of a 3" I. D. and 4-1/2" O. D. steel cylinder which is 6 ft. long. The chamber is sealed on one end by a blank flange and on the other by the diaphragm section. Ports are provided in the blank flange for the driver gas inlet and for the compression chamber pressure indicator.

(2) The diaphragm section has the following features: two 1-1/2" diameter bolts extend from the downstream compression chamber flange through mating holes in the flanges at the end of the low pressure tube, so that the diaphragm is clamped between these two sections. The flange on the compression chamber also has a smooth transition from the 3" I. D. of the compression chamber to the 2-7/8" square of the low pressure tube. The end faces of both the compression chamber flange and the low pressure tube are smoothly machined to facilitate good sealing. The diaphragms generally used were made of copper. The copper plate is scribed to a specific depth with a pre-set scriber so that a certain control of breakage pressure is obtained. The diaphragms were generally broken by pressure, although at first a plunger was used.

(3) The low pressure tube has a 2-7/8" x 2-7/8" square cross section, and the 20 ft. length is divided into two 10 ft. sections. At the junction a 1" neoprene gasket isolates the instrumented 10 ft. section from the vibrations in the rest of the tube caused by the diaphragm breakage. These sections are assembled from cold-rolled steel plates, and their inside surfaces are smoothly ground. The side plates are 2-7/8" high and 1" thick and an "O" ring grove is machined into them. The top and bottom plates are 5" wide by 1/2" thick. The tube is bolted together after the sections have been aligned and doweled. The

second 10 ft. section is provided with instrumentation facilities and testing area. Five ports 1-1/2" in diameter are spaced 2 feet apart on one side wall. These ports are used for the positioning of the different wall gages for pressure and heat transfer measurements. In addition two observation windows 4-1/2" in diameter are located 15' and 19' from the diaphragm section; the 19' station was used for most of the experiments.

(4) The divergent nozzle section provides for a two-dimensional expansion in the vertical direction to a 45" height. It is the same section designed and built by Y. Yoler and described in Ref. 5. The only modifications in this section are the addition of three more windows along the nozzle axis, enabling tests at different area ratios with the same nozzle setting, and the insertion of 1-1/2" ports along two rays 15^{o} from the nozzle axis. With these modifications a complete survey of the flow in the nozzle can be made.

B. High Pressure System

Helium and nitrogen are used as driver gases in the shock tube. These gases are obtained commercially in high pressure bottles at about 2200 psi. The bottle pressure is measured on a 3000 psi full scale gage, and a 800 psi laboratory gage is used for measuring the compression chamber pressure to an accuracy of $\pm$ 10 psi.

C. Vacuum System

A high vacuum, Welch Duo-Seal No. 1428B pump is used for reaching pressure as low as 0.8 mm Hg in the low pressure tube. The pressure is

measured by a 50 mm Hg full-scale Wallace-Tiernan vacuum gage. This gage is calibrated against a Macleod gage, with a resolution of $\pm$ 0.05 mm Hg, thus permitting about 1 per cent accuracy.

An oil diffusion pump is connected to the system for use in providing a much lower vacuum in the hypersonic nozzle section to facilitate the starting of flow in the nozzle. This pump will be used when the nozzle investigation is underway.

D. Instrumentation

Instrumentation was developed for making the following measurements in the shock tube: (1) the shock wave speed; (2) heat transfer rates on shock tube wall and on model surface; (3) static pressure behind shock wave on shock tube wall. In addition a schlieren system was built for flow studies. Since a detailed discussion of instrumentation techniques applicable to shock tube work is presented in Section III, only a brief description of the apparatus used is given here. A block diagram of the instrumentation is shown in fig. 3; the arrangement of the electronic instruments is shown in fig. 4.

1. Shock Wave Speed Measurement

The shock wave speed is determined by measuring the time for the shock to travel between two monitoring stations spaced 2' $\pm$ 0.005" apart. For detection devices, thin film gages mounted flush on the tube wall are used (Section III). The gage output is fed through pulse amplifiers to the "start" and "stop" channels of a 7360 Berkeley counter. This counter has a resolution time of 1 μ sec. Thus the wave speed is

measured within at least 1/2 per cent accuracy.

2. Heat Transfer Gage

The initial resistance of the thin platinum film is measured on a Wheatstone bridge, and the initial current is measured by a milli-ammeter, both to an accuracy of 1 per cent. The gage output is fed through a Tektronix-121 wide-band amplifier to a 535 Tektronix oscilloscope. This combination of amplifier-oscilloscope has a sensitivity of 0.5×10^{-3} volts/cm. with a noise level of about 0.1×10^{-3} volts. The oscilloscope trace is recorded with a Du-Mont oscilloscope Polaroid Land camera type 297.

3. Optical System

A schlieren system utilizing a capacitor-thyraton discharge spark unit of about 2 μsec spark duration is used for flow visualization. The spark is triggered by the platinum film gage output through an electronic time delay. The spark is focussed by a condenser lens system to a slit which is situated at the focal point of a 3" diameter lens. The parallel beam is then passed through the test section, and focused on the knife edge by a 75" focal length spherical mirror. The records are obtained on a polaroid type 44 film (Polapan 400). With this system satisfactory pictures are obtained with densities behind the starting shock waves of the order of 3×10^{-2} of an atmosphere. The schlieren system is seen in fig. 2, except for the spherical mirror which is further upstream.

4. Pressure Instrumentation

A piezoelectric pressure transducer utilizing barium-titanate disks was successfully developed for static pressure measurements with weak shock waves. (This gage is discussed in Section III.) The gage output is fed through a cathode follower to the oscilloscope and is again recorded with a polaroid camera.

III. INSTRUMENTATION FOR AERODYNAMIC INVESTIGATIONS IN A SHOCK TUBE

A few years ago very little was known about the physico-chemical processes occurring in the hot gas behind a bow shock wave at hypersonic flight speeds. For this reason the shock tube became an invaluable source of controlled high temperature gas flow for studies of relaxation phenomena, radiation from the gas, electrical conductivity, etc. In parallel to such investigations the need exists for studies at elevated gas temperatures, of the macroscopic quantities important in fluid mechanics, such as the shock wave shape, flow pattern, surface heat transfer rate, temperature and pressure distribution, lift and drag forces and moments. In its application to such aerodynamic studies the shock tube serves as a short duration wind tunnel, where by short duration one means 50 μsec to a few milliseconds of useful flow time. This short duration of the flow dictates the instruments which can be used, and also the problems which can be investigated experimentally in the shock tube. Just as in a more conventional wind tunnel, before experimental data can be interpreted, one has to know the characteristics of the shock tube flow such as Mach number, Reynolds number, pressure, temperature, composition, chemical processes and their rates, and of course flow uniformity, effect of disturbances, etc. One purpose of preparing this rather formidable list is to indicate the goals for development of new techniques, and particularly to help evaluate current techniques. Available experimental results must then be examined critically for the assumptions employed in interpreting the actual measurements.

This section is divided into two subsections: The first sub-section describes in detail the technique developed during the course of this work for measuring heat transfer rates and surface temperatures. The second part presents a short account of the development of piezoelectric pressure gages.

A. Heat Transfer Measurement Technique

It is certainly not surprising that the first shock tube investigations were carried out almost exclusively by utilizing optical techniques such as schlieren, shadowgraph, and interferometry. These optical techniques have extremely fast response time and thus are particularily suited for shock tube application. The optical methods are applicable to two dimensional or axially-symmetric model geometries. However, they do not yield local measurements for bodies of arbitrary geometry. Thus a need exists for techniques for measuring local quantities such as pressures and heat transfer rates. Now, pressure transducers and other force measuring devices are extremely sensitive to tube vibrations which are rather strong because of the sudden loading when the diaphragm is ruptured. Much work has been done on the pressure measurement problem including some studies here at GALCIT, but to the best of our knowledge this problem is still unsolved for strong shocks. So the only local quantities which can be measured in the shock tube with an acceptable degree of accuracy are the heat transfer rate and surface temperature. These quantities are measured by utilizing the fast response of a thin metallic film acting as a resistance thermometer. The idea of utilizing this technique was pursued at a number of labora-

tories and reported in Refs. 8, 9, 10, 11, 12, 13, 22, and 30. Since this technique is still quite a new one, a detailed discussion will be included here.

The idea of using a small mass to obtain fast response has been used for a long time in the hot-wire technique, and in fast-response thermocouples. Actually the hot wire has been used successfully in the shock tube for weak shock waves $M_s < 3$ (Refs. 14, 15, and 16). For strong shock waves the closely related problems of mechanical strength and suitable response characteristics make the hot-wire applications questionable. The next step is to use a thin metallic film bounded to a strong base as a sensing element. This idea was employed for obtaining resistance thermometers and thermocouples of low thermal-inertia. A film thermocouple developed at the Midwest Research Institute (Ref. 17) is constructed by evaporating a thin nickel film ($\sim 10^{-6}$ cm thick) on a steel housing, thus obtaining a Ni-Fe junction. This thermocouple shows an extremely fast rise time ($\sim 1\ \mu$sec). However the output is low ($\sim 18 \times 10^{-6}$ volts/^{o}F), and it is also non-linear. This thermocouple was used for measuring surface temperatures in gun barrels.

For shock tube research the use of thin films as resistance thermometers appears more promising. The various shock tube research groups which investigated this technique use different methods of application of the metallic film, such as painting, evaporation, and sputtering. Of course the simplest technique is to apply a thin film by using a special metallic paint, e. g., the platinum base paint known as "Hanovia Paste". The film is painted on an electrical insulating material such as glass, and then baked in order to evaporate the sol-

vent and insure better adherence to the backing material (Ref. 22). Another method used is the evaporation of metal to produce a film on some insulating backing material (Refs. 8 and 9). Films of gold were obtained this way. The sputtering technique used at GALCIT (Refs. 10 and 11) provides a controllable method for applying a thin metallic film. The film thickness (and therefore its electrical resistance) is controlled by the sputtering time. The sputtering process produces an extremely strong and rugged film which, after baking, shows excellent resistance to erosion, at least up to shock Mach numbers of 7 - 8. However, the sputtering technique is still an art and requires a considerable amount of trial and error before satisfactory results are obtained. For this reason the sputtering procedure which is used at GALCIT will be described in some detail.

1. Sputtering Technique

The sputtering phenomenon at the cathode of a glow discharge was discovered in 1852 by W. R. Grove, and has been used for some time for coating mirrors. After the perfection of modern vaporizing techniques the sputtering method did not find much application. The exact mechanism of the process is not fully understood (Ref. 18). However, the apparatus and general procedure are well known, although the exact geometry and best sputtering conditions have to be determined empirically. A typical set-up for the sputtering process following Strong's method (Ref. 18) is shown in fig. 5. A standard 5" x 9" bell jar is used. In its top a hole is drilled for the cathode connection. The bell jar stands on a smoothly ground steel base, and a vacuum seal is

vacuum
provided by a layer of high/silicone grease. An aluminum tube of adjustable height is screwed into the base to serve as the anode and a seat for the element to be sputtered. The cathode is a 0.065" x 0.25" platinum bar 2" long, which is suspended over the table from the top of the bell jar. On the table a 3" glass cylinder encloses the cathode and the sputtered element so as to prevent the sputtered metal from spreading all over the bell jar. Quartz tube is used to cover the rod on which the platinum cathode is suspended.

The importance of eliminating contaminating materials from the sputtering system cannot be over-emphasized. A small rubber or plastic gasket that can outgas when heated, or other impurities introduced into the system, will cause many frustrating hours of unsuccessful trials.

The important parameters for setting up the sputtering apparatus are: (1) sputtering metal, (2) gas environment, (3) vacuum level and gas circulation, (4) current and voltage applied, and (5) distance between cathode and model. A list of possible sputtering metals is given by Strong, who also mentions the various gases which can be used in the apparatus. For simplicity air is used exclusively in the present apparatus although faster sputtering occurs in an argon atmosphere. The conditions found to be best with the GALCIT apparatus for sputtering of platinum are: (1) pressure level of 2 to 3 mm Hg. abs. (a small air leak, balanced by the vacuum pump, is maintained), (2) a voltage of 800 - 1100 volts and a current of 50 ma, (3) the distance between the platinum cathode and the sputtered surface is between 1-1/2" - 2". During the sputtering process the platinum glows with a reddish-blue halo, and a glow also appears around the sputtered element. A dark

zone of about 3/4" is maintained between the two glowing parts.

2. Construction of Heat Transfer Gage

The film is sputtered on an electrical insulator element, which is generally glass or quartz, although other similar materials can be used. Two methods of gage construction have been employed. In one method a sputtered element is inserted directly into the model. The other method is to build the model out of glass or similar material and sputter the film directly on the model. In both cases the film is baked at 1100°F for about 1/2 hour. Electrical leads are then soft-soldered to the edges of the film, or for the case of the model insert, the unexposed edges are sputtered and the leads are soldered there. The gage is then flush-mounted in a groove in the model. A strip of blotting paper is inserted behind the element to absorb the shock and reduce the danger of breakage of the glass. Gages at various stages of assembly are shown in fig. 6.

3. Response Characteristics of a Surface Resistance Thermometer

The time required for heat to diffuse from the outer surface of the film to the interface between the metallic film and the backing material provides a measure of the response time of the film itself. Roughly, this diffusion time, td, is given by

$$t_d \cong \left(\frac{\rho C_p}{K}\right)_f \cdot \delta^2 \qquad (1)$$

where δ is the film thickness, and the subscript "f" denotes the pro-

perties of the film material. For platinum $(\rho C_p)/k = 4.04$ (cgs.), and if $\delta \sim 10^{-6}$ cm, or 100 Å, then $t_d \sim 4 \times 10^{-12}$ sec. Thus under almost all transient conditions the temperature of such a thin film is uniform across its thickness and is equal to the instantaneous surface temperature of the backing material itself.

So far as the backing material is concerned, the metallic film act as a thermal capacitance of extremely small "thermal-inertia". The surface temperature of the backing material approaches within a few per cent of the ideal response for zero film thickness in a "lag-time" t_ℓ, of the order of $100 \left\{ [(C_p\rho)_f]^2 / (k\rho C_p)_b \right\} \cdot \delta^2$. (Here "b" refers to the backing material.) If the backing material is quartz, and a platinum film of 10^{-6} cm is used, then $t_\ell \sim 6 \times 10^{-9}$ sec. For glass backing material $t_\ell \sim 6 \times 10^{-8}$ sec. Experimental evidence, although not capable yet of showing the exactness of this calculation shows that indeed the response time is less than 0.10 μ sec (fig. 9).

When the thin metallic film is utilized as a resistance thermometer its temperature rise appears as a voltage variation. If this temperature rise is not very large, experimental calibration shows that the relation between film temperature and its electrical resistance is linear. So the instantaneous film resistance R_f can be calculated from the relation

$$R_f = R_o [1 + \alpha (T_f - T_o)] \qquad (2)$$

where α is the coefficient of resistivity, the subscript "o" refers to initial conditions, and "f" refers to the instantaneous film conditions. With a constant current flow through the film, the instantaneous voltage

rise is $\Delta E = I_o(R_f - R_o)$ so that

$$T_f - T_o = \frac{\Delta E}{I_o R_o \alpha} \tag{3}$$

For a typical gage, R_o = 50 ohms, $I_o = 20 \times 10^{-3}$ amp. and α = 0.002 - 0.003/°C so that an output of 2 - 3 mv per degree centrigrade is recorded. Surface temperature variations of less than 0.2°C - 0.3°C can be resolved with the present electronic equipment.

For the testing times available in the shock tube (less than 1×10^{-3} sec.) the heat pulse penetrates only a very shallow layer near the surface of the glass element. The depth of this layer can be roughly estimated as $\delta_b \sim 3\sqrt{\left(\frac{K}{\rho c_p}\right)_b \cdot t}$. Now for $t = 10^{-3}$ sec, $\delta_b \sim$ 0.004 cm. for glass, and $\delta_b \sim$ 0.010 cm. for quartz. Since the backing element is usually at least 0.25 cm. thick and the scale of the temperature variation along the surface of the model is at least 10 times larger than δ_b, the backing element acts practically like a semi-infinite, one-dimensional heat sink. Thus the required relation between the surface heat transfer rate and the known film (= surface) temperature change is obtained by solving the classical, one-dimensional heat conduction equation

$$\frac{\partial T}{\partial X} = \chi \frac{\partial^2 T}{\partial X^2} \tag{4}$$

for the region $x > 0$, subject to the boundary conditions

$$T(x, 0) = 0 , \quad q(x, 0) = 0 , \quad T(0, t) = f(t) \tag{5}$$

and

$$q(X,t) \longrightarrow 0 \qquad T(X,t) \longrightarrow 0 \qquad \text{as } X \longrightarrow \infty \ .$$

Here $T \equiv T_f - T_o$ and $\chi = \left(\frac{K}{\rho C_p}\right)_b$. For the case of unit step function in surface temperature, i.e., $T(0,t) = 0$ for $t \leqq 0$ and $T(0,t) = 1$ for $t > 0$, we know that

$$q(0,t) = \frac{K}{\sqrt{\pi \chi t}} = \sqrt{\frac{(K\rho C_p)_b}{\pi}} \cdot \frac{1}{\sqrt{t}} \tag{6}$$

(see for example, Ref. 19). Therefore, the heat transfer rate for an arbitrary surface temperature time history $T(0,\tau)$ is given by the relation:

$$q(0,t) = \sqrt{\frac{(K\rho C_p)_b}{\pi}} \int_0^t \frac{1}{\sqrt{t-\tau}} \frac{df}{d\tau} d\tau \tag{7}$$

where $f(\tau) = T(0,\tau)$, or by introducing

$$\theta = \sin^{-1}\sqrt{\frac{\tau}{t}} \quad \text{and} \quad g(\tau) = 2\sqrt{\tau}\,\frac{df}{d\tau} = \frac{df}{d\sqrt{\tau}}$$

equation 7 can be written as

$$q(0,t) = \sqrt{\frac{(K\rho C_p)_b}{\pi}} \int_0^{\frac{\pi}{2}} g(\theta)\, d\theta \tag{8}$$

The inverse relation connecting the surface temperature and the applied heat transfer rate is also useful. According to Carslaw and Jaeger (Ref. 19, page 59, equation 9)

$$T(0,t) = \frac{1}{\sqrt{\pi (\rho C_p K)_b}} \int_0^t \frac{q(0,\tau)}{\sqrt{t-\tau}}\, d\tau \tag{9}$$

The explicit solution of equation 9 for several heat rate input functions is useful for future reference and will be written out.

a. Step Function Heat Transfer Rate

In this case $q(0, t) = 0$ for $t \leq 0$ and $q(0, t) = q_o$ = constant for $t > 0$. The solution is then

$$T(0,t) = \frac{2 q_o}{\sqrt{\pi (\rho C_p K)_b}} \cdot \sqrt{t} \tag{10}$$

b. Heat Transfer Rate Decreasing like $1/\sqrt{t}$

Here $q(0, t) = \frac{\sqrt{(\rho C_p K)_b}}{\sqrt{\pi}} \cdot \frac{1}{\sqrt{t}}$ for $t > 0$. Then

$$\begin{aligned} T(0, t) &= 1 \qquad t > 0 \\ &= 0 \qquad t \leq 0 \end{aligned} \tag{11}$$

c. Periodic Heat Transfer Rate

Here $q(0, t) = q_o \sin(\omega t + \epsilon)$, and the "steady-state" periodic part is then

$$T(0,t) = \frac{q_o}{\sqrt{(\rho C_p K)_b}} \cdot \frac{1}{\sqrt{\omega}} \cdot \left[\sin\left(\omega t + \epsilon - \frac{\pi}{4}\right)\right] \tag{12}$$

4. Method of Calibration

The quantitative measurement of the heat transfer rate from the output of the surface resistance thermometer depends on accurate determination of the quantities $(\rho C_p k)_b$ and α, the coefficient of resistivity.

For the short duration of flow in the shock tube the surface temperature of a model is not increased to more than 100°C provided $M_{s_{max}} \cong 7 - 8$, so that determination of the coefficient of resistivity between the ice point (0°C) and the water boiling point (100°C) is sufficient. For these thin films α is dependent on the film thickness and lies below the value for the bulk metal, which is 0.0038/°C for platinum. The experimentally measured values range between 0.0018 and 0.0025/°C.

The determination of $(\rho C_p k)_b$ of the backing material presented a more difficult problem. Because of the interpenetration of metal and glass that occurs at the interface between the thin film and the glass element, and the very shallow layer affected by the heat pulse, the physical quantities k, ρ, and C_p cannot be considered to be that of the bulk material. In addition the properties of glass may vary over a wide range between various specimens, so that one is forced to devise a method for calibration of every gage under actual transient conditions. The simplest solution is to use a known transient heat rate input, measure the gage output, and thereby determine directly the parameter $\frac{1}{(\rho C_p k)_b}$.

A step function heat rate input was chosen. This input was obtained by the discharge of a large capacitor into the film. The capacitor was selected so that the time constant of its discharge through the gage would be much larger than the required test time. The gage was placed on one leg of a balanced bridge circuit (fig. 7), so that only

the output generated by the increase of the gage resistance is recorded. The characteristics of this calibration circuit are shown in fig. 8. First a stable 57 Ω 2 watt resistor was substituted for the gage and the output is shown in fig. 8a. For the first 200 μsec the discharge current is very well described by a step function. (Note that in the traces for fast sweeps all initial transients decay in about 1 μsec.) Fig. 8b shows the output when the gage is connected in the bridge. The output is very well described by a parabolic time variation for the first few hundred microseconds. This surface temperature variation is predicted by the solution of the heat conduction equation (equation 10). Now, the numerical value of $1/(\rho C_p k)_b$ is determined by the following procedure:

The heat input q_o in cal/cm^2/sec. is given by

$$q_o \cong \frac{I_o^2 R_o}{4.19\, A} \tag{13}$$

where I_o is the current in the gage in amperes, R_o is the intial gage resistance in ohms, and A is the film area in cm^2. Note that for q_o to be a true step function we require that the film strip be of uniform thickness and width, and that the per cent change in film resistance and current be very small, so that throughout the test q_o is uniform and constant. The film uniformity is insured by the sputtering process. Films are tested on an optical comparator for uniformity of width, and if they are excessively irregular they are rejected. Another source of error is the end effects. Particularily at the corners of the element the film may be thinner and this results in a "hot spot" which distorts the gage response. This difficulty is eliminated by covering the edges

with a layer of conducting silver paint which is covered on installation in the test section so that only the film is exposed to the gas flow. Now $\Delta R/R_o$ and $\Delta I/I_o$ are generally of the order of 1 per cent or less, so that their effect on the heat rate input is practically negligible. In cases where this assumption is violated this effect can be accounted for in the calculations. Although such calculation will require much more labor, the calibration procedure will still be valid.

By analyzing the bridge circuit one finds that the voltage output ΔE caused by the heating of the film is related to the resistance change ΔR by

$$\Delta R = \frac{\Delta E}{V} \cdot \frac{(R_o + R_2)^2}{R_2} \tag{14}$$

where R_2 is the second resistance in the bridge (fig. 7), and I_o is given by

$$I_o = \frac{V}{R_o + R_2} \tag{15}$$

Now $T_f - T_o = \Delta R/\alpha R_o$, and by equation 10

$$\frac{\alpha}{\sqrt{(\rho c_p k)_b}} = \frac{4.19\sqrt{\pi} \cdot A \cdot \Delta R}{2 \cdot R_o^2 \cdot I_o^2 \sqrt{t}} \tag{16}$$

When a gage is calibrated only for heat transfer rate measurement the separate determination of α is not required, since this method actually determines the quantity $\frac{\alpha}{\sqrt{(\rho c_p k)_b}}$ which appears in this relation between ΔE and $q(0, t)$. Resistances and voltages can be measured to relatively high accuracy, and this coefficient $\frac{\alpha}{\sqrt{(\rho c_p k)_b}}$ can be

determined within a few per cent. For heat transfer calculations it is convenient to use the parameter $\frac{\sqrt{\pi (\rho C_p k)_b}}{2\alpha}$. The experimental values for this parameter for platinum film on glass range between 11 and 17 in c. g. s. units. Comparing these results to the handbook values of $(\rho C_p k)$ for glass shows that these are in the same range. The differences in values are explainable by the variation of α and the use of different glasses.

5. Application of Gage to Shock Tube Research

The film resistance thermometer described in the previous sections can be utilized in the shock tube either as a heat transfer rate gage or as a shock wave detection device for shock wave speed measurement, or for other timing or triggering applications.

When used as a heat transfer rate measuring device the gage is operated in a circuit similar to that used for hot wire anemometer operation at constant current. The accuracy of the heat transfer data depends on the accuracy of the calibration procedure and the accuracy of measuring of the current, initial resistance, and output voltage. With ordinary laboratory techniques overall accuracy of about 5 per cent can be achieved and with special care particularily in the calibration, this accuracy can probably be improved.

When the gage is employed for shock detection device, the requirements on the film are much relaxed. There is no need for gage calibration and the only requirement on gage size is that its width be small enough so that the shock wave will traverse it in a short enough time. Films of width of 0.010" were obtained so this traversing time is

as short as 0.5 μsec even at shock Mach number of 2; of course this transit time decreases linearily with shock speed. Fig. 3 shows an arrangement for using the gages as shock speed detectors. Here the initial jump caused by the hot gas behind the shock is amplified and fed to the electronic counter. Similarily this pulse can be utilized for triggering associated equipment such as oscilloscopes, time delays, spark for schlieren system, etc.

The response of the resistance film gage in the shock tube flow is represented in figs. 9, 10, and 11. Fig. 9 shows the response time of a gage at the stagnation line of a cylinder utilizing a fast sweep. The fast response time is evident. Figs. 10 and 11 show typical traces of gages at the stagnation region of a cylinder and on the shock tube wall, respectively.

The stagnation point traces show the shock arrival, the "hot" flow for about 200 μsec and then the arrival of the "contact region" and the "cold" non-uniform flow behind it.

The gage response on the shock tube wall shows the temperature jump when the shock arrives, and the almost uniform temperature thereafter, which indicates that the boundary layer just behind the shock is laminar. After 100 - 200 μsec the temperature again rises because of laminar-turbulent transition and turbulent flow in the boundary layer.

A detailed discussion of the application of this gage will be given in the discussion of the actual experiments conducted in the shock tube (Sections IV and V).

B. Piezoelectric Pressure Gage

The direct measurement of local pressures either on model surfaces or on the shock tube wall presents a very difficult problem. Some work on pressure transducers for shock tube application is reported in Refs. 5, 20, 21, and 22. The present very brief account is included to illustrate various problems encountered in the development of pressure transducers suitable for extremely short flow times (of about 100 μ sec).

The fast response time required can be achieved by the utilization of piezoelectric materials such as quartz or barium-titanate. However, the sudden loading of the gage by the pressure jump across the shock wave excites resonance vibrations in the gage housing and/or the piezoelectric material itself, so that the "noise" is a large fraction of the signal. An additional difficulty is caused by waves travelling in the shock tube wall generated by the diaphragm breakage. These waves are largely eliminated by proper gage mounting, or by a rubber isolating section such as the one used in the GALCIT shock tube (see fig. 1).

The pressure transducer utilized in the present work employs two barium-titanate discs 1/2" in diameter and 0.10" thick. These discs are connected in parallel and inserted into a housing behind a thin (0.050") diaphragm. Fig. 12 presents the response of this gage mounted on the shock tube wall as a function of shock strength and initial pressure. For weak shock waves ($M_s < 3$) the noise caused by vibration is comparatively small, and the gage output is very satisfactory. Thus this gage can be utilized for shock wave detection and for quantitative pressure measurements up to this range of shock strength.

As the shock wave speed increases the noise also increases, and for relatively strong shocks ($M_s \sim 6$) the vibration signal is about 50 per cent of the total output. These disturbances cannot be connected with waves in the shock tube wall, because no signal is received before the arrival of the shock. Also, the high noise frequency of 50 - 100 KC excludes the possibility of structural vibrations other than vibrations of the gage housing and diaphragm and/or the piezoelectric elements themselves. No satisfactory solution of these problems has been found for flow times of the order of 100 μ sec. It should be pointed out that the signal to noise ratio becomes acceptable in about 500 μ sec, so that the barium-titanate gage should be satisfactory for uniform flow times longer than 500 μ sec.

The measurement of pressures on model surfaces in the shock tube is even more difficult than the problem of measuring static pressures on the shock tube wall. Considering the difficulties encountered with this problem the task of measuring pressures on model surfaces is left for future development of new techniques.

IV. SHOCK TUBE PERFORMANCE AND CALIBRATION

Idealized shock tube theory has been discussed and described in many reports (Refs. 1, 4, and others). On the basis of this theory the shock wave speed and flow history are uniquely determined once the following initial conditions are given: (1) gas combination, i.e., driver gas and test gas in the low pressure section; (2) ratio of initial driver gas pressure to initial test gas pressure, p_4/p_1; (3) ratio of initial driver gas temperature to initial test gas temperature, T_4/T_1. Some of the most important (and most questionable) assumptions of this theory are:

1. Instantaneous diaphragm breakage and shock formation.
2. Distinct "contact surface" separating the "hot" and "cold" gas.
3. No effects of viscosity and heat conduction at the tube walls.

Experimental evidence shows that these assumptions are seriously violated in the shock tube, and this fact has a strong effect on the actual flow produced. To include these effects properly in a theoretical calculation of shock tube performance is an extremely difficult task. For example the breakage of the diaphragm may depend on such non-accountable factors as material uniformity, tearing properties, etc., and in general is a rather random variable. Thus, to be able to use the shock tube as an experimental aerodynamic tool the tube must be calibrated experimentally so that its actual performance can be established. Calibration of the GALCIT shock tube and studies of the flow produced in the straight section will be the subject of part B of this section.

Once the shock wave speed is determined experimentally the flow

conditions to be expected "far" behind the shock can be calculated with the aid of the existing data on the properties of air in thermodynamic equilibrium, including dissociation and ionization. Until recently the available calculations were based on the older incorrect value for the dissociation energy for nitrogen. Correct results that have since become available are suitable mainly for a particular application. Thus it was decided to perform these calculations for the initial conditions of the GALCIT shock tube. Conditions behind a normal shock wave were computed for shock Mach numbers from 3 to 20, and for initial pressures of 1, 5, and 10 mm Hg in the low pressure section, with $T_1 = 298^{\circ}K$. Flow quantities behind a detached bow wave in the "hot" flow and at the forward stagnation point of a blunt body were also obtained for the same range of parameters. These results are directly applicable to the heat transfer rate calculations of Section V.

Equilibrium thermodynamic properties of air as a function of temperature and density were obtained from tables in Refs. 23 and 24, which are based on recent National Bureau of Standards data (Ref. 25). A brief outline of the method of computation employed and a discussion of the results obtained is given in part A of this section.

A. Flow Conditions in Shock Tube

1. Thermodynamic Equilibrium Conditions Behind a Strong Shock Wave in Air

In "shock coordinates" the continuity, momentum and energy equations and the equation of state across a normal shock wave are as follows:

continuity: $$\rho_1 V_1 = \rho_2 V_2 \tag{17}$$

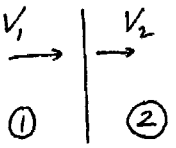

momentum: $$P_1 + \rho_1 V_1^2 = P_2 + \rho_2 V_2^2 \tag{18}$$

energy: $$\frac{V_1^2}{2} + H_1(\rho_1, T_1) = \frac{V_2^2}{2} + H_2(\rho_2, T_2) \tag{19}$$

state: $$P = \rho \frac{\bar{R}}{m} T \tag{20}$$

where the subscript 1 refers to conditions upstream of the shock wave and 2 refers to equilibrium conditions behind the shock wave. Here H(ρ, T) is the enthalpy per unit mass <u>including</u> the chemical enthalpy.

Now the starting shock wave in the shock tube is moving with velocity U_s into a stationary gas so that

$$V_1 = U_s$$

and

$$V_2 = U_s - U_2$$

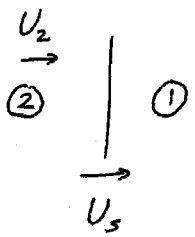

For this case, equations 17, 18, 19, and 20 can be combined and re-written in the following form:

$$H_2 - H_1 = \frac{U_s^2}{2}\left[1 - \left(\frac{\rho_1}{\rho_2}\right)^2\right] \tag{21}$$

$$\frac{P_2}{P_1} = 1 + \frac{\rho_1}{P_1} U_s^2 \left[1 - \frac{\rho_1}{\rho_2}\right] \tag{22}$$

$$\frac{\rho_1}{\rho_2} = \frac{P_1}{P_2} \cdot \frac{m_1}{m_2} \cdot \frac{T_2}{T_1} \tag{23}$$

Once the enthalpy, H, and the molecular weight, m, are known as functions of the temperature and density these equations can be solved for the conditions behind the shock wave. Starting with the known initial conditions, namely, $\rho_1 p_1$, T_1, m_1 of the undisturbed air, and a particular value of the shock velocity U_s, select a trial value $\rho_1/\rho_2 = (\rho_1/\rho_2)^o$ (for example, the perfect gas value). From equation 21 obtain H_2^o. Now from the known properties of air obtain T_2^o using the values of H_2^o and ρ_2^o, and also obtain $(m_1/m_2)^o$. From equation 22, compute $(p_2/p_1)^o$. These values of $(p_1/p_2)^o$, $(T_2/T_1)^o$, and $(m_1/m_2)^o$ are now substituted into equation 23 to obtain a new value of $\rho_1/\rho_2 = (\rho_1/\rho_2)^1$. This procedure is now repeated with the new $(\rho_1/\rho_2)^1$ until $(\rho_1/\rho_2)^{i+1} = (\rho_1/\rho_2)^i$ to the required accuracy. This procedure converges very fast and generally 2 to 3 iterations were sufficient for 1 per cent accuracy. This fast convergence arises from the fact that the enthalpy H_2 for strong shock waves is equal to $\frac{U_s^2}{2}\left[1 - \left(\frac{\rho_1}{\rho_2}\right)^2\right]$ while $\rho_1/\rho_2 << 1$, so that H_2 is fairly independent of the density ratio, and so T_2 is also almost independent of ρ_1/ρ_2. However, the pressure ratio p_2/p_1 is much more sensitive to the density ratio ρ_1/ρ_2, and is adjusted sufficiently fast to enable fast convergence of the entire procedure.

The results of these calculations are shown in figs. 12 - 20. The speed of sound and Mach number in region 2 are also shown based on the data of Refs. 23a, b, c. One can easily see the large effects produced by the inclusion of the real gas properties, particularly on the density, temperature and Mach number behind the shock wave. However the effect on the pressure behind the shock wave is not so appreciable.

2. Conditions Behind a Bow Wave on a Blunt Nosed Body in the Shock Tube

A strong shock wave generates a supersonic flow behind it, and if a blunt body is placed in this stream a detached bow wave will be established in front of the body. In the stagnation region this bow wave is nearly normal and the conditions behind this wave will be determined by the normal shock relations. However, the initial conditions in this case are those which were calculated previously for the hot flow produced behind the moving shock wave (Section IV. A. 1).

The shock equations in this case are

$$H_{5'} - H_2 = \frac{U_2^2}{2}\left[1-\left(\frac{\rho_2}{\rho_{5'}}\right)^2\right] \tag{24}$$

$$\frac{P_{5'}}{P_2} = 1 + \frac{\rho_2}{P_2} U_2^2 \left[1 - \left(\frac{\rho_2}{\rho_{5'}}\right)\right] \tag{25}$$

$$\frac{\rho_2}{\rho_{5'}} = \frac{P_2}{P_{5'}} \cdot \frac{m_2}{m_{5'}} \cdot \frac{T_{5'}}{T_2} \tag{26}$$

$$U_2 = U_s\left[1 - \frac{\rho_1}{\rho_2}\right] \tag{27}$$

where state 2 corresponds to the hot flow ahead of the body and state 5' refers to conditions just behind the bow shock on the axis of symmetry. By the same procedure described in Section III, one can solve for the conditions at the stagnation region.

By assuming adiabatic compression between the shock wave and the forward stagnation point one obtains

$$\frac{p_o'}{p_{5'}} = \left[1 + \frac{\bar{\gamma}-1}{2} M_{5'}^2\right]^{\frac{\bar{\gamma}}{\bar{\gamma}-1}} \tag{28}$$

$$\frac{\rho_o'}{\rho_{5'}} = \left(\frac{p_o'}{p_{5'}}\right)^{\frac{1}{\bar{\gamma}}} \tag{29}$$

$$\frac{T_o'}{T_{5'}} = \left(\frac{p_o'}{p_{5'}}\right)^{\frac{\bar{\gamma}-1}{\bar{\gamma}}} \tag{30}$$

where p_o' is the stagnation pressure behind the bow shock, $M_{5'} = U_{5'}/a_{5'}$, $a_{5'}^2 = (\gamma_{5'} p_{5'})/\rho_{5'}$, and $\bar{\gamma}$ is some mean value of γ at the conditions of the "shocked" air. For strong shock waves $(\rho_1/\rho_2) << 1$ and also $(\rho_2/\rho_{5'}) << 1$, so that by neglecting terms of order $(\rho_1/\rho_2)^3$ and $(\rho_2/\rho_{5'})^3$ one obtains

$$\frac{p_o'}{p_{5'}} \cong 1 + \frac{1}{2} \frac{\rho_2/\rho_{5'}}{1 - \rho_2/\rho_{5'}} \tag{31}$$

$$\frac{\rho_o'}{\rho_{5'}} \cong 1 + \frac{1}{2\bar{\gamma}} \cdot \frac{\rho_2/\rho_{5'}}{1 - \rho_2/\rho_{5'}} \tag{32}$$

$$T_o' \cong T_{5'} \tag{33}$$

3. Accuracy of Calculations

Although the iteration procedure described in Section A. 1 can be carried out to any degree of accuracy required the absolute accuracy of the calculations is obviously determined by the accuracy of the tabulated properties of air. The data available to the author at this time is given in temperature steps of 1000°K, which requires some imaginative interpolation, particularly in the regions where the properties of air are changing rapidly with increase in temperature (e. g., 3000° - 4000°K and 8000° - 9000°K). This fact accounts for some scatter in the calculations which can be avoided when more detailed data becomes available with smaller temperature intervals. However, even with this handicap the calculated values are probably accurate to within a few per cent.

4. Viscosity of Air Behind a Shock Wave

For temperatures below 2000°K in air the viscosity coefficient can be obtained by the semi-empirical Sutherland formula

$$\mu \times 10^7 = 145.8 \frac{T^{3/2}}{110.4 + T} \tag{34}$$

where μ is in gr/cm-sec. Available experimental data up to 1900°K agrees very well with equation 34. For higher temperatures a more refined calculation is required and a good approximation can be obtained by using the Lennard-Jones potential for the intermolecular force field. For this case, from Ref. 26,

$$\mu \times 10^7 = 266.93 \frac{\sqrt{mT}}{r_0^2} \cdot \frac{J(\tau)}{Y(2,2,\tau)} \tag{35}$$

where

$J(\tau)$ = correction factor ~ 1

$\Upsilon(2,2,\tau)$ = the second collision integral

$\tau = kT/\epsilon$

The functions $J(\tau)$ and $\Upsilon(2,2,\tau)$ are tabulated in Ref. 26.

For air

$\epsilon/k = 97.0$

$r_o = 3.617$ A

The results of this calculation are shown in fig. 21, which also shows the viscosity values obtained from an extrapolation of the Sutherland formula. It is interesting to note that the difference between the two curves is not more than 10 per cent at most.

By using equation 35 the Reynolds number of the flow behind the shock wave of strength M_s can be calculated. The results are plotted in fig. 22, where $Re/cm = (\rho_2 U_2)/\mu_2$ is calculated for various initial pressures.

B. Experimental Determination of Shock Tube Performance

1. Relation Between Shock Strength and Shock Tube Initial Conditions

As discussed in the Introduction to part A of this section, the simplified shock tube theory relates all conditions in the shock tube to the initial conditions. The relation for the strength of the shock generated in the tube is as follows (Ref. 4):

$$\frac{p_4}{p_1} = \frac{p_2}{p_1}\left[1 - \left(\frac{p_2}{p_1} - 1\right)\frac{\frac{\gamma_4 - 1}{2\gamma_4}\frac{E_1}{E_4}}{\frac{\gamma_1 + 1}{\gamma_1 - 1}\frac{p_2}{p_1} + 1}\right]^{-\frac{2\gamma_4}{\gamma_4 - 1}} \tag{36}$$

where subscript "1" refers to conditions ahead of the shock wave, "2" to conditions behind the shock, and "4" to the conditions of the driver gas in the compression chamber. E_1 and E_4 are the internal energies of the gases across the diaphragm. Since the pressure ratio across the shock p_2/p_1 is uniquely related to the shock Mach number (fig. 15), equation 36 also determines the shock Mach number M_s in terms of the initial conditions. A direct test of this theory is to try to verify this relation experimentally.

The results of numerous runs with helium as the driver gas and air in the low pressure tube are shown in fig. 23. The shock velocity was measured by using the film resistance thermometer for shock detection. Two gages were placed 2 feet apart and the outputs were fed through pulse amplifiers to the start and stop channels respectively, of a 1 mc Berkeley counter. The errors in this measurement are estimated to be within the resolving time of the counter, which is about 1 μsec, so that the error in shock velocity is not more than 1/2 per cent. Also the error in p_4/p_1 is not expected to exceed a few per cent. Fig. 23 shows scatter much in excess of the experimental inaccuracy, and one suspects a more fundamental reason.

Examination of the diaphragm opening process shows that it is definitely not instantaneous; actually the diaphragm opens in a time of about 200 - 300 μsec. Examination of drum camera schlieren pictures

taken near the diaphragm (Ref. 4) indicates that vortices and other disturbances are generated at the diaphragm. These pictures were taken for plastic diaphragms which tend to shatter. In Ref. 4 the authors note that the same initial condition, p_4/p_1, results in different shock strengths, depending on the thickness of the diaphragm, the number of layers of plastic diaphragm used, and the amount of stressing that the diaphragm material was subjected to before its breakage. One is led to suspect that metallic diaphragms, which do not shatter, consume much more time for opening, and therefore affect the shock strength to a much larger extent.

In the present experiments soft copper diaphragms 0.010" and 0.020" thick were used. They were scribed to a depth of 1/3 to 2/3 of their thickness. The experiments represented in fig. 23 were conducted over a period of about 2 years, so the scribing is more or less random, and so are the corresponding shock speeds. Fig. 23 shows some concentration of points near an average curve with runs occurring less frequently away from the average, which is a characteristic of a random process. The theoretical line (equation 36) is included in fig. 23. Our conclusion, which is confirmed by many shock tube investigators, is that p_4/p_1 cannot be used for shock speed prediction, and that shock speed must be measured for each run. For this reason the shock speed measurement is the basic datum from which all quantities can be predicted theoretically (part IV. A), and which is used for checking and reducing the experimental data. However, before one can proceed to use the shock tube for actual studies two questions still have to be clarified: (1) Duration and uniformity of flow in the shock tube; (2) Possibility of making two or more independent experimental

measurements of the gas properties behind the shock.

2. Duration and Uniformity of Flow in the Shock Tube

The duration of the "hot" flow, defined as the transit time of the slug of air between the shock front and the contact surface, can be easily calculated from the wave system in an ideal shock tube. If the tube is properly designed and no reflected wave appears at the test area before the contact surface arrives, the hot flow time is $t_h = (L/U_2) - (L/U_s)$, where U_s is the shock velocity and U_2 is the flow velocity behind the shock. But $U_2 = U_s \left[1 - (\rho_1/\rho_2)\right]$ so that $t_h = \dfrac{(\rho_1/\rho_2)\, L}{U_s \left[1 - \rho_1/\rho_2\right]}$, where L is the distance from the diaphragm to the test section. Now for $M_s \sim 6$, $\rho_2/\rho_1 \cong 6.0$ (fig. 13), so that $t_h \sim 750$ μsec when L = 20 ft. Actually the observed flow times are one-half to one-third of this value. The flow duration was determined by two independent techniques:

a. Heat Transfer Gage

An accurate determination of uniform flow duration was obtained from the heat transfer records on circular cylinders 12.5 mm and 5 mm in diameter. The heat transfer records using helium driver gas show a distinct change from a smooth curve to a rugged curve with a certain "jump" at the point of transition (fig. 10). To confirm the statement that this transition occurs when the cold flow arrives, test runs were also conducted using nitrogen as the driver gas. A distinct jump in heat transfer-rate was again observed, and the flow duration checked very well with the results obtained with the helium driver gas.

b. Schlieren Studies

The second determination of hot flow duration is obtained from a schlieren study of the flow over a rake of three 45° cones (figs. 25 and 26). Both shock arrival and contact region were detected by the change in shock wave angle and by the sudden thickening of the wall boundary layer. Although the flow durations determined by this method are not as accurate as the results obtained from the heat transfer records, they serve as an independent check on those results, as seen in fig. 24.

The explanation of this reduction of test time so far below the theoretical values must lie in the deviation from the simple shock tube theory, particularly the imperfect diaphragm removal. One suspects that the shock wave growth process generated by the gradual diaphragm opening actually reduces the "effective" length of the shock tube. However, it is hard to expect this effect alone to be so big that it is responsible for the reduction of the test time by 60 to 70 per cent. An additional phenomenon may be jet formation which produces a transition region extending deep into the hot flow region. Such effects have been noticed in heat transfer studies where a typical flow history at $M_s = 5.5$ seems to be as follows: about 250 μ sec of hot flow, followed by 250 μ sec of "mixing", followed by smoothing out of the gage output curve and a later decay of the flow. In addition the Mach number in the "cold" region as observed in cone-schlieren studies seems to lie much below the theoretically predicted value. At $M_s = 6.2$ the predicted Mach number in the cold flow is about 4.4, while the measured value is only 2.6.

The question of the uniformity of the actual hot flow was investigated to determine if this flow is suitable for aerodynamic investigations. For these tests both the schlieren technique and the heat transfer rate measurements are used.

In the schlieren studies the history of the flow Mach number is determined by measuring the shock wave angles on a 45^{o} cone rake. The cone rake (fig. 25) consists of three 45^{o} cones placed 3/4" apart on a double-wedge support. The center cone is placed at the center of the test section, and the outside cones are about 3/4" from the shock tube walls. In successive runs the schlieren spark is triggered at various times after the shock wave passage. Time intervals increasing by 20 μ sec steps are obtained by the use of an electronic time delay capable of resolution of 1 μ sec steps. The triggering pulse is obtained from a wall temperature gage used for shock speed measurements, which is placed two feet forward of the test section. The shock speed is recorded for every shot. The information obtained from this test is: (1) Flow Mach number uniformity at various times (distances) behind the shock wave; (2) Flow uniformity across the test section; (3) Boundary layer growth on shock tube wall obtained from shock wave boundary layer interaction.

The flow Mach number is determined from the shock wave angle using Kopal's cone tables (Ref. 35) for $\gamma = 4/3$ and $\gamma = 1.4$. In this range of flow Mach numbers (1.3 - 2.0) the effect of γ on shock angle is very small. Typical schlieren pictures before and after contact region arrival are shown in fig. 26. The results of runs at two shock strengths $M_s = 4.75 \pm 0.1$ and $M_s = 6.2 \pm 0.1$ are shown in figs. 27

and 28. Actually the repeatability of the shock, M_s, is within about $\pm$ 0.1 of a Mach number, but the flow Mach number is not very sensitive to M_s; in fact the corresponding uncertainty in M_2 is $\pm$ 0.01 - 0.02. If the non-uniformity in M_2 were larger than $\pm$ 0.01 - 0.02 the data presented in figs. 27 and 28 would show it. Actually the results show a very small scatter and a constant flow Mach number both across the tube cross section and at various times after the shock wave passage.

The only direct and simple characteristic of the flow behind the shock is the flow Mach number, M_2, which is obtained from the wave angle on the cones. The measured values of M_2 as a function of shock Mach number are shown in fig. 29. The results of calculations of M_2 for an ideal gas, for a gas with variable specific heats including rotation and vibration, and for air including dissociation are also shown in fig. 29. The experimental results follow the equilibrium-air calculations, although they are slightly lower. Although no direct measurement of temperature, pressure, or density was attempted, this Mach number measurement indicates that the equilibrium conditions are realized in the shock tube flow, and that the calculations of equilibrium flow conditions (part A) represent a good approximation.

A much more sensitive test for uniformity of flow is the heat transfer rate at the stagnation region of a blunt body. The heat transfer calculations show that the heat transfer rate at the stagnation point, $\dot{q}_o$, is proportional to the total stagnation enthalpy, h_{s_e}, and to the square root of the product of external velocity and density, $\sqrt{(\rho_e U_e)}$. For a strong shock wave, $\rho_e/\rho_1 >> 1$ and the enthalpy $h_{s_e} \sim U_s^2$, so that $\dot{q}_o \sim U_s^2 \sqrt{\rho_e U_2}$. If the shock tube flow is uniform then U_s, U_2, and ρ_2 are constant and so q_o should be constant. Now the response of

the heat transfer gage to such a heat rate input is obtained from equation 10 of Section III. The instantaneous surface temperature should increase parabolically as $\sqrt{t}$. This response characteristic is actually observed in the shock tube and is discussed in more detail in Section V. Now the heat transfer rate depends strongly on the shock velocity, so that it is extremely sensitive to non-uniformities of the shock wave speed for such effects as shock attenuation, etc. ($\dot{q}_o \sim U_s^n$, where $3 \leq n \leq 3.5$).

To summarize: the various experiments* which were made to determine the uniformity and duration of the "hot" flow in the shock tube definitely indicate that a uniform high temperature flow is established in this shock tube in a very short time ($< 50 \mu$ sec). The shock strength and flow duration are not very well predicted by the simple shock tube theory.

Upon examination of the schlieren photographs one can easily observe the interaction between the shock wave generated by the models with the boundary layer on the shock tube wall (figs. 26 and 42). These pictures of shock-wave boundary layer interaction can serve for an estimation of the boundary layer thickness and show if the boundary layer is laminar or turbulent. Both of these observations are of interest for discussion of shock wave attenuation. In this particular tube the wall boundary layer is very thin up to the time of arrival of the contact region. Within the contact region the boundary layer thickens extremely fast. Moreover, until the contact region arrives the interaction of the shock wave with the boundary layer is

---

* For $M_s < 3$, static pressure measurements on the shock tube wall also confirmed the results obtained by all the other methods.

typical of a laminar boundary layer. Beyond the contact region there seems to be a transition to a turbulent boundary layer. The boundary layer growth and its effect on the shock tube flow has received considerable theoretical and experimental attention. The theoretical calculations of shock wave attenuation (Refs. 36 and 37) indicate a very small attenuation (less than 4 per cent) in the case of a laminar boundary layer for a 20' tube, and a rather large attenuation (15 per cent) for turbulent boundary layers. The experimental studies of Refs. 37 and 38 indicate that the wall boundary layer is turbulent in those cases. The direct boundary layer observations in the GALCIT tube indicate a laminar boundary layer, and no measurable effects of attenuation as measured by the stagnation region heat transfer rate are observed. The GALCIT shock tube walls are smoothly ground while most shock tubes are cold-rolled steel surfaces. It would be interesting if the difference between laminar and turbulent boundary layers (Refs. 37 and 38) can be attributed to wall roughness.

V. HEAT TRANSFER STUDIES ON A CIRCULAR CYLINDER IN SHOCK TUBE

The development of the fast-response resistance thermometer, which is described in Section III. A, enables one to investigate experimentally the heat transfer problem in the high temperature flow in the shock tube. The present section will describe the measurements of heat transfer rates on a circular cylinder at enthalpies in the range of 400 to 1300 cal./gr. of air, which correspond to enthalpies encountered in free flight Mach number of approximately 4 to 10. The experimental results are compared to the heat transfer rate calculations based on the theoretical analysis of L. Lees (Ref. 28), using air properties at these conditions calculated in Section IV. A.

Part A of this section presents the experimental heat transfer results at the stagnation point of a circular cylinder and compares these results with the theoretical calculations.

Part B presents the heat transfer rate distribution measured over the circumference of a circular cylinder and these are compared with the theory.

A. Heat Transfer Rate at the Stagnation Region of a Circular Cylinder

1. Theory and Calculations

When the boundary layer in the stagnation region of a blunt body at hypersonic speeds is laminar, the heat transfer problem can be

treated analytically. At a high enthalpy level where the gas is dissociated and ionized, one has to make various assumptions as to the mechanism of heat transfer at the wall. In Reference 28, L. Lees examines two opposite limiting cases: (1) thermodynamic equilibrium; (2) diffusion as a rate-governing for heat transfer. It is also shown that under various assumptions the difference between the heat rate in the two limiting cases will be proportional to $\left[\frac{\rho D_{12} \bar{C}_p}{k}\right]_w^{2/3}$, which is of the order of 1.3.

For the case of complete thermodynamic equilibrium, the stagnation point heat ransfer rate, q_0, is (equation 12a of Reference 28):

$$q_0 = \frac{(\sqrt{2})^k}{2} (\bar{P}r)^{-2/3} \sqrt{\rho_e \mu_e} \sqrt{u_\infty} (h_{s_e} - h_w) \frac{\left[\frac{R}{u_\infty}\left(\frac{du_e}{ds}\right)\right]_0^{1/2}}{\sqrt{R_0}} \qquad (37)$$

where k = 0 for two-dimensional bodies and k = 1 for axially-symmetric bodies. The analysis assumes that Prandtl number is constant across the boundary layer and is represented by an average $\overline{Pr}$. Here $\overline{Pr}$ is taken to be 0.70.

The velocity gradient at the stagnation point $\left[\frac{R}{u_\infty}\left(\frac{du_e}{ds}\right)\right]_0$ is obtained in terms of M_∞, γ_∞ and an average $\bar{\gamma}$, by assuming a modified Newtonian pressure distribution (equation 13, Reference 28). It is convenient to express this velocity gradient in terms of gas densities which are obtained directly in the calculation. For a circular cylinder $ds = R_0 d\theta$. Let $\frac{c_p}{c_{p_{max}}} = \cos^2\theta$, and from Bernoulli's equation

$$\frac{d\rho_e}{d\theta} = -\rho_e u_e \frac{du_e}{d\theta} \tag{38}$$

so that $\left[\frac{1}{u_\infty}\left(\frac{du_e}{d\theta}\right)\right]_0 = \sqrt{2\rho_2/\rho_e \cdot \frac{p_2}{\rho_2 u_2^2}\left(\frac{p_o'}{p_2} - 1\right)}$

Now, one expresses $\frac{p_o'}{p_2}$ and $\frac{\rho_e}{\rho_2}$ in terms of $\frac{\rho_2}{\rho_3}$ (Part IV. A). (Note that state "2" in the shock tube corresponds to state "∞" in Reference 28). The expression is then simplified to [neglecting terms of $\left(\frac{\rho_2}{\rho_3}\right)^3$]:

$$\left[\frac{1}{u_\infty}\left(\frac{du_e}{d\theta}\right)\right]_0 = \sqrt{2\,\frac{\rho_2}{\rho_3}\left[1 - \frac{\gamma+1}{2\gamma}\frac{\rho_2}{\rho_3}\right]} \tag{39}$$

Since $\frac{\rho_2}{\rho_3} << 1$, $\frac{\gamma+1}{2\gamma}\frac{\rho_2}{\rho_3}$ is a small correction, so that an average value of γ will be a good approximation. Using $\overline{\gamma} = 1.3$

$$\left[\frac{1}{u_\infty}\left(\frac{du_e}{d\theta}\right)\right]_0 = \sqrt{2\,\frac{\rho_2}{\rho_3}\left[1 - 0.885\,\frac{\rho_2}{\rho_3}\right]} \tag{40}$$

Values of the stagnation point velocity gradient calculated from equation 40 compare vey well with the measured values on a hemisphere-cylinder body of Reference 29 even at M_2 as low as 1.7 (fig. 31). However, for lower M_2 the results of Reference 29 are used directly in the heat transfer calculations.

If $\frac{h_{se}}{h_w} >> 1$ the product $\rho\mu$ is almost constant over the boundary layer and can be equated to the value of $(\rho\mu)_e$ at the outer edge of the boundary layer. Actually, one can improve on the value

of $\rho\mu$ to be used in equation 37, by computing $\rho\mu$ at the average temperature $T_{ave} = \frac{T_w + T_e}{2}$ and local pressure, or at temperatures corresponding to the average enthalpy $\frac{h_w + h_e}{2}$, and local pressure*. Figure 30 shows the results of the stagnation point heat transfer calculations obtained by inserting in equation 37 values of $\rho\mu$: (1) At the surface (wall); (2) at $T_{ave} = \frac{T_w + T_e}{2}$ (3) at $T_h = F\left(\frac{h_w + h_e}{2}\right)$, and (4) at the outer edge of the boundary layer $(\rho\mu)_e$. Here R_o is the radius of the cylinder in cm, and p_1 is the initial pressure in the test section in mm Hg (In all cases the initial temperature is 298°K.).

2. Experimental Results

The heat transfer rate at the stagnation point of a circular cylinder spanning the shock tube test section is measured by utilizing the film resistance thermometer described in Section III. A. Two brass cylinders 12.5 mm and 5 mm in diameter were investigated to determine the scale effect (if any). The sputtered film, which is .020" wide and 1" long for the 12.5 mm cylinder and .010" x 1/2" for the 5 mm cylinder, is positioned at the "stagnation line" of the cylinder, as shown in fig. 32.

The heat transfer rate at the stagnation region of a blunt body in the hot flow of the shock tube is well described by a step function in heat rate; i.e., q_o is initially zero, then jumps to a constant value of q_o when the shock arrives, and remains at that value until

---

* The exact solution will involve step by step integration of the boundary layer equations which can be done with modern computing apparatus.
Such a solution is given by Rose and Riddell (Ref. 30) who show that $\sqrt{(\rho\mu)_e}$ in equation 37 is replaced by $(\rho\mu)_e^{0.4}(\rho\mu)_w^{0.1}$

the hot flow terminates. For such a heat rate input the surface temperature increases like $\sqrt{t}$. By using equations 3 and 10 of Section III one can easily show that the heat rate q_o is related to gage response ΔE by the expression

$$q_o = \frac{\sqrt{\pi(\rho C_p K)_b}}{2\alpha} \cdot \frac{\Delta E}{I_o R_o \sqrt{t}} \tag{41}$$

The quantity $\frac{\sqrt{\pi(\rho C_p K)_b}}{2\alpha}$ is the gage constant determined by calibration (Section III). It is assumed that I_o, R_o, and this calibration constant do not change during the test. I_o is kept constant by the heating panel circuit, while R_o is measured before and after each run. Its value increases by 2 - 3 per cent of the initial value at most, because of damage to the film and the glass backing produced by pitting caused by small particles in the air. However, most of this pitting occurs after the arrival of the contact region, because this flow is particularly turbulent and probably carries small diaphragm chips, and dirt particles scoured from the tube wall. The proof that the calibration constant actually remains constant during the "useful" life of the gage is obtained by repeated experiments at the same flow conditions. These tests did not show any significant variation in gage constant even for gages that lasted for 30 to 40 runs.

The experimental heat transfer rates are plotted as $q_o \cdot \sqrt{\frac{R_o}{P_1}}$ vs. M_s in fig. 33. These results are compared with the heat transfer rates calculated from equation 37 with various $(\rho\mu)$ values. The experimental results fall generally between the values of the heat transfer rates based on the external $(\rho\mu)_e$ and those based on

$(\rho\mu)_{average}$. (Note that at this range of M_s, $(\rho\mu)_{average}$ based on average temperature and average anthalpy are almost identical). At the lower Mach numbers, $(4 < M_s < 6)$, the heat transfer rate tends to be closer to values obtained using $(\rho\mu)_{average}$; but as M_s increases a shift towards the rates predicted by using $(\rho\mu)_e$ is apparent. The scatter of the experimental results is rather small and actually falls within the expected accuracy of about $\pm$ 5 per cent.

The theoretical prediction based on the analysis of Reference 28 agrees very well with the experimental results. The fact that at high Mach numbers the heat rates approach the values based on $(\rho\mu)_e$ may be caused by inaccuracies in our knowledge of the transport properties such as $\overline{Pr}$ and μ. It would be very interesting to observe how this trend developes at higher Mach numbers.

Although the stagnation enthalpy experienced in these tests corresponds to free flight Mach numbers up to 10, the flow Mach number in these tests ranges from about 1.6 to 2.0. Even at these low Mach numbers, however, the pressure distribution on a cylinder obtained in wind tunnel tests follows the modified Newtonian approximation very closely over the first 40^o - 50^o, i.e., $C_p/C_{p_{max}} = \cos^2\theta$. This fact will be discussed in more detail when the heat transfer rate distribution over the cylinder is described. It is sufficient to note now that although only the high enthalpy is exactly simulated, the flow Mach number is still high enough to enable useful data. It will be of interest to repeat these experiments in an expanding nozzle where both the enthalpy and the Mach number may be simulated.

B. Heat Transfer Rate Distribution over the Surface of a Circular Cylinder

1. Theory and Calculations

The calculation of the heat transfer rate on a body with a known pressure distribution and a laminar boundary layer at a very high stagnation enthalpy is also discussed in Reference 28. The existence of a laminar boundary layer over the forward portion of a circular cylinder in the shock tube flow can be justified mainly by the low Reynolds numbers experienced (fig. 22). This a priori assumption can be checked later by comparing the experimental data with the predicted laminar values.

The heat transfer rate distribution is given in equations 12 and 12a of Reference 28, as follows:

$$\frac{q_w}{q_0} = \frac{\frac{1}{\sqrt{2}}\left(\frac{\rho}{\rho'}\right)\left(\frac{u_e}{u_\infty}\right)\left(\frac{\omega_e}{\omega_{e_0}}\right) r_0^{\,k}}{\left[\int_0^s \left(\frac{\rho}{\rho'}\right)\left(\frac{u_e}{u_\infty}\right)\left(\frac{\omega_e}{\omega_{e_0}}\right) r_0^{\,2k}\, ds\right]^{1/2}} \cdot \frac{\sqrt{R_0}\; 2^{-k/2}}{\sqrt{\frac{R_0}{u_\infty}\left(\frac{du_e}{ds}\right)_0}} \qquad (42)$$

where $\dot{q}_0$ is the heat transfer rate at the forward stagnation point, and $\omega = \mu/RT$.

The additional approximations involved in the derivation of this relation are as follows: (1) The effect of the local pressure gradient parameter, β, on the local heat transfer rate is negligible for $\frac{h_{se}}{h_w} >> 1$. (2) The local recovery enthalpy is identical with the stagnation point enthalpy h_{se}. (3) $\frac{\omega_e}{\omega_{e_0}}$ is a constant over the body surface. In Appendix A the effect of each of these approximations is

examined in some detail, and the individual corrections to the heat transfer rate are found to be small. Moreover the effect of the variable $\bar{\beta}$ and ω_e/ω_{e_o} over the cylinder surface tend to increase q by about 2 to 3 per cent, while the effect of the corrected recovery enthalpy is to reduce q by about 5 per cent. Thus these corrections tend to cancel each other, at least for $\frac{h_{se}}{h_w} >> 1$.

The local pressure and velocity are related by the momentum equation. Since the expansion around the body surface is isentropic this relation can be written as:

$$\left(\frac{u_e}{u_\infty}\right)^2 = \frac{2\bar{\gamma}}{\bar{\gamma}-1} \cdot \frac{p_0'}{u_\infty^2 \rho_0'} \left[1 - \left(\frac{p}{p_0'}\right)^{\frac{\bar{\gamma}-1}{\bar{\gamma}}}\right] \tag{43}$$

Therefore, equation 42 can be rewritten as

$$\frac{q_w}{q_0} = \frac{\sqrt{R_0}}{\sqrt{\sigma}} \cdot 2^{-\frac{k+1}{2}} \frac{\left[\frac{2\bar{\gamma}}{\bar{\gamma}-1} \frac{p_0'}{u_\infty^2 \rho_0'}\right]^{1/4} \left\{\left(\frac{p}{p_0'}\right)^2 \left[1 - \left(\frac{p}{p_0'}\right)^{\frac{\bar{\gamma}-1}{\bar{\gamma}}}\right]\right\}^{1/2} r_0^k}{\left[\int_0^s \left\{\left(\frac{p}{p_0'}\right)^2 \left[1 - \left(\frac{p}{p_0'}\right)^{\frac{\bar{\gamma}-1}{\bar{\gamma}}}\right]\right\}^{1/2} r_0^{2k} ds\right]^{1/2}} \tag{44}$$

where

$$\sigma = \left[\frac{R_0}{u_\infty}\left(\frac{du_e}{ds}\right)\right]_0$$

By utilizing this equation one can calculate the local heat transfer rate from the known flow properties and local pressure distribution.

For the case of the circular cylinder k = 0, $ds = R_0\, d\theta$ and the relation for the heat rate distribution is then

$$\frac{q_w}{q_0} = \frac{\left[\frac{2\bar{\gamma}}{\bar{\gamma}-1}\cdot\frac{P_0'}{u_\infty^2\rho_0'}\right]^{1/4}\cdot\left\{\left(\frac{P}{P_0'}\right)^2\left[1-\left(\frac{P}{P_0'}\right)^{\frac{\bar{\gamma}-1}{\bar{\gamma}}}\right]\right\}^{1/2}}{\left[\int_0^\theta\left\{\left(\frac{P}{P_0'}\right)^2\left[1-\left(\frac{P}{P_0'}\right)^{\frac{\bar{\gamma}-1}{\bar{\gamma}}}\right]\right\}^{1/2}d\theta\right]^{1/2}} \qquad (45)$$

The experimentally-measured pressure distribution on a circular cylinder at various Mach numbers in wind tunnel and a shock tube is shown in fig. 34. These measurements are obtained in a wind tunnel (Ref. 31) and in a shock tube (Ref. 32). When these measurements are reduced to the form of $C_p/C_{p_{max}}$, one immediately notes that in this range of Mach numbers, 1.8 to 6.0, $C_p/C_{p_{max}}$ is very well approximated by the $\cos^2\theta$ relation predicted by the modified Newtonian theory, at least for $0 \leq \theta \leq 40^\circ - 50^\circ$. Therefore for this range, one can solve for the heat transfer rate distribution explicitly:

Now,

$$\frac{C_p}{C_{p_{max}}} = \frac{P-P_\infty}{P_0'-P_\infty} = \cos^2\theta \qquad 0^\circ < \theta < 50^\circ \qquad (46)$$

then $$\frac{P}{P_0'} = \cos^2\theta + \frac{P_\infty}{P_0'}\sin^2\theta \quad ; \quad \frac{P_\infty}{P_0'} \cong \frac{1}{\gamma_\infty M_\infty^2}$$

and $$\frac{u_e}{u_\infty} \cong \sin\theta$$

The heat transfer rate distribution is then calculated to be (for θ $0^\circ < \theta < 50^\circ$)

$$\frac{q_w}{q_0} = \frac{\sqrt{2}\left(\cos^2\theta + \frac{1}{\gamma_\infty M_\infty^2}\sin^2\theta\right)\theta}{\left[\theta^2\left(1+\frac{1}{\gamma_\infty M_\infty^2}\right) + \left(1-\frac{1}{\gamma_\infty M_\infty^2}\right)(\theta\sin 2\theta - \sin^2\theta)\right]^{1/2}} \tag{47}$$

The measured heat transfer rates on a cylinder indicated a smooth distribution up to $\theta = 120^\circ$, so that a more exact calculation of predicted heat rate distribution seems to be in order. According to equation 45, the heat transfer rate can be calculated for any arbitrary pressure distribution by the following method:

At a fixed flow Mach number the relation

$$\frac{c_p}{c_{p_{max}}} = \frac{p - p_\infty}{p_0' - p_\infty} = f(\theta)$$

is known (in this case from fig. 34) so that

$$\frac{p}{p_0'} = g(\theta) = f(\theta)\left(1 - \frac{p_\infty}{p_0'}\right) + \frac{p_\infty}{p_0'}$$ and $\frac{p_\infty}{p_0'}$ is a known function of Mach number and γ. Now the function

$$G(\theta) = \left[g^2(\theta)\left\{1 - [g(\theta)]^{\frac{\gamma-1}{\gamma}}\right\}\right]^{1/2} \tag{48}$$

is plotted vs. θ, and the quantity

$$H(\theta) = \frac{G(\theta)}{\left[\int_0^\theta G(\theta)\, d\theta\right]^{1/2}} \tag{49}$$

is evaluated by numerical integration.

From equation 45, q_w/q_o is then given by:

$$\frac{q_w}{q_o} = \frac{\left[\frac{2\bar{\gamma}}{\bar{\gamma}-1}\cdot\frac{P_o'}{u_\infty^2\rho_\infty'}\right]^{1/4}}{\sqrt{2\sigma}}\cdot H(\theta) \qquad (50)$$

This calculation was carried out for the flow conditions in the shock tube at $M_\infty = M_2 = 1.85$ and for $0^\circ < \theta < 120^\circ$. The results of this calculation are shown in fig. 35.

2. Experimental Results

The heat transfer rate distribution on the surface of a circular cylinder is measured by using the same technique and models that are used for the stagnation heat rate measurements described in Part A. 2 of this section. The model (seen in fig. 32) is rotated to position the gage at different angles from the horizontal axis. This procedure was repeated in steps of 10° up to 120°, and then a few tests were run at 150° and 180° measured from the forward stagnation point. The shock speed is measured for each run. Because of the extremely small scatter of the stagnation heat transfer rate data, the stagnation heat transfer rate is very well defined. Consequently the ratio of local to stagnation heat transfer rate can be obtained with about 5 - 6 per cent accuracy, as shown in fig. 39. The shock strength for these tests was kept between M_s of 5.5 to 6.0, so that the average M_2 is about 1.85. Although M_s changes slightly between runs, the effect on the flow Mach number M_2 is very small, and this effect is even smaller on the pressure distribution and hence also on the heat rate distribution.

In fig. 39, this data is compared with the results of the calculations (equation 50) described in the preceding section, and the agreement seems to be rather good.

3. Determination of Local Pressure Distribution from the Measured Heat Transfer Rate Distribution over the Surface of the Model

The pressure measurements in the continuous wind tunnel are probably the most accurate measurements available in wind tunnel experimental technique. Therefore, it is customary to express the calculated quantities in aerodynamical analysis as a function of pressures. This statement is particularly true for the heat transfer analysis, where the local heat transfer rate is expressed in terms of local pressures and pressure gradients.

The measurement of pressures in the shock tube is very difficult. However, the heat transfer rate can be measured to a fairly good accuracy, as is evident from the present data. In many cases one would like to know the local pressure on models in the shock tube flow. The heat transfer rate distribution is related to the local pressure by equation 42 of V.B. If $w_e \cong w_{e_0}$, then

$$\frac{q_w}{q_0} = \frac{\frac{1}{\sqrt{2}}\left(\frac{\rho}{\rho_0}\cdot\frac{u_e}{u_\infty}\right) r_0^{\kappa}}{\left[\int_0^s \left(\frac{\rho}{\rho_0}\frac{u_e}{u_\infty}\right) r_0^{2\kappa}\, ds\right]^{1/2}} \cdot \frac{\sqrt{R_0}}{2^{\kappa/2}\sqrt{\frac{R_0}{u_\infty}\left(\frac{du_e}{ds}\right)_0}} \qquad (51)$$

Let $Q = q_w/q_o$ and $P = (p/p_o')\,(u_e/u_\infty)$, now by squaring and differentiating with respect to s, equation 51 becomes

$$r_o^{\,k}\left[\frac{1}{Q}\frac{dP}{ds} - \frac{P}{Q^2}\frac{dQ}{ds} + \frac{k\,P}{Q\,r_o}\frac{dr_o}{ds} - \frac{2^k\sigma\,Q}{R_o}\right] = 0$$

or

$$\frac{d}{ds}\left[\frac{P}{Q}\,r_o^{\,k}\right] = \frac{(2r_o)^k\,\sigma\,Q}{R_o}$$

By integrating this last equation one obtains

$$P = \frac{\sigma\,Q}{r_o^{\,k}R_o}\int_0^s (2r_o)^k\,Q\,ds \tag{52}$$

This equation can be solved for some special cases

(1) Circular Cylinder

Here $k = 0$, $ds = R_o\,d\theta$, and equation 52 becomes

$$P = \sigma\,Q\int_0^\theta Q\,d\theta \tag{53}$$

(2) Sphere

$k = 1$, $ds = R_o\,d\theta$, $r_o = R_o \sin\theta$, and the relation becomes

$$P = 2\sigma\,\frac{Q}{\sin\theta}\int_0^\theta Q\sin\theta\,d\theta \tag{54}$$

and P can be expressed in terms of p/p_o' by the relation

$$P = \left\{ \frac{2\bar{\gamma}}{\bar{\gamma}-1} \cdot \frac{p_0'}{u_\infty^2 \rho_0'} \cdot \left(\frac{p}{p_0'}\right)^{\frac{2}{\bar{\gamma}}} \left[1 - \left(\frac{p}{p_0'}\right)^{\frac{\bar{\gamma}-1}{\bar{\gamma}}} \right] \right\}^{1/2} \qquad (55)$$

The heat transfer distribution over the circular cylinder is measured as shown in fig. 39. So, combining equations 53 and 55 one can compute the local pressure on the cylinder. This result is shown in fig. 40 where $C_p/C_{p_{max}} = \dfrac{p/p_0' - p_\infty/p_0'}{1 - p_\infty/p_0'}$ is compared with the pressure distribution measured in the wind tunnel tests at the same flow Mach number (Ref. 31). The agreement of these results is remarkable and adds to our confidence in the experimental results and in the theoretical analysis of Reference 28.

4. Schlieren Study of Flow History on a Circular Cylinder

The application of data obtained in the quasi-steady shock tube flow to problems of steady flow depends on the possibility of establishing equilibrium conditions in the flow around the model. Therefore a study of the process of formation of the pattern on a circular cylinder was made. Schlieren pictures taken at various times after the shock wave passage were obtained (fig. 41). From a series of such photographs one can observe an equilibrium shock position which is reached in about 50 μ sec. Figure 42 shows a typical flow pattern on a 1/4" circular cylinder in the shock tube. This time delay for the establishment of the equilibrium flow checks with the observed behavior of the stagnation point heat transfer rate, which starts almost with a jump, and takes up the parabolic rise only after about 25 - 30 μ sec.

The equilibrium detachment distance is plotted as a function of the flow Mach number in fig. 43, and compared with wind tunnel data (Ref. 33). In the shock tube flow the shock wave is closer to the body, and this result is expected because of real gas effects, i.e., the increase in density ratio across the shock wave compared with wind tunnel conditions.

VI. SUMMARY AND CONCLUSIONS

This report presents a systematic investigation of various applications of the shock tube to aerodynamic research. Because of the extremely short duration of uniform flow the experimental technique presents a major obstacle. Therefore the thin platinum film resistance thermometer was developed as an instrument for measurement of local heat transfer rate. By utilizing this heat transfer gage and a schlieren optical system the shock tube flow can be accurately calibrated, thus providing a known environment for experimental studies.

The thin platinum film gage, properly calibrated, provides an accurate measurement of heat transfer rate distribution on the surface of the model. This technique was evaluated on a body of simple geometry, where a theoretical analysis is also available -- i.e. a circular cylinder. The theory also makes possible the inverse process, namely, the evaluation of the surface pressure distribution from the experimental heat transfer data. This technique for heat transfer measurements can be extended to models of other geometries and to heat transfer studies in various interesting flow fields such as wakes, nozzles, etc.

The direct pressure measurements in the shock tube present a very difficult problem. Inherently the shock tube flow is transient for any mechanical system, exciting resonance vibrations and demanding extreme response time. Further work on the development of pressure gages and other techniques for transient measurements is required.

However even with the present available instrumentation techniques the shock tube can be very useful for the following applications:

1. Heat transfer and aerodynamic studies at high stagnation temperatures.
2. Low Reynolds number investigations.
3. Physical-Chemical investigations at high temperatures.
4. Magneto-hydrodynamic investigations.

The extremely short duration of the shock tube flow, although presenting a very difficult experimental problem, enables one to obtain very high temperatures and velocities contained within ordinary laboratory structures.

REFERENCES

1. Geiger, F. W. and Mautz, C. W.: The Shock Tube as an Instrument for Investigation of Transonic and Supersonic Flow Patterns. University of Michigan, Engineering Research Institute, Project M 720-4, June, 1949.

2. Bitondo, D. and Lobb, R. K.: Design and Construction of a Shock Tube. Institute of Aerophysics, University of Toronto, UTIA Report No. 3, December, 1950.

3. Lobb, R. K.: On the Length of a Shock Tube. Institute of Aerophysics, University of Toronto, UTIA Report No. 4, July, 1950.

4. Glass, I. I.; Martin, W.; and Patterson, G. N.: A Theoretical and Experimental Study of the Shock Tube. Institute of Aerophysics, University of Toronto, UTIA Report No. 2, November, 1953.

5. Yoler, Y.: Hypersonic Shock Tube. GALCIT Hypersonic Wind Tunnel, Memorandum No. 18, July 19, 1954.

6. Glick, H. S.; Hertzberg, A.; and Smith, W. E.: Flow Phenomena in Starting a Hypersonic Shock Tunnel. AEDC-TN-5516, March, 1955.

7. Hertzberg, A.; Smith, W. E.; Glick, H. S.; and Squire, W.: Modification of the Shock Tube for Generation of Hypersonic Flow. AEDC-TN-5515, March, 1955.

8. Blackman, V. H.: Vibration Relaxation in Oxygen and Nitrogen. Princeton University, Department of Physics, Report NA-061-020, May, 1955. Also, Journal of Fluid Mechanics, Vol. 1, Part 1, pp. 61-85, May, 1956.

9. Chabai, A. J. and Emrich, R. J.: Measurement of Wall Temperature and Heat Flow in Shock Tube. Journal of Applied Physics, Vol. 26, No. 6, pp. 779-780, June, 1955.

10. Rabinowicz, J.; Jessey, M. E.; and Bartsch, C. A.: Resistance Thermometer for Transient High Temperature Studies. Journal of Applied Physics, Vol. 27, No. 1, pp. 97-98, January, 1956.

11. Rabinowicz, J.; Jessey, M. E.; and Bartsch, C. A.: Resistance Thermometer for Heat Transfer Measurement in a Shock Tube. GALCIT Hypersonic Research Project, Memorandum No. 33, July 2, 1956.

12. Hertzberg, A.: The Application of the Shock Tube to the Study of the Problems of Hypersonic Flight. Jet Propulsion, pp. 549-554, July, 1956.

13. Bershader, D. and Allport, T.: On the Laminar Boundary Layer Induced by a Traveling Shock Wave. Princeton University, Department of Physics, NR-061-020, May, 1956.

14. Billington, I. J.: The Hot Wire Anemometer and Its Use in Non-Steady Flow. Institute of Aerophysics, University of Toronto, UTIA Technical Note No. 5, September, 1955.

15. Dosanjh, D. S.; Kovasznay, L. S. G.; and Glarken, P. C.: Study of Transient Hot Wire Response in a Shock Tube. The Johns Hopkins University, Department of Aeronautics, Report No. CM 725, March, 1952.

16. Dosanjh, D. S.: Use of a Hot Wire Anemometer in Shock Tube Investigations. NACA TN 3163, December, 1954.

17. Bendersky, D.: A Special Thermocouple for Measuring Transient Temperatures. Mechanical Engineering, Vol. 75, pp. 117-121, February, 1953.

18. Strong, J.: Procedures in Experimental Physics. Prentice Hall, Inc., 1946.

19. Carslaw, H. S. and Jaeger, J. C.: Conduction of Heat in Solids. Oxford, Clarendon Press, 1947.

20. Emrich, R. J. and Petterson, R. L.: Pressure Variation with Time in the Shock Tube. Lehigh University, Technical Report No. 7, March 15, 1956.

21. Yoler, Y. A. and Nagamatsu, H. T.: A Study of Piezoelectric Elements for the Measurement of Transient Forces. GALCIT Hypersonic Wind Tunnel, Memorandum No. 23, February 1, 1955.

22. Vidal, R.: Model Instrumentation for Heat Transfer and Force Measurement in a Hypersonic Shock Tunnel. C.A.L. Report AD-917-A-1, February, 1955.

23. a. Logan, J. G., Jr.: The Calculation of the Thermodynamic Properties of Air at High Temperatures. AF OSR-TN-56-344, AD-95220, May, 1956.
    b. Treano, C. E. and Logan, J. G., Jr.: Tables of Thermodynamic Properties of Air from 3000°K to 10,000°K. AF OSR-TN-56-343, AD-95219, June, 1956.
    c. Logan, J. G., Jr.: Thermodynamic Charts for High Temperature Air Calculations. AF OSR-TN-56-342, AD-95218, July, 1956.

24. Gilmore, F. R.: Equilibrium Composition and Thermodynamic Properties of Air to 24,000°K. RAND Report RM-1543, August, 1955.

25. Hilsenrath, J. and Beckett, C. W.: Thermodynamic Properties of Argon Free Air. National Bureau of Standards, Report No. 3991, April, 1955.

26. Hirschfelder, J. O.; Curtiss, C. F.; Bird, R. B.; and Spotz, E. L.: Transport Properties of Gases and Gas Mixture. Thermodynamic and Physics of Matter. Princeton Series on High Speed Aerodynamics, Vol. I, Sec. D, pp. 339-418, Princeton University Press, 195 .

27. Mirels, H.: Boundary Layer Behind Shock or Thin Expansion Wave Moving into Stationary Fluid. NACA TN 3712, May, 1956.

28. Lees, L.: Laminar Heat Transfer over Blunt Nosed Bodies at Hypersonic Flight Speeds. Jet Propulsion, Vol. 26, pp. 259-269, April, 1956.

29. Korobkin, I.: Laminar Heat Transfer Characteristics of a Hemisphere for the Mach Number Range 1.9 to 4.9. NAVORD Report 3841, October, 1954.

30. Rose, P. H., and Riddell, F. R.: An Investigation of Stagnation Point Heat Transfer in Dissociated Air. To be presented at the 1957 Heat Transfer and Fluid Mechanics Institute, June 19-21, 1957, at the California Institute of Technology.

31. Howarth, L. (editor): Modern Development in Fluid Dynamics High-Speed Flow. Vol. II, Fig. 220, p. 685, Oxford, The Clarendon Press, 1953.

32. Kim, C. S.: Supersonic Flow Past Circular Cylinder. Journal of the Physical Society of Japan, pp. 439-445, April, 1956.

33. Alperin, M.: Experimental Information on Two-Dimensional Detached Shock Waves. JPL Progress Report No. 4-44, 1950.

34. Cohen, C. B. and Reshotko, E.: Similar Solutions for the Compressible Laminar Boundary Layers with Heat Transfer and Pressure Gradient. NACA TN 3325, April, 1956.

35. Kopal, Z.: Tables of Supersonic Flow around Cones. Massachusetts Institute of Technology, Technical Report No. 1, 1947.

36. Mirels, H.: Attenuation in a Shock Tube due to Unsteady Boundary Layer Action. NACA TN 3278, August, 1956.

37. Trimpi, R. and Cohen, N.: A Theory for Predicting the Flow of Real Gases in Shock Tubes with Experimental Verification. NACA TN 3375, March, 1955.

38. Boyer, D. W.: Effect of Kinematic Viscosity and Wave Speed on Shock Wave Attenuation. University of Toronto, Institute of Aerophysics, Technical Note No. 8, May, 1956.

APPENDIX A

EFFECT OF CERTAIN APPROXIMATIONS ON THE CALCULATED LOCAL HEAT TRANSFER RATE

In deriving equation 42 (Part V.B.1) for the heat transfer rate distribution over an arbitrary body, the following approximations are introduced: (1) The effect of the local pressure gradient on the heat transfer rate is negligible for $h_{se}/h_w >> 1$; (2) the local recovery enthalpy is given by the stagnation enthalpy; (3) the quantity $\omega_e = \mu/\rho T$ is a constant over the body surface equal to ω_{e_o}. Each of these approximations is now examined to determine the overall error involved in the predicted local heat transfer rate.

1. Effect of Local Pressure Gradient on Heat Transfer Rate

As an example of the effect of the local pressure gradient on local heat transfer, we may refer to the calculation of Cohen and Reshotko (Ref. 34) for the "similar solutions" with constant specific heats, $Pr = 1$, and $\rho\mu = \text{const}$. The heat transfer rate function $\frac{g'_w}{1-g_w} = -\frac{S'_w}{S_w}$ is calculated in Reference 34 as a function of $\bar{\beta}$ for various initial enthalpy ratios $g(o) \equiv g_w = \frac{h_w}{h_{se}}$. Here $\bar{\beta}$ is a pressure gradient parameter given by $\bar{\beta} = \frac{2\tilde{s}}{M_e}\frac{dM_e}{d\tilde{s}}$, where $\tilde{s}$ is a distorted distance along the surface defined by the relation

$$\tilde{s} = \int_0^s \rho_e \mu_e u_e r_o^{2k} ds$$

(Refs. 28 and 34.) At the forward stagnation point of a circular cylinder $\bar{\beta} = 1$ and $\frac{g'_w}{1-g_w} \cong 0.50$ for $h_w/h_{se} << 1$. Now $\bar{\beta}$ varies over the cylinder, but the function $\frac{g'_w}{1-g_w}$ is not very sensitive to the value of $\bar{\beta}$ when $g_w << 1$; therefore the variation in this

function can be estimated by using the local similarity approximation.

By the definition of $\bar{\beta}$ and $\tilde{s}$ for a two-dimensional body ($k = 0$)

$$\bar{\beta} = \frac{2 \int_0^s \rho_e \mu_e u_e \, ds}{M_e \rho_e \mu_e u_e} \frac{dM_e}{ds} \qquad \text{A-1}$$

But $\frac{P_0'}{P} = \left(1 - \frac{\bar{\gamma}-1}{\bar{\gamma}} M_e^2 \right)^{\bar{\gamma}/\bar{\gamma}-1}$, and $\rho = \frac{P}{RT}$, so that

$$\bar{\beta}(\theta) = \frac{\frac{\bar{\gamma}-1}{\bar{\gamma}} \int_0^\theta \left(\frac{P}{P_0'}\right)\left(\frac{u_e}{u_\infty}\right)\left(\frac{w_e}{w_{e_0}}\right) ds}{\left(\frac{P}{P_0'}\right)^2 \left(\frac{u_e}{u_\infty}\right)\left(\frac{w_e}{w_{e_0}}\right)} \cdot \frac{1}{\left[1 - \left(\frac{P}{P_0'}\right)^{\frac{\bar{\gamma}-1}{\bar{\gamma}}}\right]} \cdot \left[- \frac{d\left(\frac{P}{P_0'}\right)}{ds} \right] \qquad \text{A-2}$$

By substituting the value of $\frac{u_e}{u_\infty}$ in terms of P/P_0' from equation 43 of Section V.B. into equation 2 above, noting that $ds = R_0 \, d\theta$ for the circular cylinder, and taking $\frac{w_e}{w_{e_0}} \cong 1$, one obtains finally

$$\beta(\theta) = \frac{\frac{\bar{\gamma}-1}{\bar{\gamma}} \int_0^\theta \left\{ \left(\frac{P}{P_0'}\right)^2 \left[1 - \left(\frac{P}{P_0'}\right)^{\frac{\bar{\gamma}-1}{\bar{\gamma}}} \right] \right\}^{\frac{1}{2}} d\theta}{\left(\frac{P}{P_0'}\right)^2 \left[1 - \left(\frac{P}{P_0'}\right)^{\frac{\bar{\gamma}-1}{\bar{\gamma}}} \right]^{3/2}} \left[- \frac{d\left(\frac{P}{P_0'}\right)}{d\theta} \right] \qquad \text{A-3}$$

Now, given the experimental pressure distribution $\frac{P}{P_0'}(\theta)$ at the required Mach number, $\bar{\beta}$ can be evaluated. The result of

such a calculation for the shock tube flow at $M_2 = 1.85$ is shown in fig. 36. This calculation shows that for the values of θ between 0 and 90°, $\bar{\beta}$ varies between 1 to 1.5, so that $\frac{g'_w}{1-g_w}$ actually increases only by 2 to 3 per cent. For θ from 90 to 120° the value of $\bar{\beta}$ drops sharply almost to zero because of the flattening of the curve of p/p'_o vs. θ, but even at $\theta = 120°$ where $\bar{\beta} = .1$ the parameter $\frac{g'_w}{1-g_w}$ is decreased by only 10 per cent as compared to the value at $\bar{\beta} = 1$ ($\theta = 0°$) (fig. 37).

2. Effect of the Recovery Factor

For simplicity the local recovery factor was assumed to be 1, so that the recovery enthalpy along the surface is constant and equal to the stagnation enthalpy. Actually the recovery factor for a laminar boundary layer is about .85, and the recovery enthalpy is slightly lower than the stagnation enthalpy. We shall proceed to show that this effect is also very small.

The recovery enthalpy h_r is defined in the following expression:

$$h_r = h_{se}\left[1 - (1-r)\frac{u_e^2}{2h_{se}}\right] \qquad \text{A-4}$$

where r is the recovery factor and has the value of about .85 for laminar boundary layer. This relation can be expressed in terms of the local pressure as

$$\frac{h_r}{h_{se}} = 1 - 0.15\,\frac{2\bar{\gamma}}{\bar{\gamma}-1}\cdot\frac{p'_o}{u_\infty^2 \rho'_o}\cdot\left[1 - \left(\frac{p}{p'_o}\right)^{\frac{\bar{\gamma}-1}{\bar{\gamma}}}\right]\frac{u_\infty^2}{2h_{se}} \qquad \text{A-5}$$

The calculated values of h_r/h_{se} are shown in fig. 37 for the circular cylinder. This calculation shows that h_r/h_{se} decreases by about 5 per cent at most over the body.

3. Variation of ω_e/ω_{e_o}

The function

$$\frac{\omega_e}{\omega_{e_o}} = \frac{\mu_e}{\mu_{e_o}} \cdot \frac{(RT)_{e_o}}{(RT)_e} = \frac{\mu_e}{\mu_{e_o}} \cdot \frac{m_e}{m_{e_o}} \cdot \frac{T_{e_o}}{T_e}$$

depends mainly on the local enthalpy and is virtually independent of pressure. In fig. 38a, b this function $\frac{\omega_e}{\omega_{e_o}}$ plotted against h/h_{298} where ω_{e_o} is evaluated at 0°C and $h_{298} = 71.3 \frac{cal}{gr.}$ for air at 298°K. For small enthalpy differences the value of the change in is rather small. At large enthalpies $\frac{h}{h_{298}} > 50$, $\frac{\omega}{\omega_o}$ becomes less sensitive to the value of the enthalpy so that the assumption that the variation in $\frac{\omega_e}{\omega_{e_o}}$ over the body surface is small is a good approximation. For the case of the cylinder, the local enthalpy, h_e, is

$$\frac{h_e}{h_{se}} = 1 - \frac{u_\infty^2}{2h_{se}} \cdot \frac{2\bar{\gamma}}{\bar{\gamma}-1} \frac{p_o'}{u_\infty^2 \rho_o'} \cdot \left[1 - \left(\frac{p}{p_o'}\right)^{\frac{\bar{\gamma}-1}{\bar{\gamma}}}\right] \qquad \text{A-6}$$

Now, the value of ω_{e_o} is obtained from fig. 38 at $\frac{h_{se}}{h_{298}}$, and ω_e is evaluated at $\frac{h_e}{h_{298}}$. The value of $\frac{\omega_e}{\omega_{e_o}}$ is about 1.15 at $\theta = 120°$. However $\frac{\omega_e}{\omega_{e_o}}$ appears both in the numerator and the denominator of the heat transfer rate expression, (equation 1, Part V.B.1), so that the effect of this change will be even smaller than the 15 per cent indicated.

Now, let us summarize the results of these estimations of the corrections to the heat transfer rate calculations. It is evident that

these corrections are indeed small. This fact justifies the a priori assumption in the analysis. Another important fact is that these small corrections of opposite sign tend to cancel each other almost everywhere on the body and the agreement of the calculated results with the experimental values can be expected to be good.

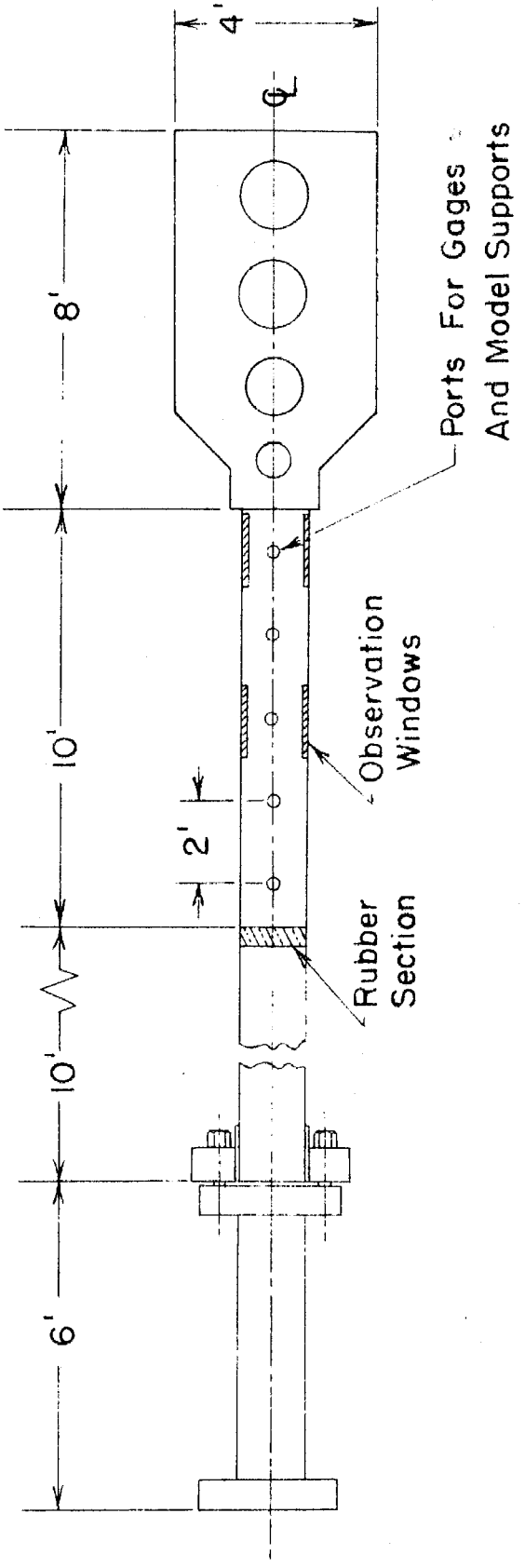

FIG. 1 – $2\frac{7}{8}$" x $2\frac{7}{8}$" GALCIT SHOCK TUBE

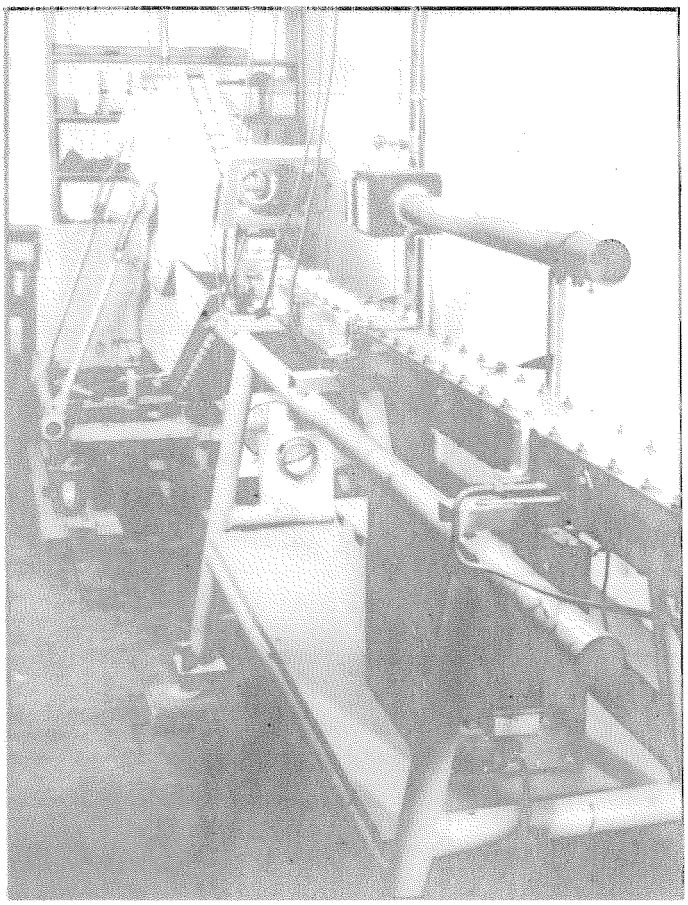

FIG. 2

VIEW OF THE 2-7/8" x 2-7/8" GALCIT SHOCK TUBE

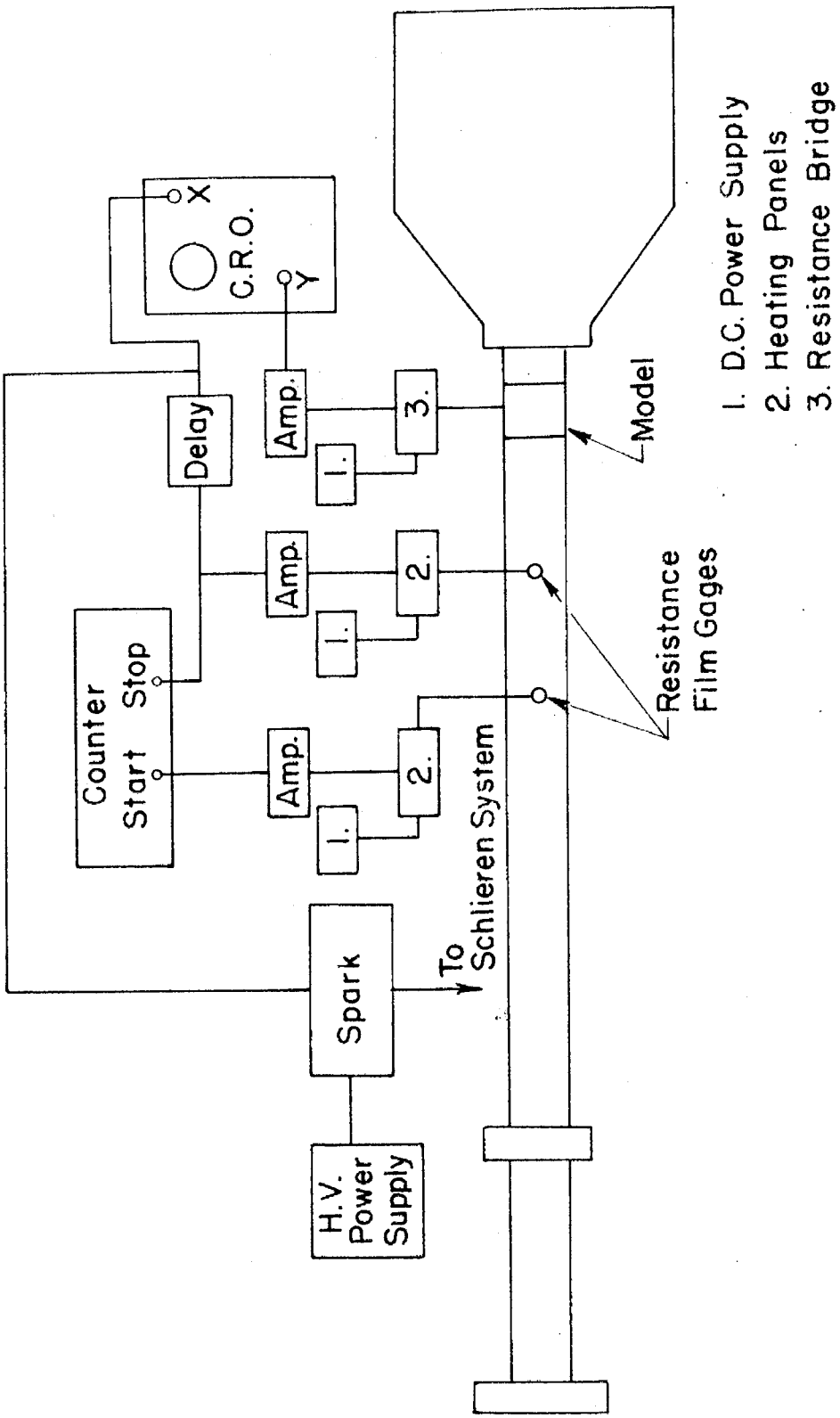

FIG. 3 – INSTRUMENTATION BLOCK DIAGRAM

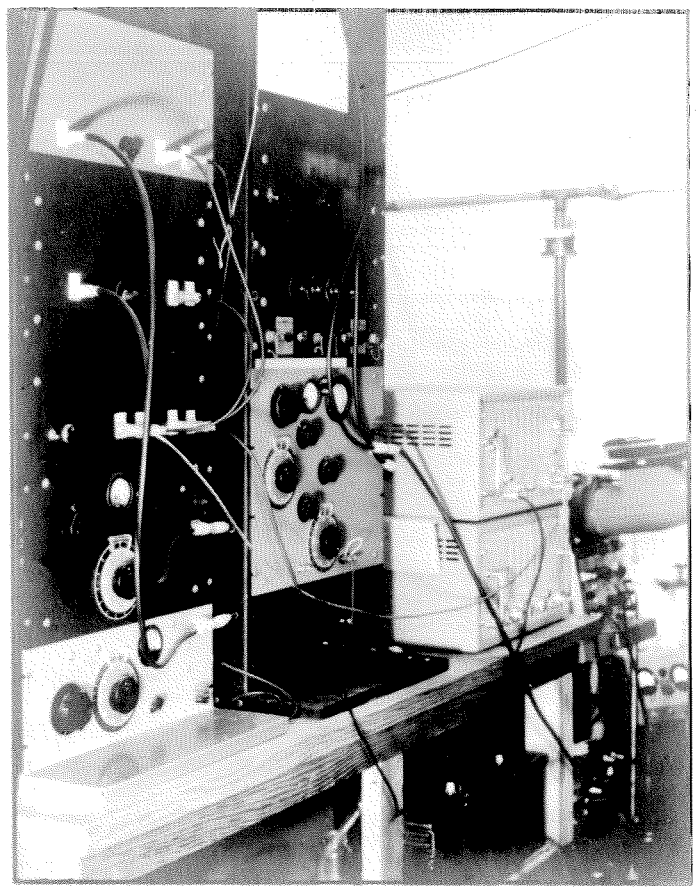

FIG. 4

VIEW OF THE ELECTRONIC APPARATUS

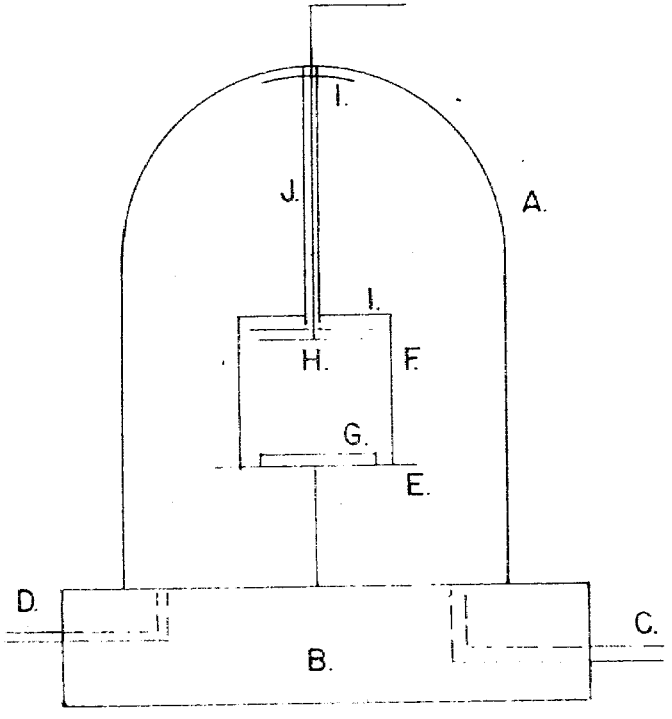

A. BELL JAR
B. STEEL BASE
C. VACUUM LINE, TO PUMP
D. CONTROLLED AIR LEAK
E. ALUMINUM BASE
F. GLASS TUBE
G. GAGE TO BE SPUTTERED
H. PLATINUM CATHODE
I. MICA INSULATION
J. PYREX TUBE

APPARATUS FOR SPUTTERING TRANSIENT TEMPERATURE GAGES

FIG. 5

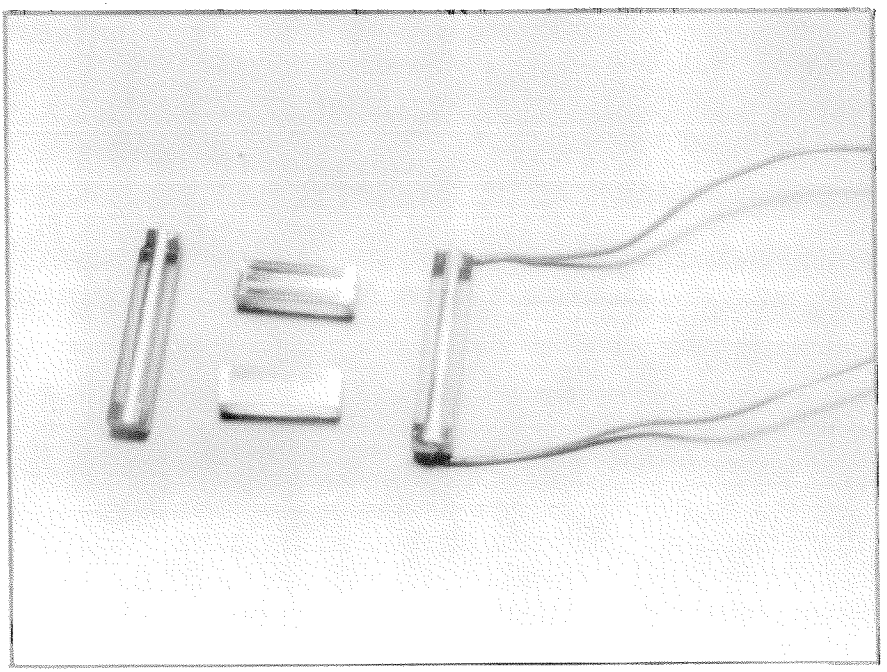

FIG. 6

RESISTANCE THERMOMETER GAGES

AT VARIOUS STAGES OF PREPARATION

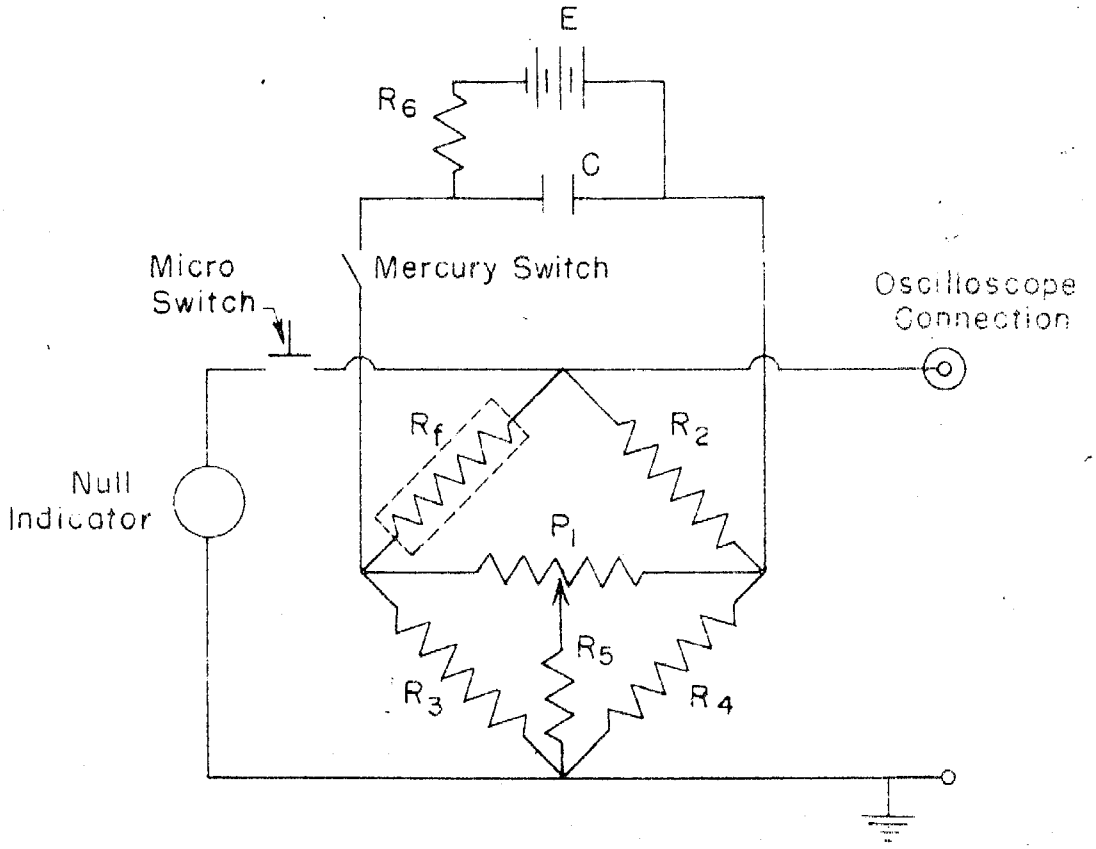

R_f = Calibrated Film

$R_2 = R_3 = R_4 = 57$ Ohm

$R_5 = 270$ Ohm

$R_6 = 1000$ Ohm

$P_1 = 1000$ Ohm Pot.

$C = 600\ \mu F$

FIG. 7 — CALIBRATION CIRCUIT

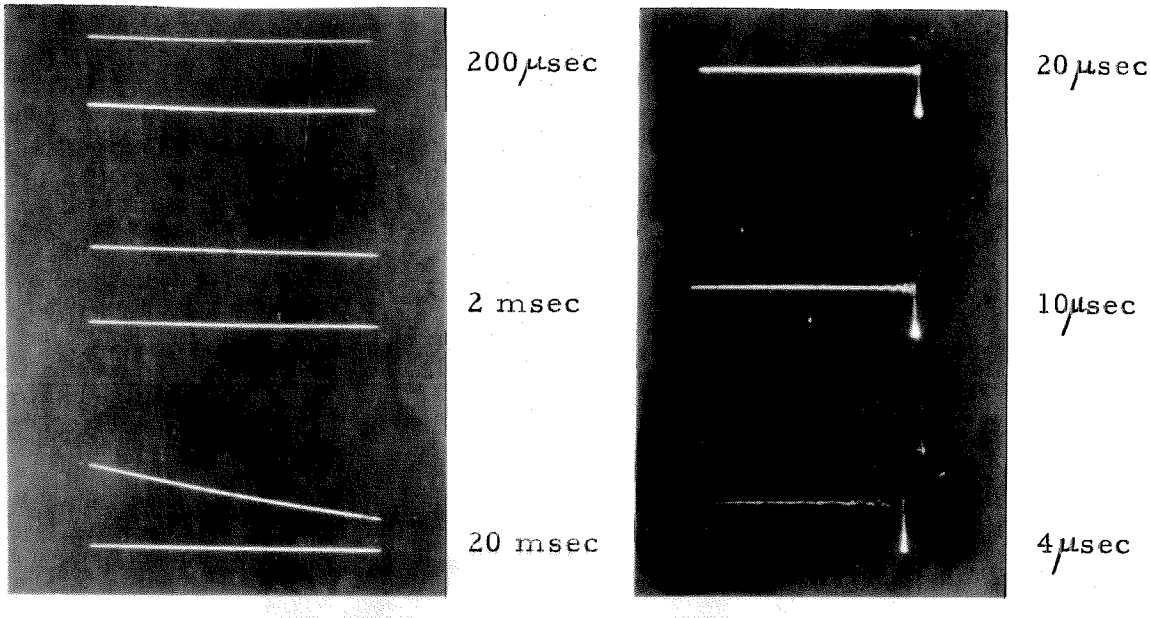

(a) Stable Resistance

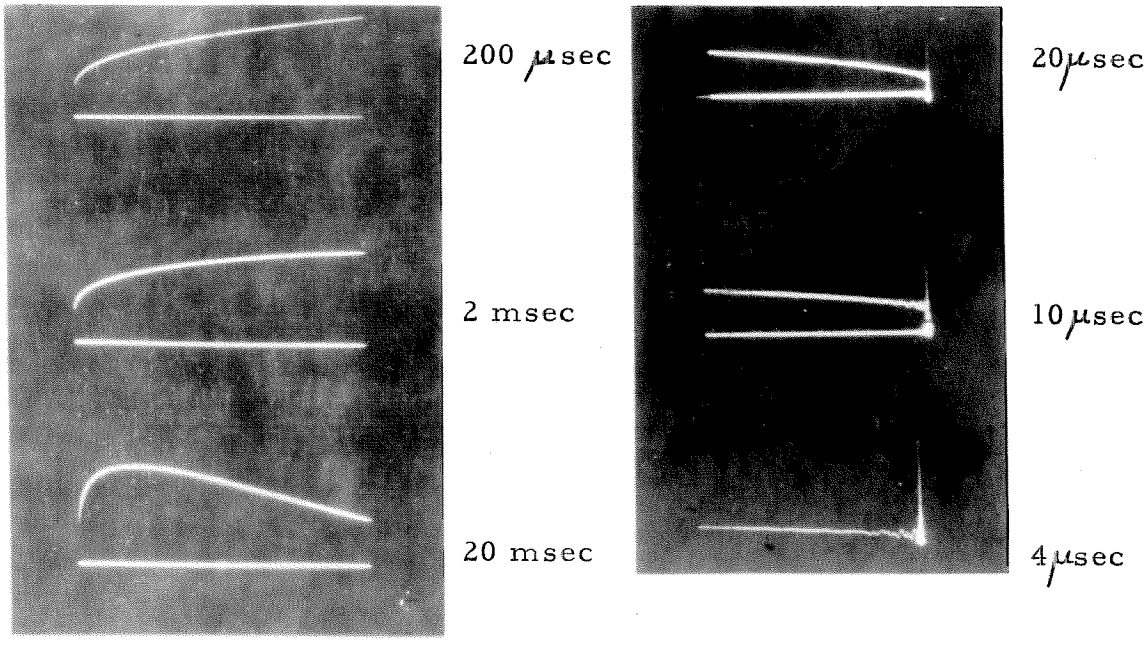

(b) Resistance Gage

FIG. 8

CHARACTERISTICS OF CALIBRATION CIRCUIT

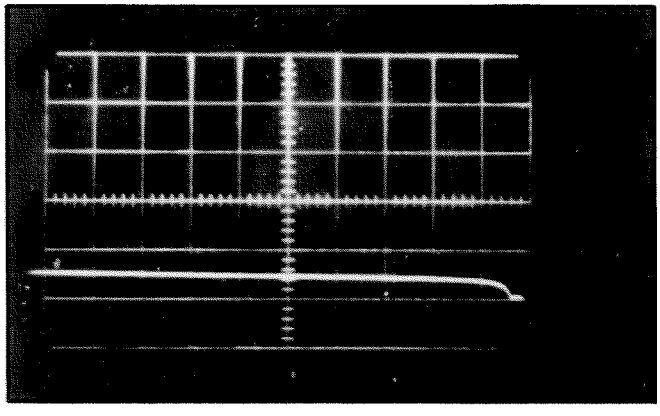

FIG. 9

RESPONSE OF GAGE AT "STAGNATION LINE" OF A CYLINDER

$M_s = 6.44$; $p_1 = 2.4$ mm Hg;

Sweep = 1 μ sec./div.; Sensitivity = .05 V/div.

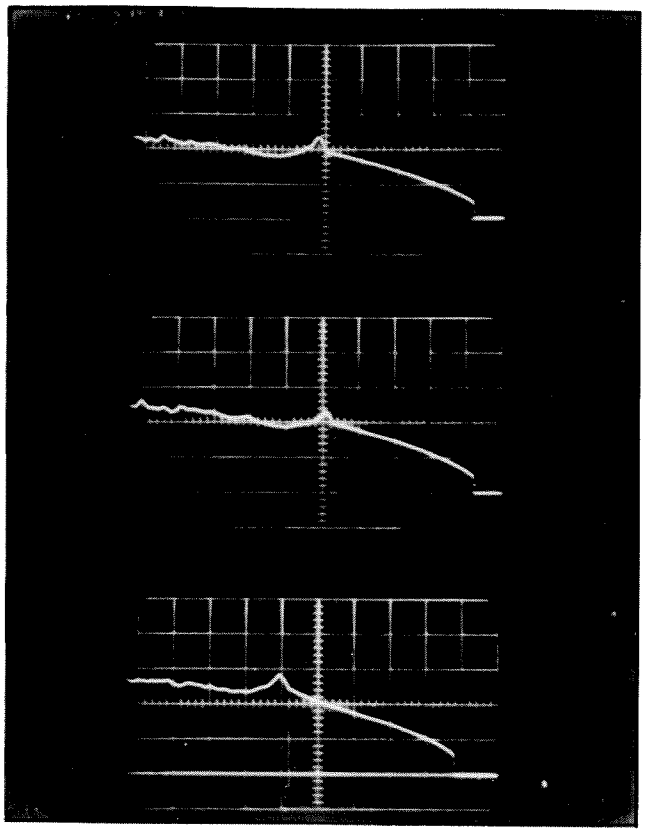

FIG. 10

GAGE RESPONSE AT THE STAGNATION POINT OF A CYLINDER

Sweep = 50 μ sec./div.; Sensitivity = .05 V/div.

Top:	M_s = 7.10	P_1 = 2.5 mm Hg	R_o = 48.9 Ω	I_o = 20 ma
Center:	M_s = 7.03	P_1 = 2.6 mm Hg	R_o = 51.5 Ω	I_o = 20 ma
Bottom:	M_s = 6.53	P_1 = 5.7 mm Hg	R_o = 52.3 Ω	I_o = 20 ma

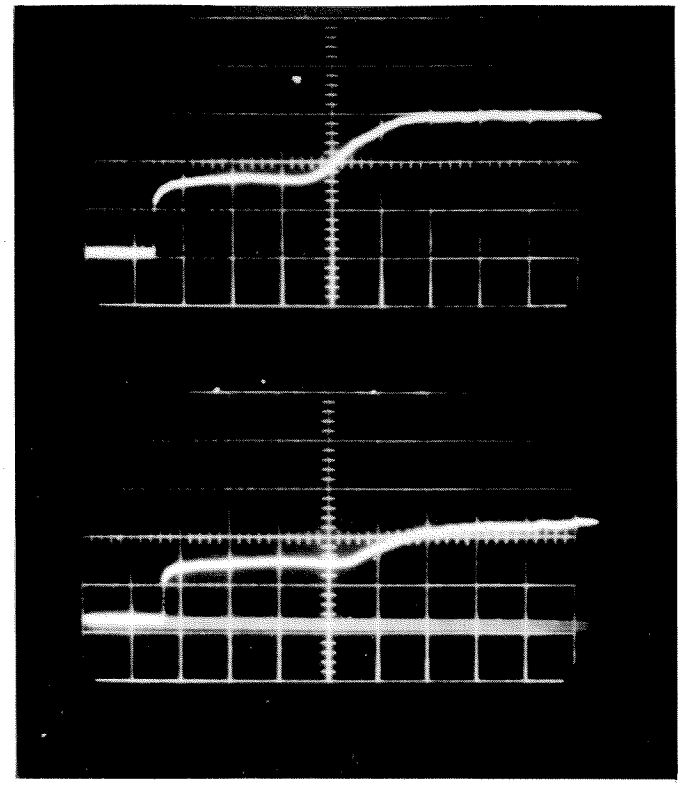

FIG. 11

GAGE RESPONSE ON THE SHOCK TUBE WALL

Sweep = 50μ sec./div.; Sensitivity = .005 V/div.

Top: M_s = 6.41 P_1 = 5.4 mm Hg I_o = 15 ma R_o = 45.3Ω

Bottom: M_s = 6.08 P_1 = 4.6 mm Hg I_o = 15 ma R_o = 45.3Ω

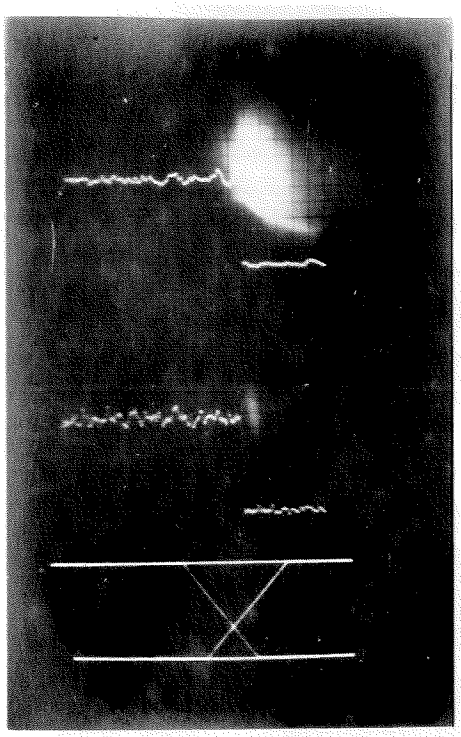

1. $M_s = 1.13$; p_1 = atm.
2. $M_s = 1.16$; p_1 = atm.

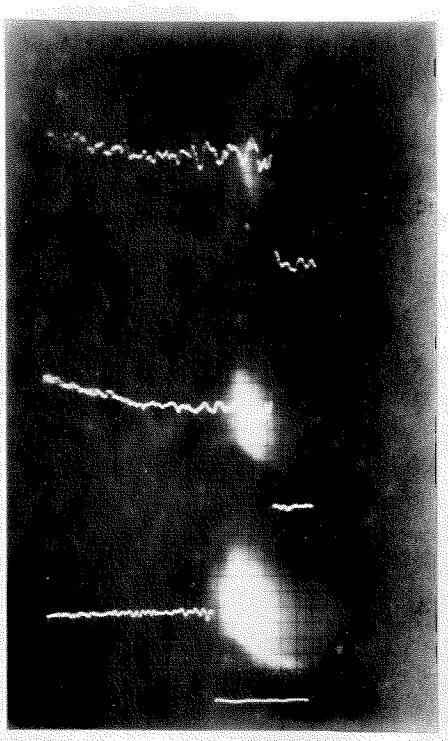

1. $M_s = 2.25$; $p_1 = 7.5$ mm Hg
2. $M_s = 2.35$; $p_1 = 6.8$ mm Hg
3. $M_s = 1.185$; p_1 = atm.

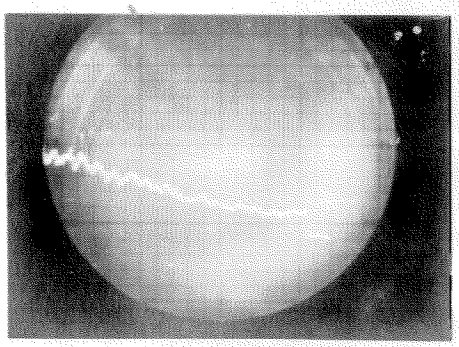

$M_s = 2.83$; $p_1 = 10$ mm

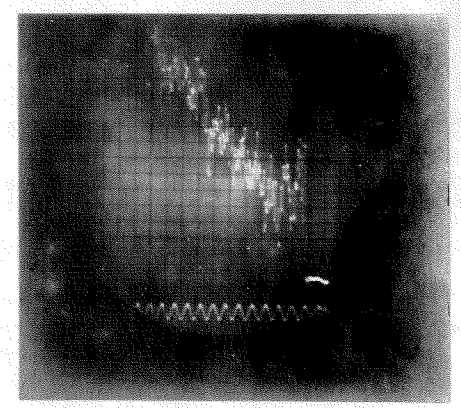

$M_s = 6.0$; $p_1 = 3$ mm Hg

FIG. 12

PIEZOELECTRIC PRESSURE GAGE RESPONSE

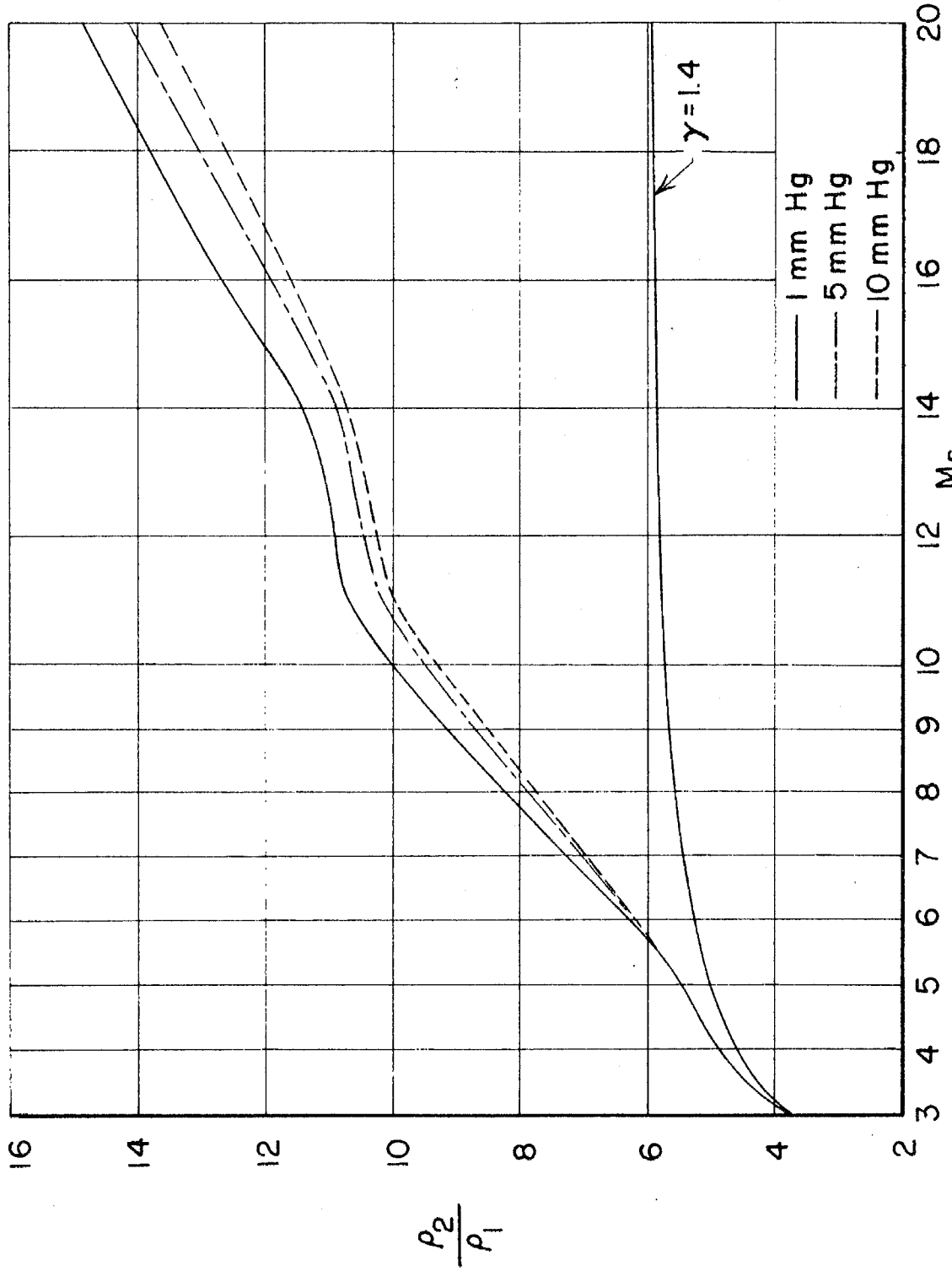

FIG. 13 – DENSITY RATIO ACROSS A NORMAL SHOCK WAVE IN AIR, $T_1 = 298°K$

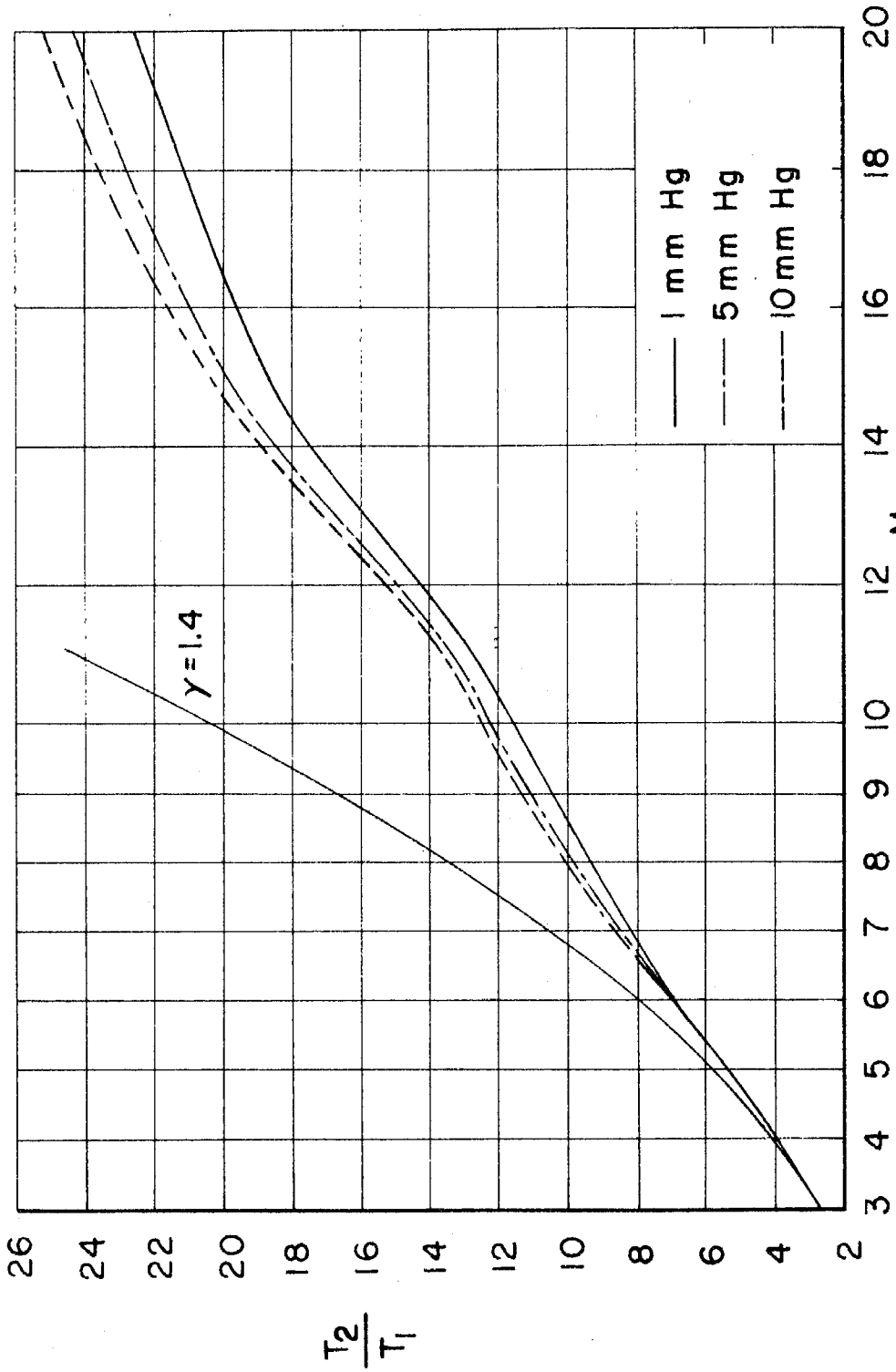

FIG. 14-TEMPERATURE RATIO ACROSS A NORMAL SHOCK IN AIR, $T_1 = 298°$ K

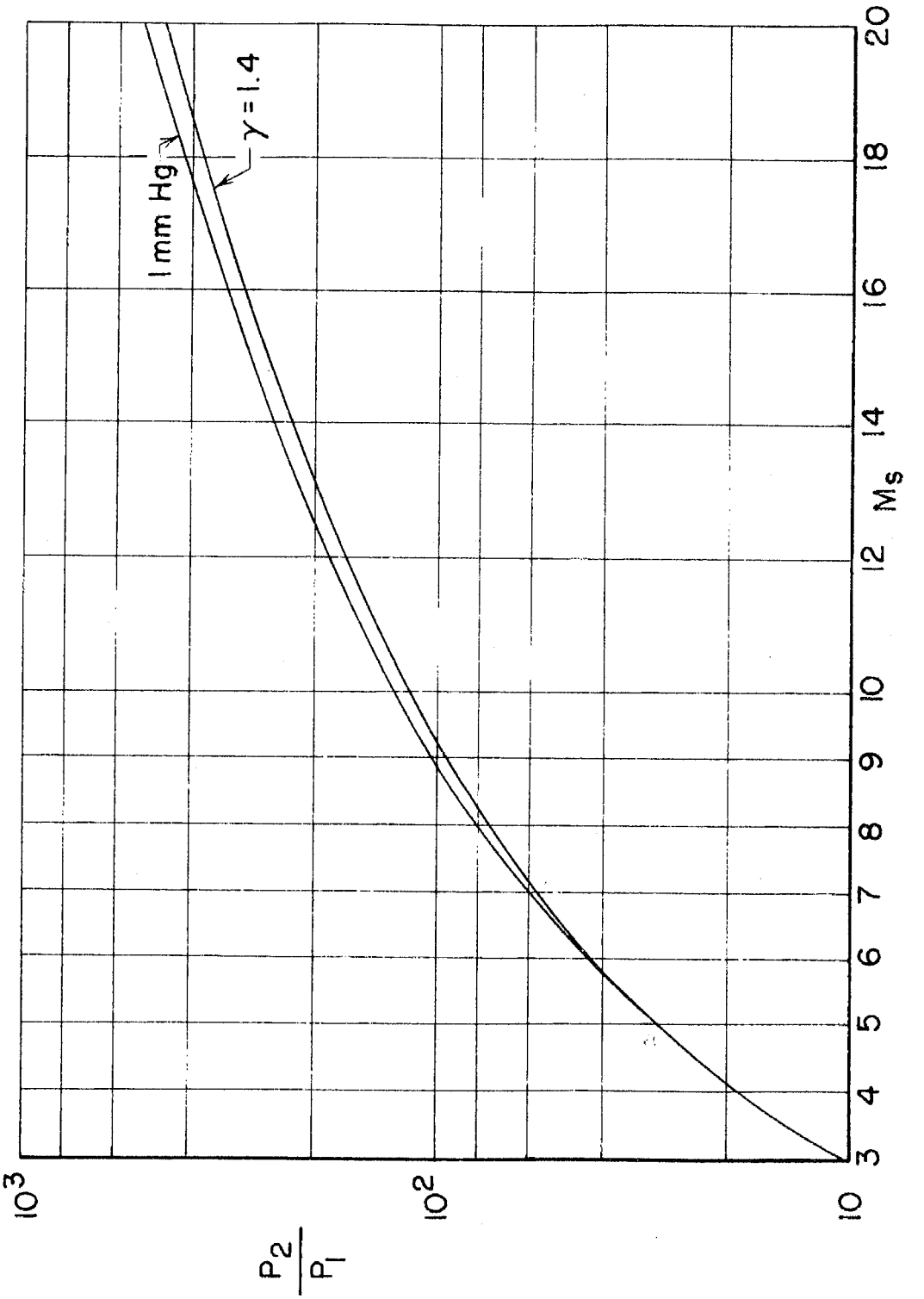

FIG. 15-PRESSURE RATIO ACROSS A NORMAL SHOCK WAVE IN AIR, $T_1 = 298°$ K

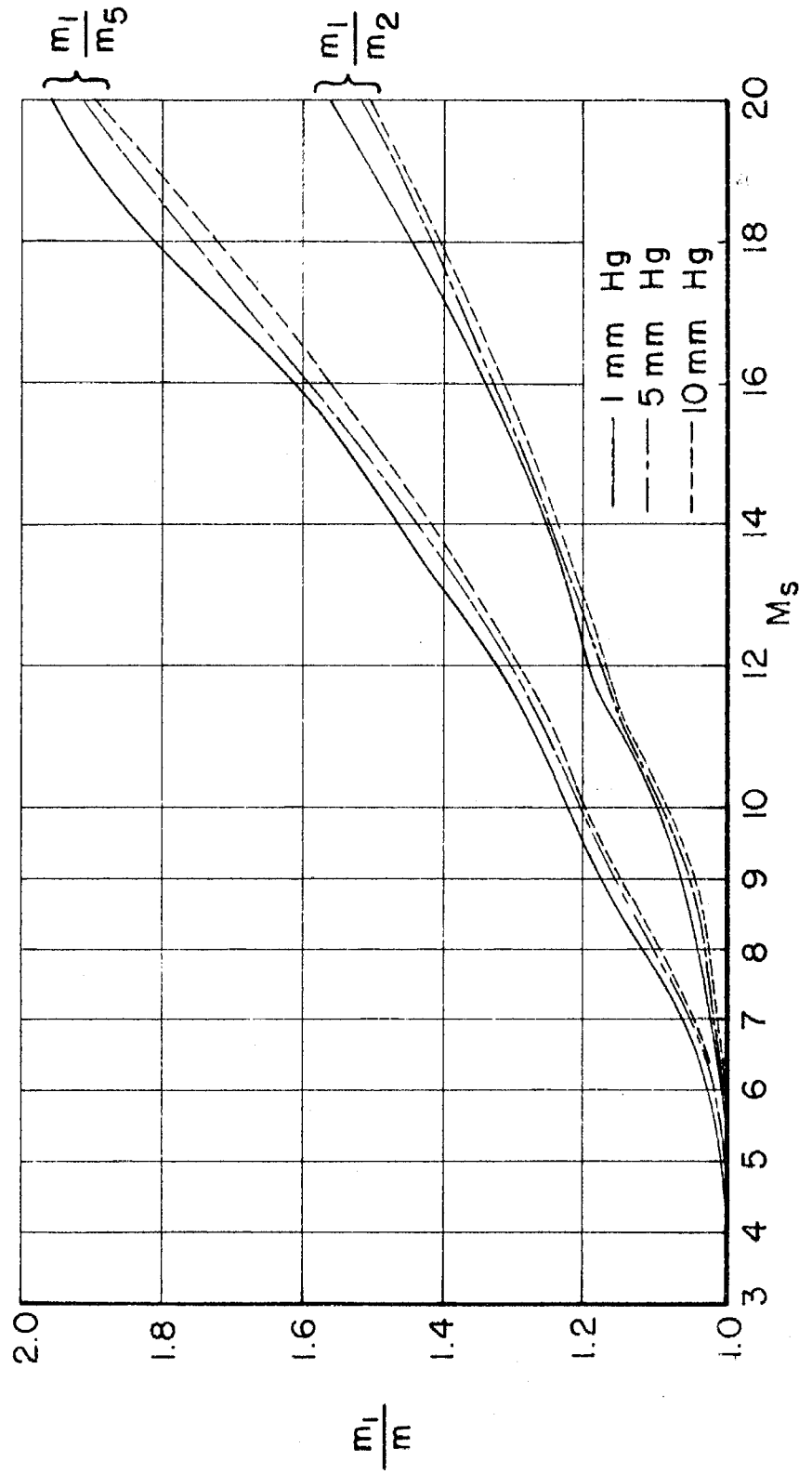

FIG.16-MOLECULAR WEIGHT RATIO ACROSS A NORMAL SHOCK WAVE AND ACROSS THE DETACHED SHOCK WAVE IN AIR, $T_1 = 298°K$

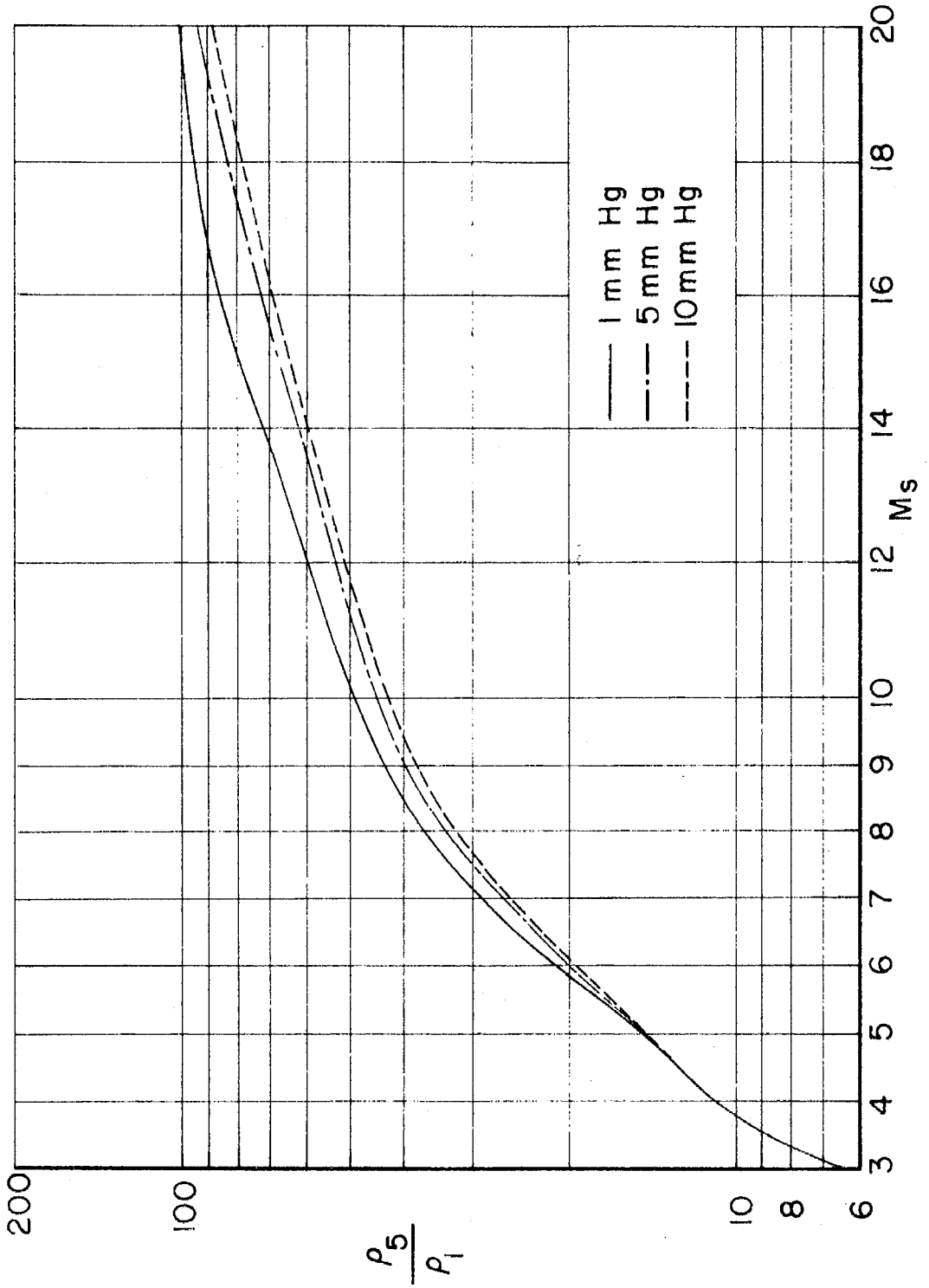

FIG. 17 – RATIO OF THE DENSITY BEHIND A DETACHED NORMAL SHOCK WAVE TO THE INITIAL AIR DENSITY, $T_1 = 298°K$

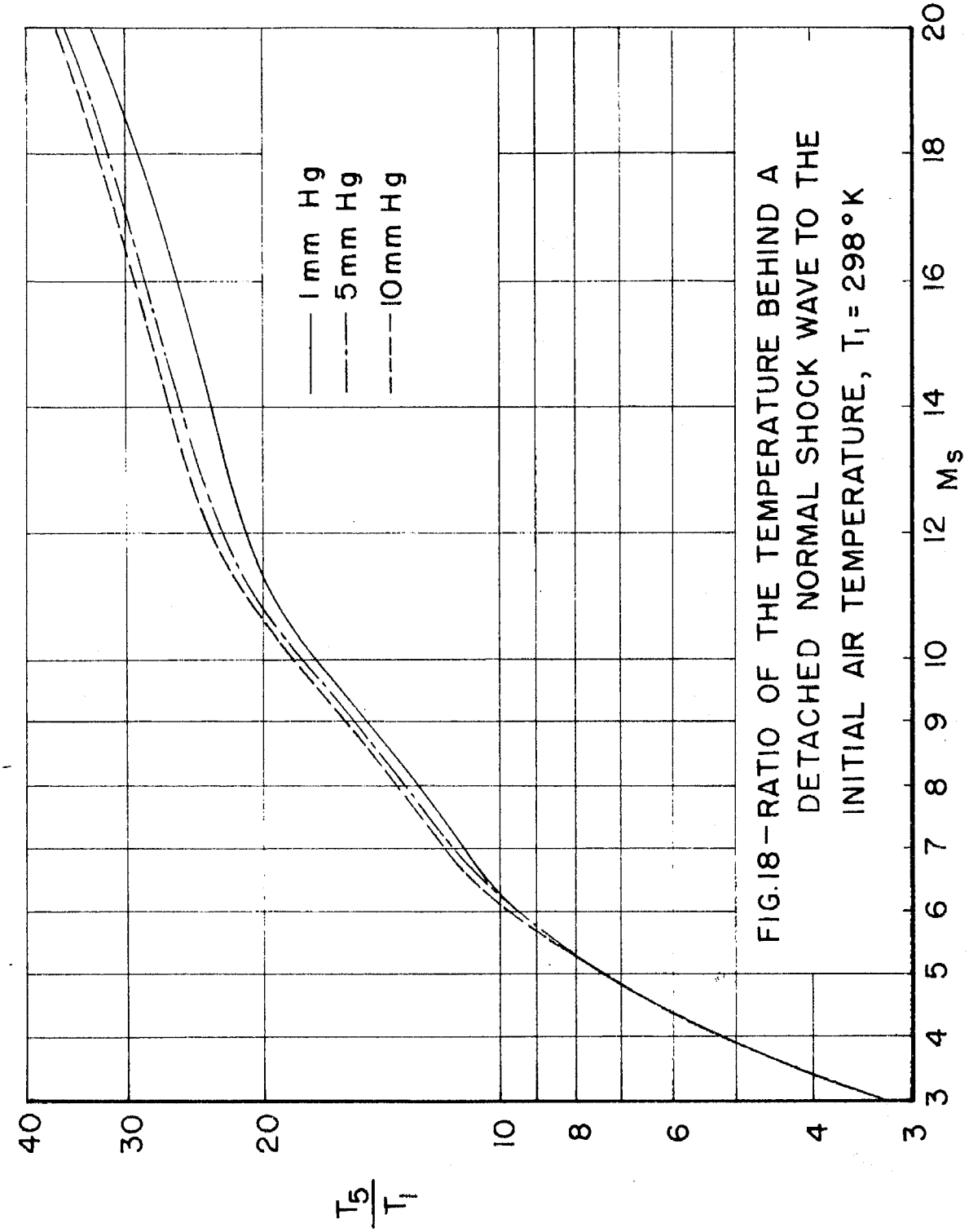

FIG. 18 – RATIO OF THE TEMPERATURE BEHIND A DETACHED NORMAL SHOCK WAVE TO THE INITIAL AIR TEMPERATURE, $T_1 = 298°K$

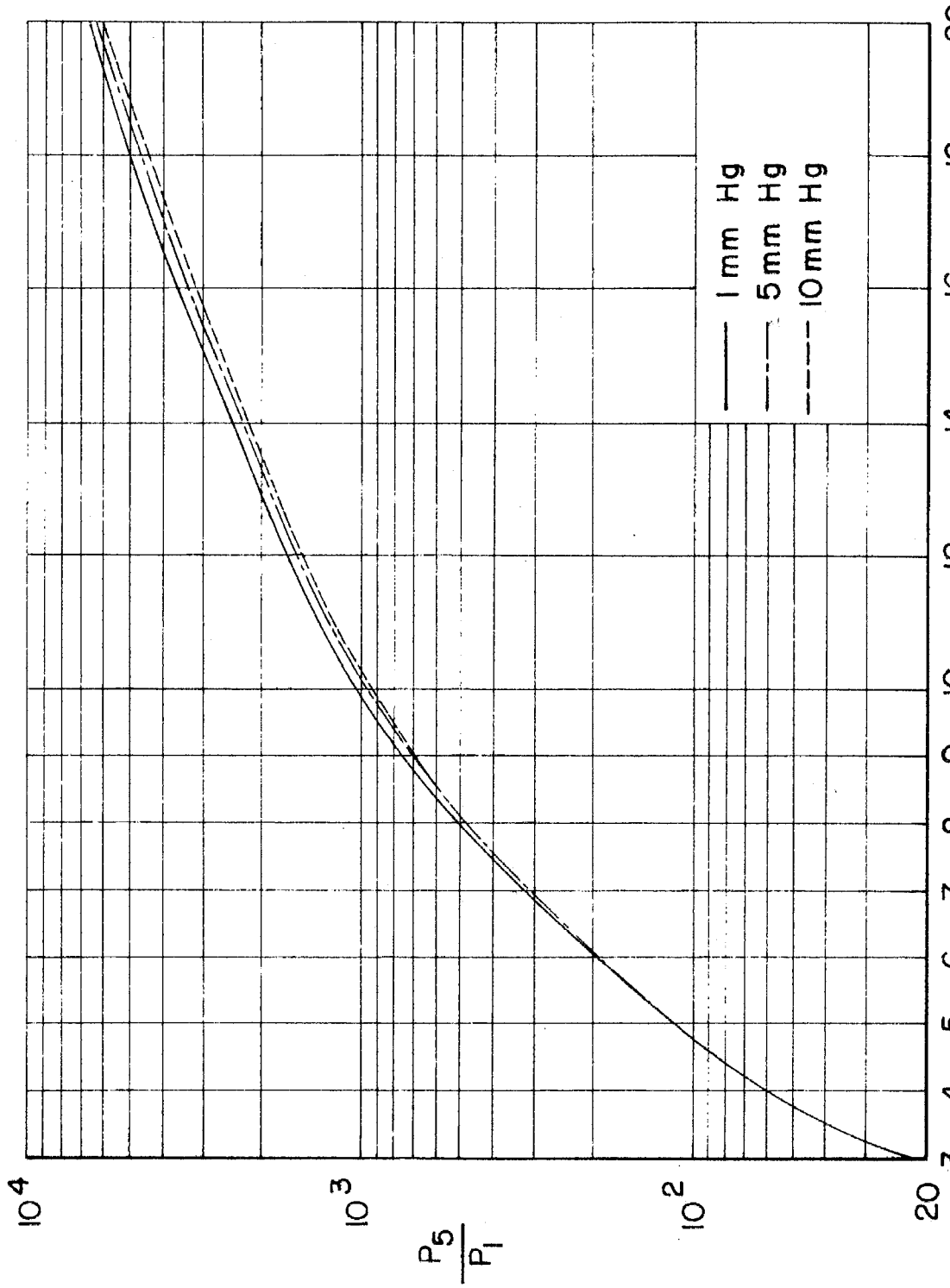

FIG. 19-RATIO OF PRESSURE BEHIND A DETACHED NORMAL SHOCK WAVE TO THE INITIAL AIR PRESSURE, $T_1 = 298°$ K

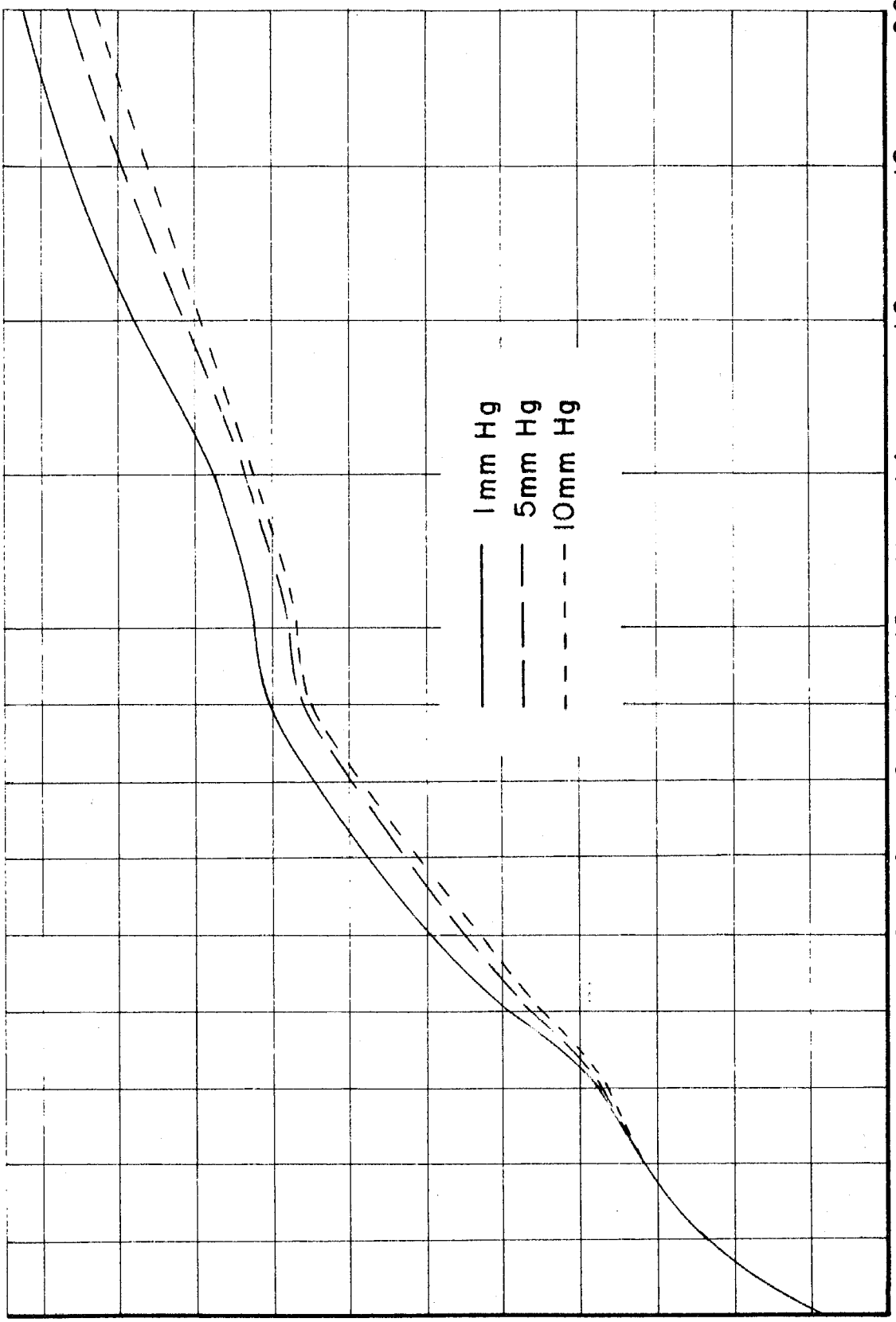

FIG. 20 – FLOW MACH NUMBER BEHIND MOVING SHOCK WAVE IN THE UNIFORM TUBE, T_1=298°K

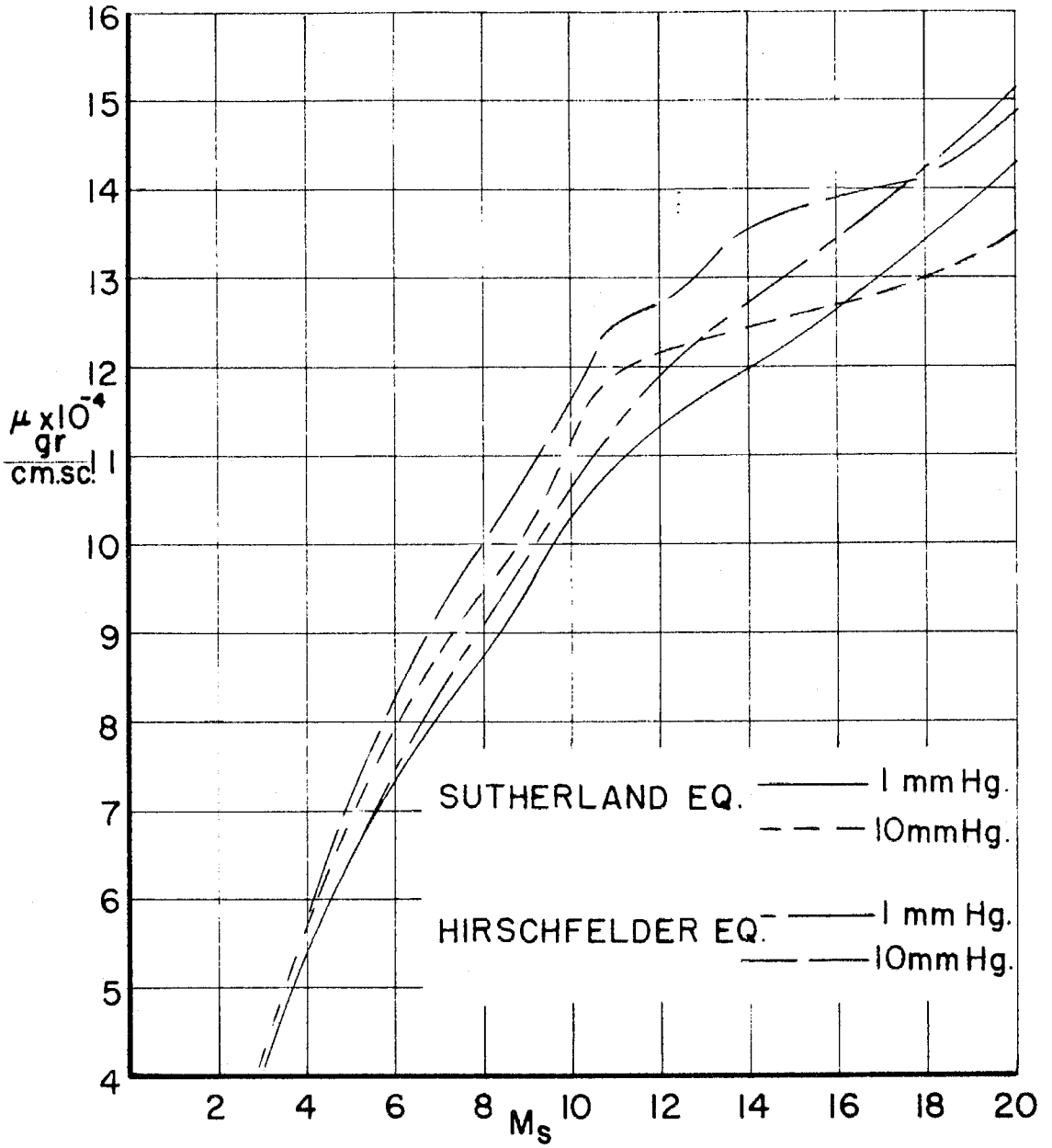

FIG. 21

VISCOSITY OF AIR BEHIND A STRONG SHOCK WAVE, $T_1 = 298°K$

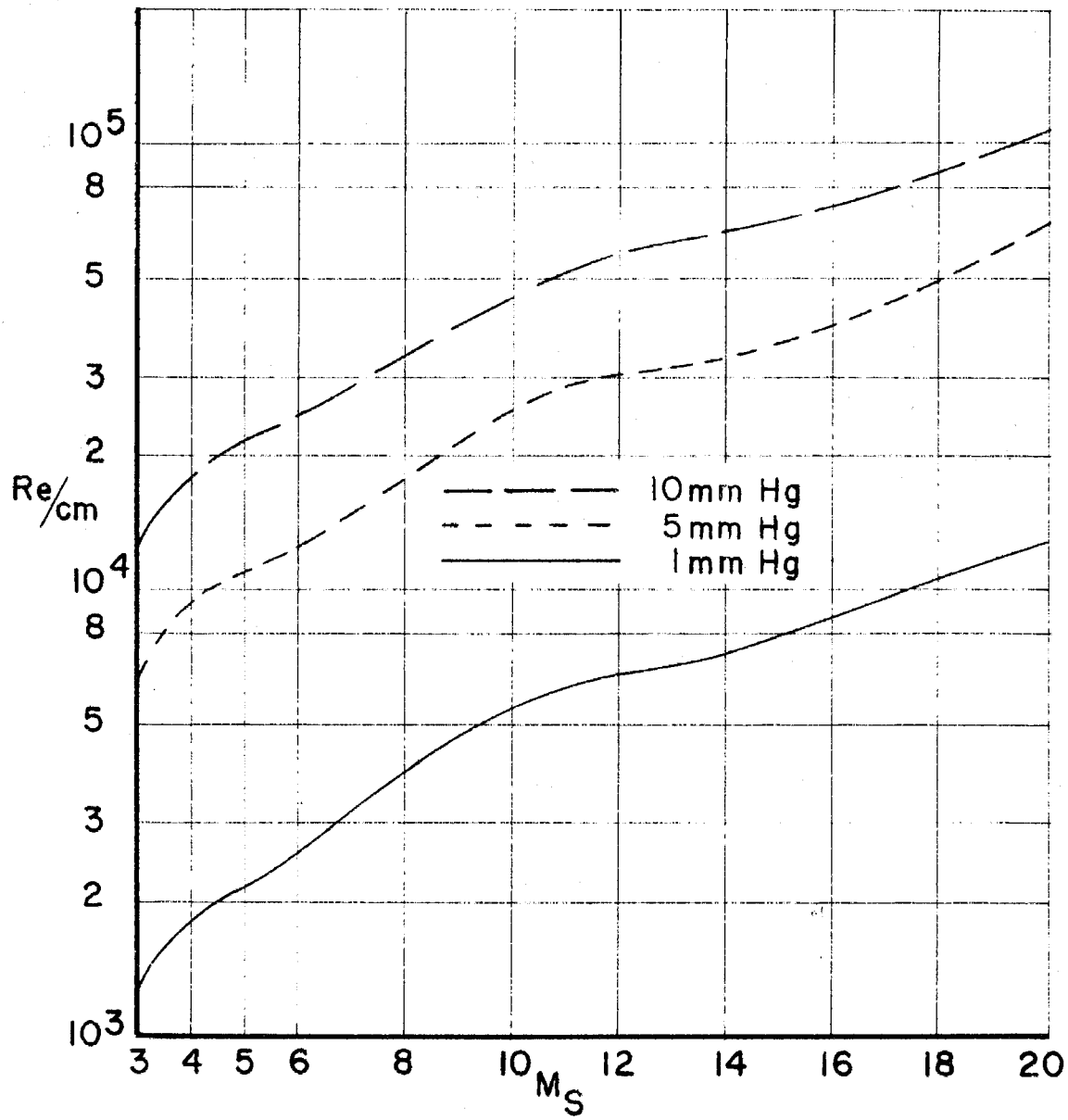

FIG. 22 – REYNOLDS NUMBER IN FLOW BEHIND THE MOVING SHOCK WAVE IN THE UNIFORM SHOCK TUBE, $T_1 = 298°K$

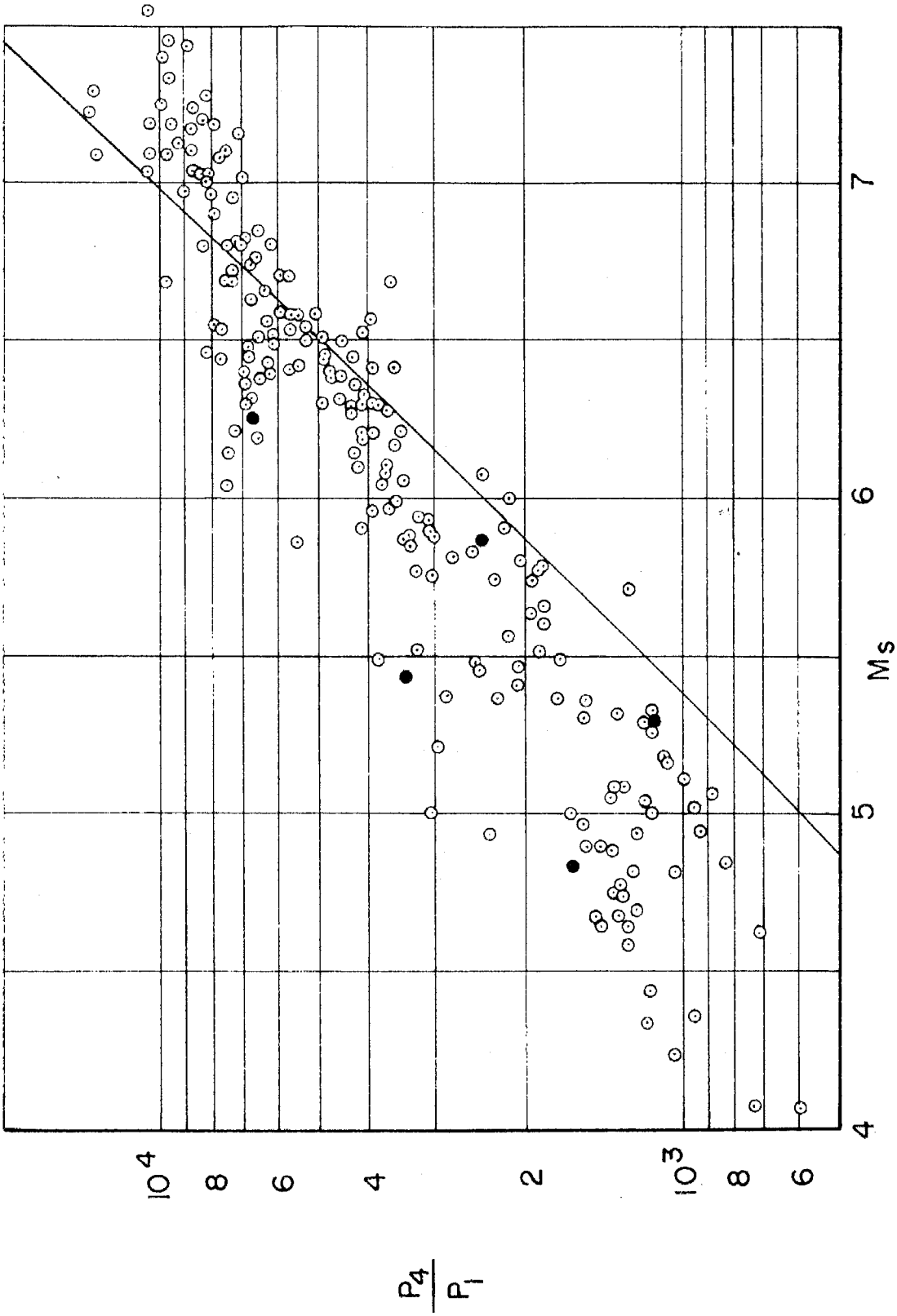

FIG. 23 - P_4/P_1 vs. M_s IN THE UNIFORM $2\frac{7}{8}$" x $2\frac{7}{8}$" SHOCK TUBE

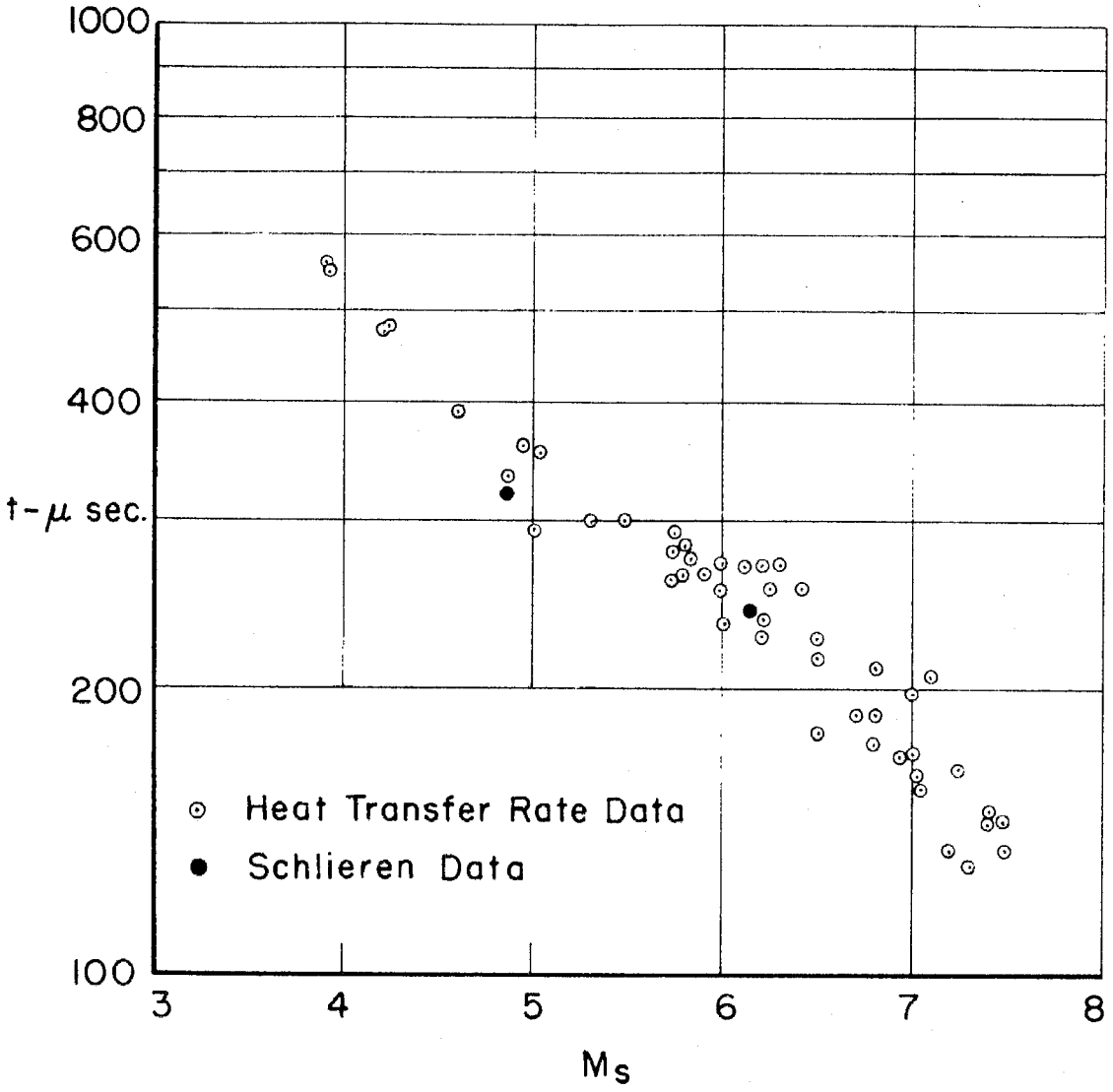

FIG.24-MEASURED DURATION OF "HOT" FLOW IN THE UNIFORM SHOCK TUBE

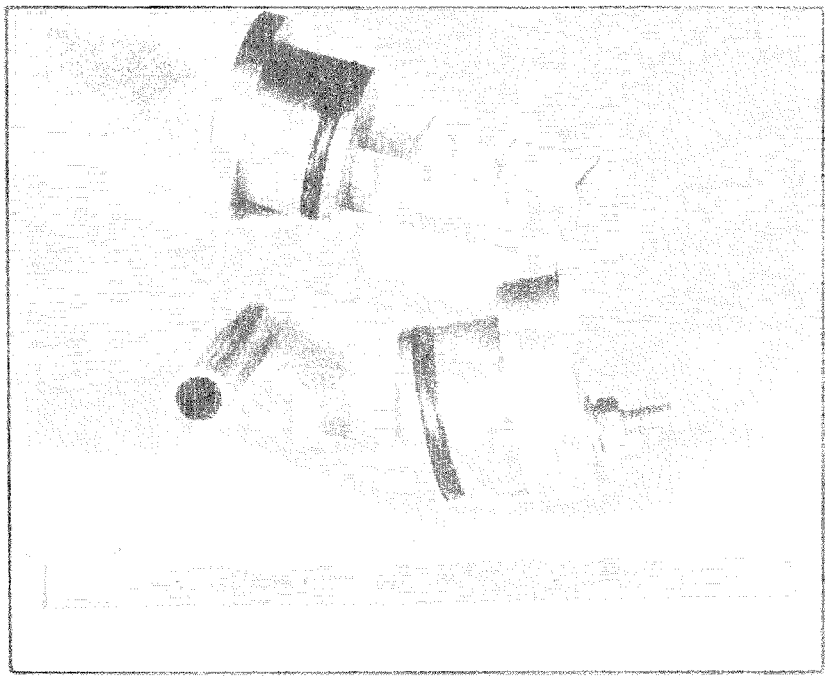

FIG. 25

CONE MODEL FOR SCHLIEREN STUDIES

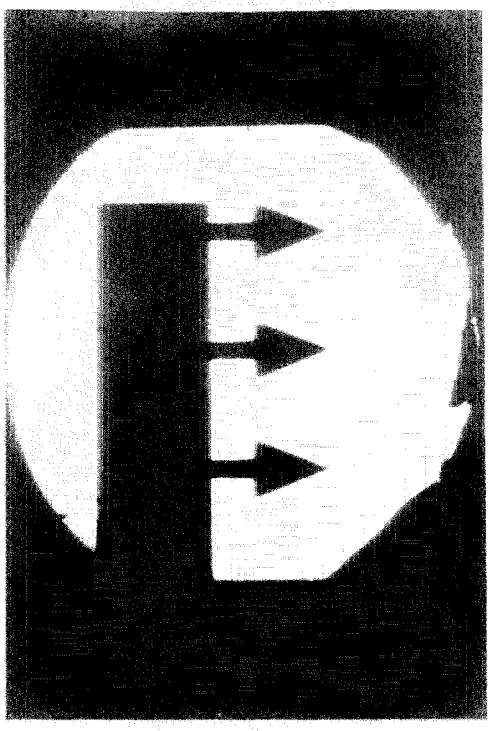

(A) During "Hot" Flow

M_s = 6.18
P_1 = 8.1
Δt = 150 μ sec

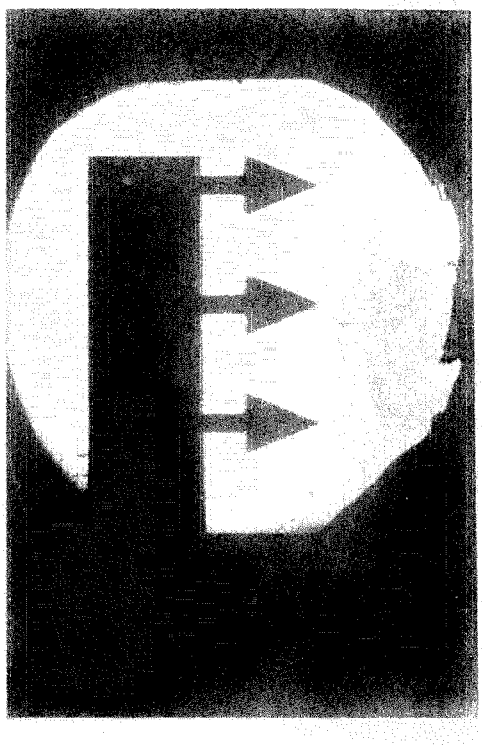

(B) After Contact Region Arrival

M_s = 6.29
P_1 = 7.2
Δt = 281 μ sec

FIG. 46

SCHLIEREN STUDIES OF FLOW OVER 45° CONES IN THE SHOCK TUBE

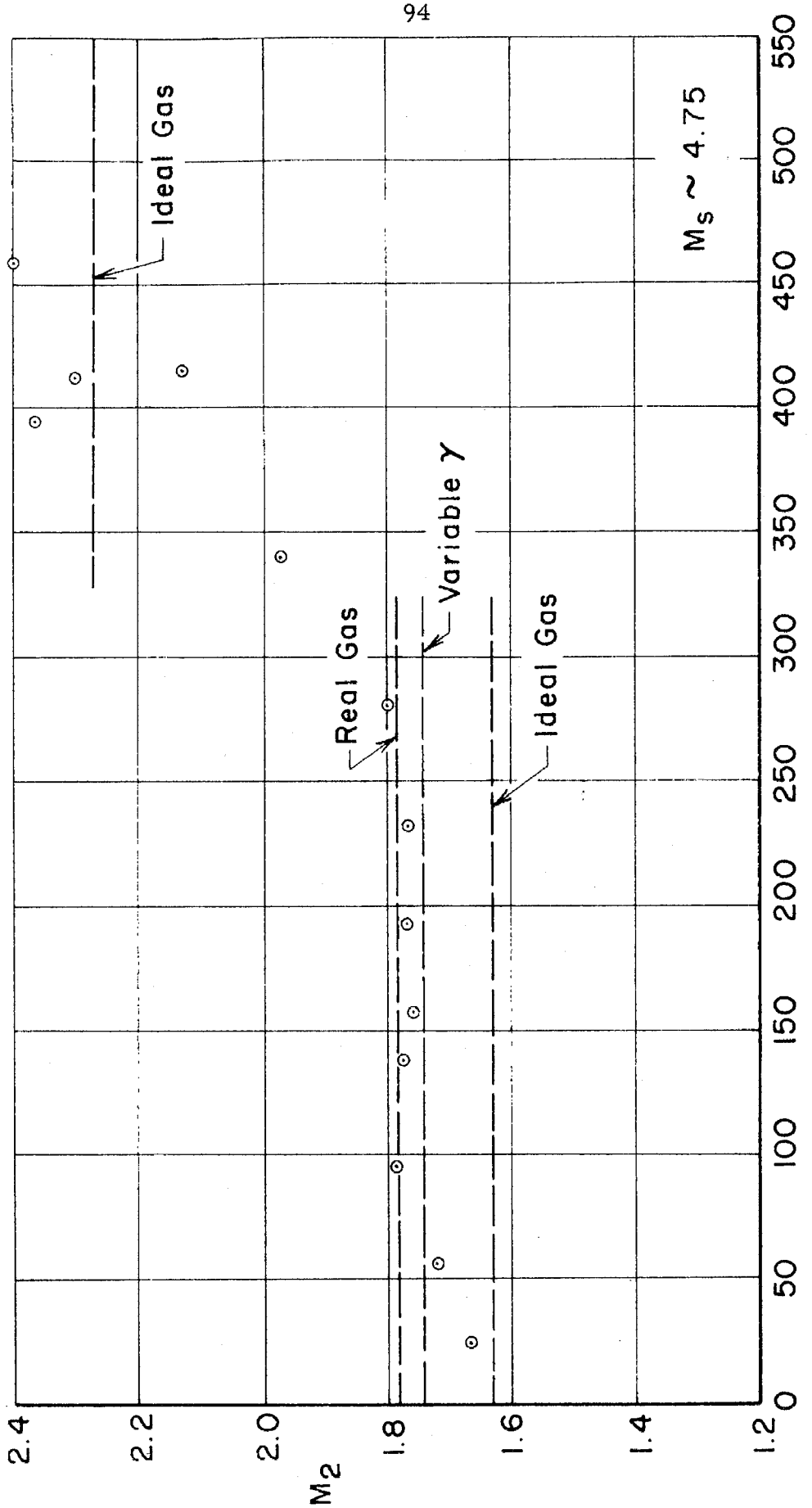

FIG.27-TIME HISTORY OF "HOT FLOW" IN THE UNIFORM SHOCK TUBE

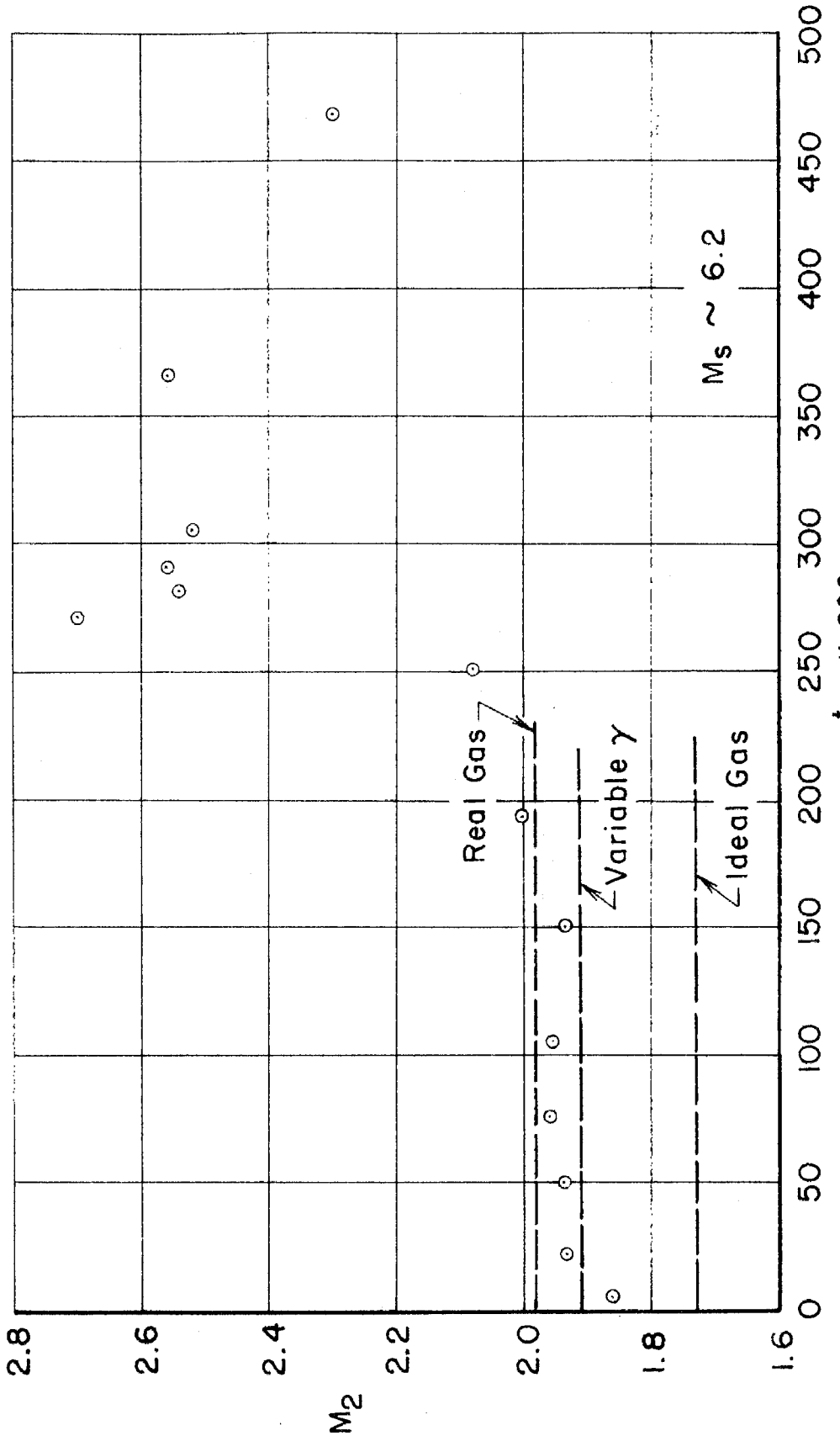

FIG. 28-TIME HISTORY OF "HOT FLOW" IN THE UNIFORM SHOCK TUBE

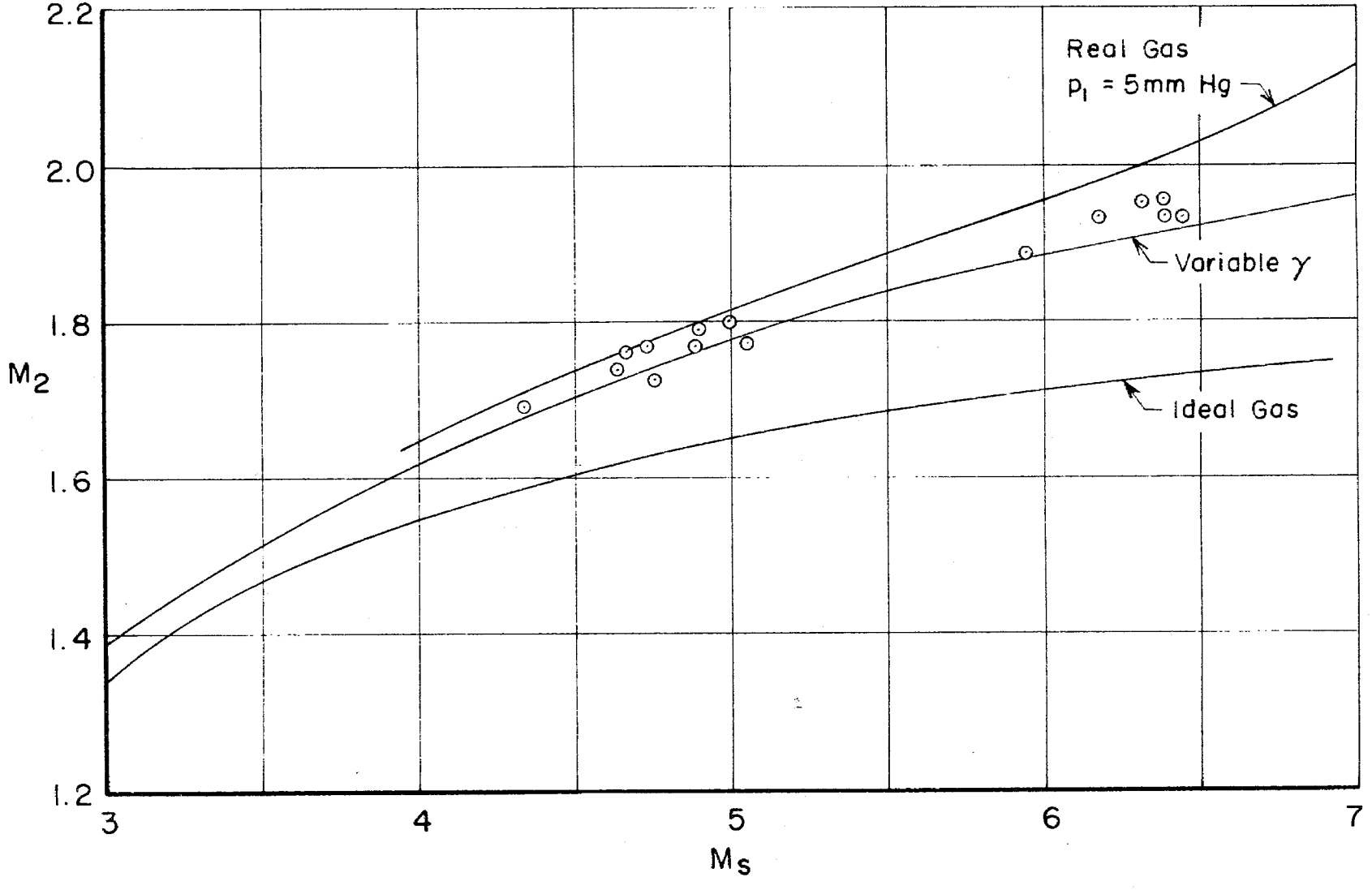

FIG. 29 - COMPARISON OF EXPERIMENTALLY MEASURED FLOW MACH NUMBER WITH THEORY

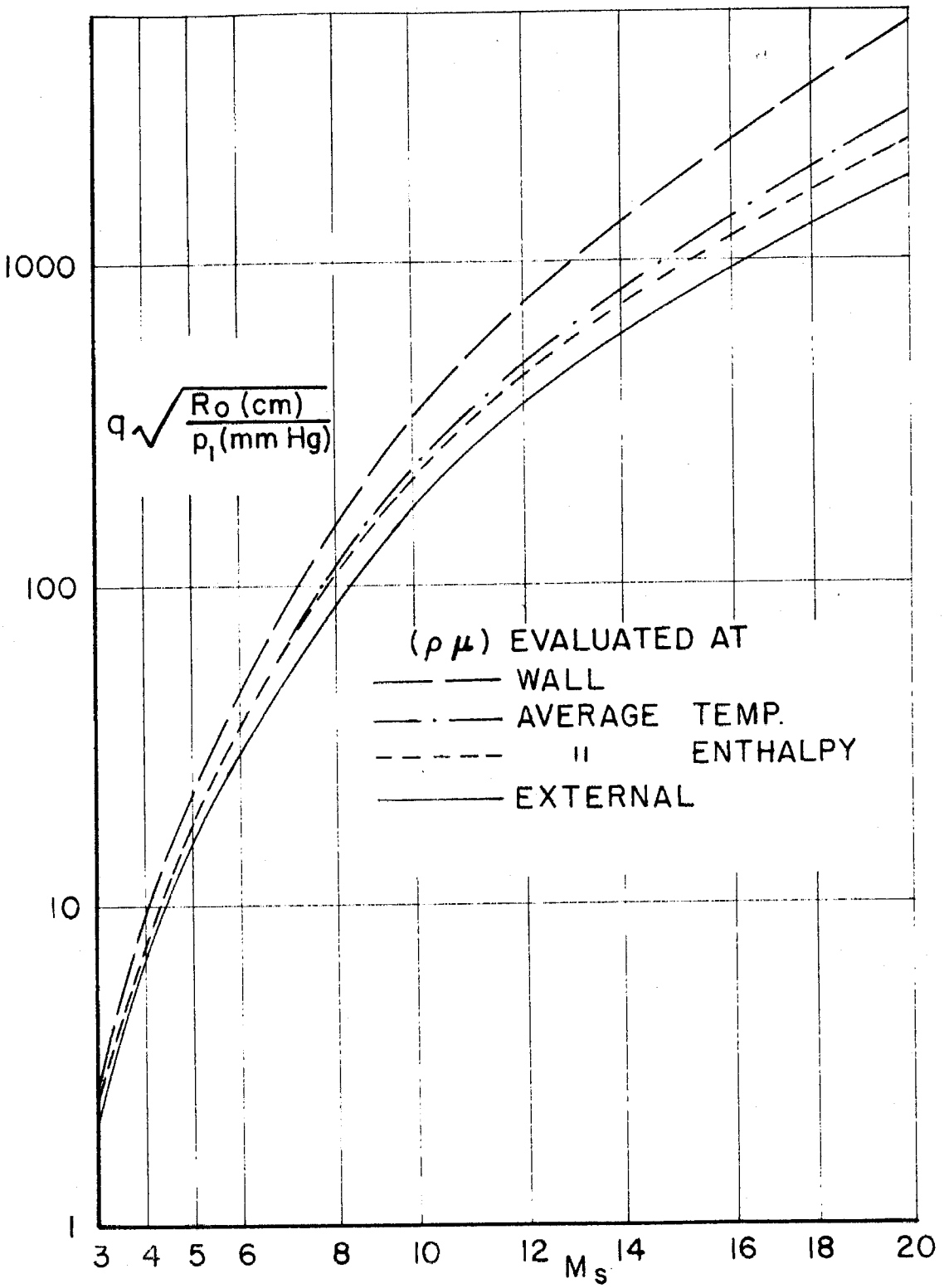

FIG. 30 — HEAT TRANSFER RATE (CAL./CM^2/SEC.) AT THE STAGNATION REGION OF A CIRCULAR CYLINDER

$T_1 = 298°\,K$

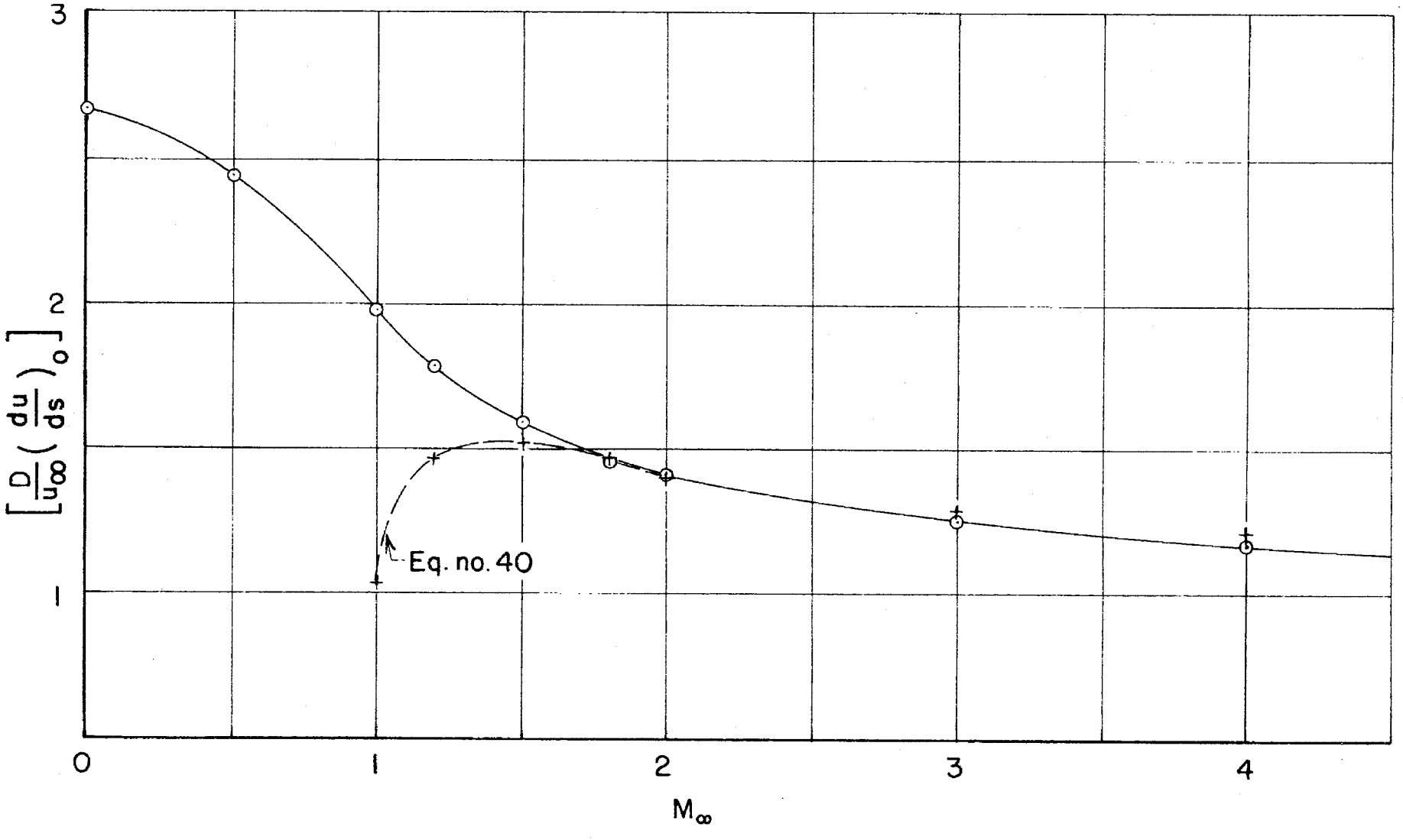

FIG. 31 $\left[\frac{D}{u_\infty}\left(\frac{du}{ds}\right)_o\right]$ vs. M_∞ (Ref. 29)

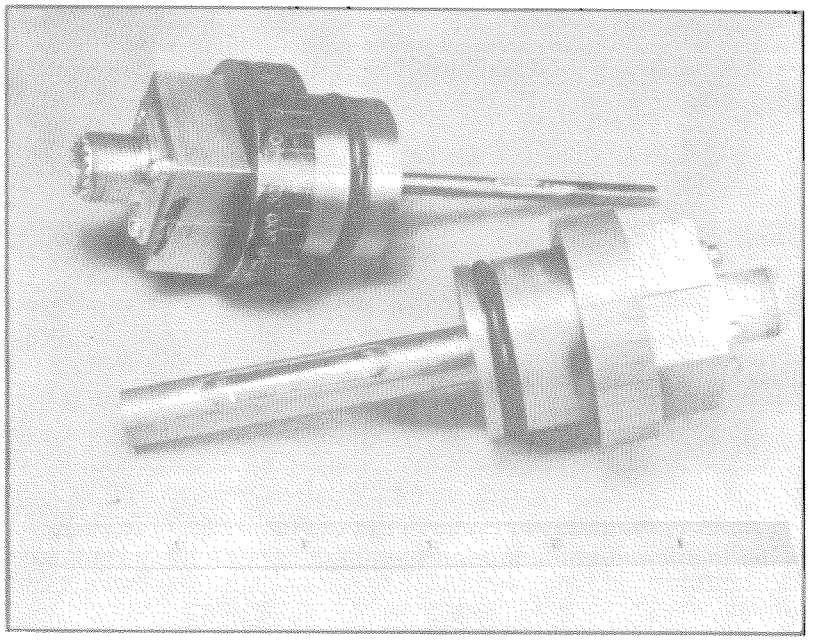

FIG. 32

CIRCULAR CYLINDER MODELS FOR HEAT TRANSFER STUDIES

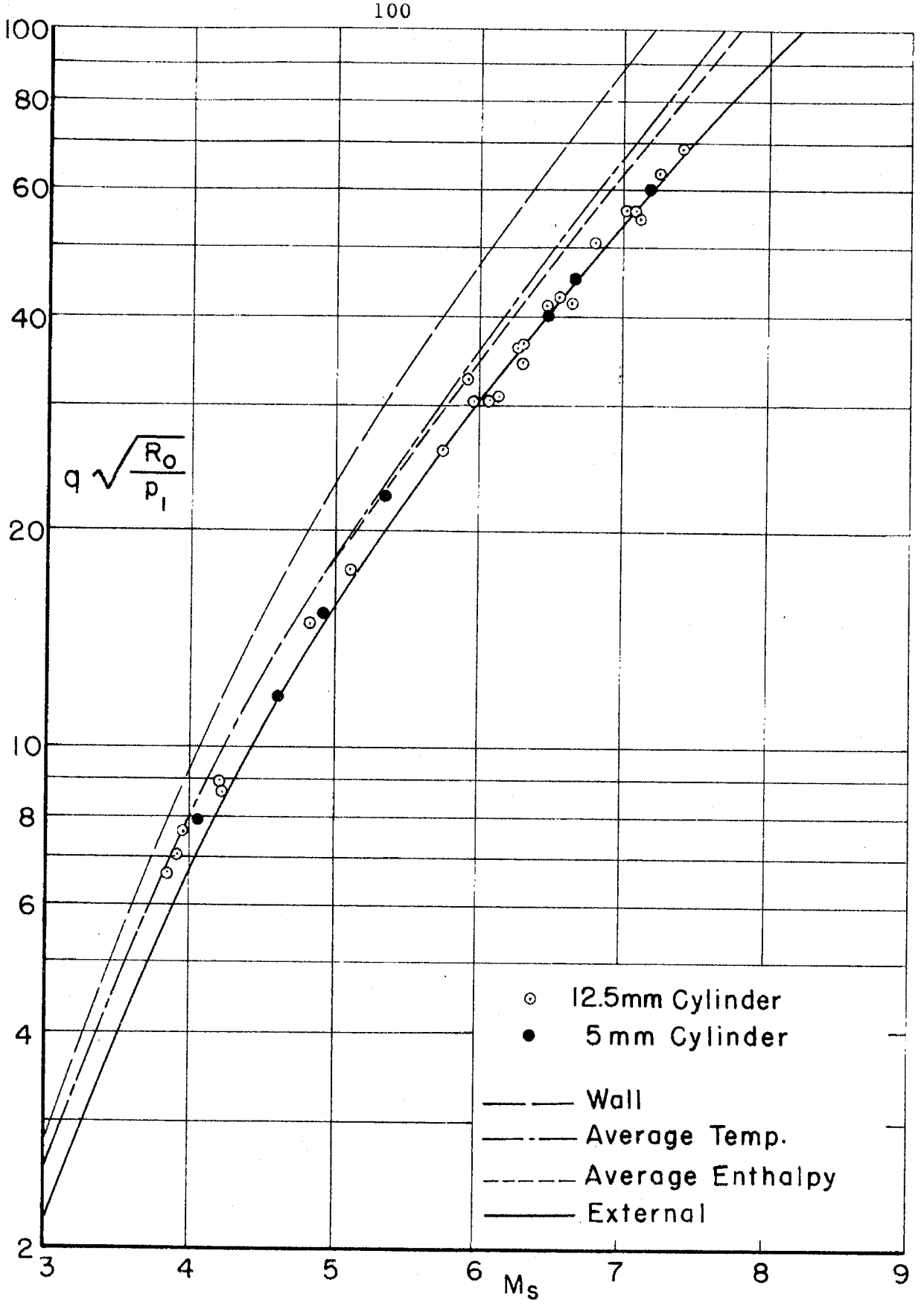

FIG.33-MEASURED HEAT TRANSFER RATE AT THE STAGNATION REGION OF A CIRCULAR CYLINDER

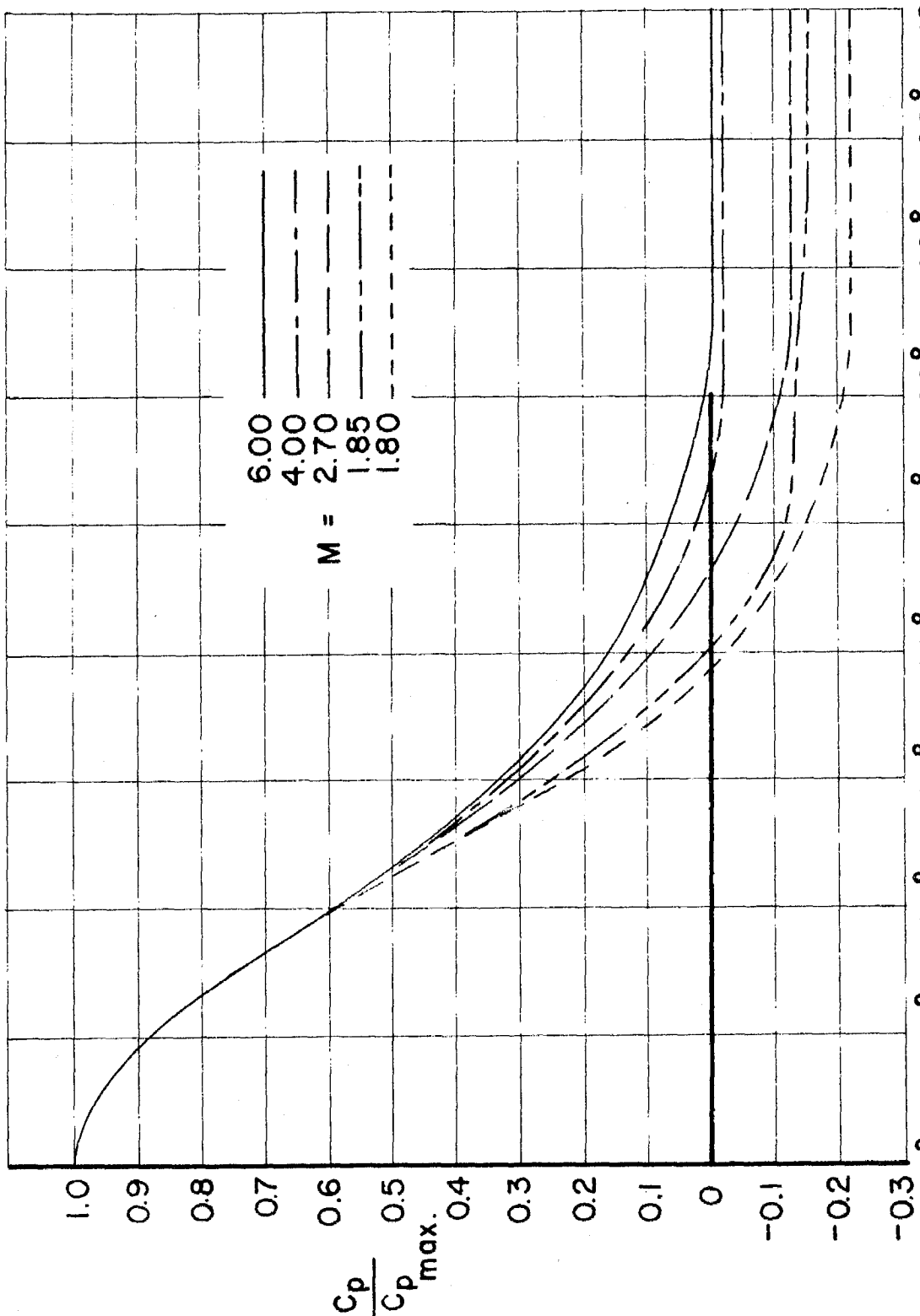

FIG. 34— PRESSURE DISTRIBUTION ON A CIRCULAR CYLINDER MEASURED IN WIND TUNNEL AND SHOCK TUBE (Ref. 31, 32)

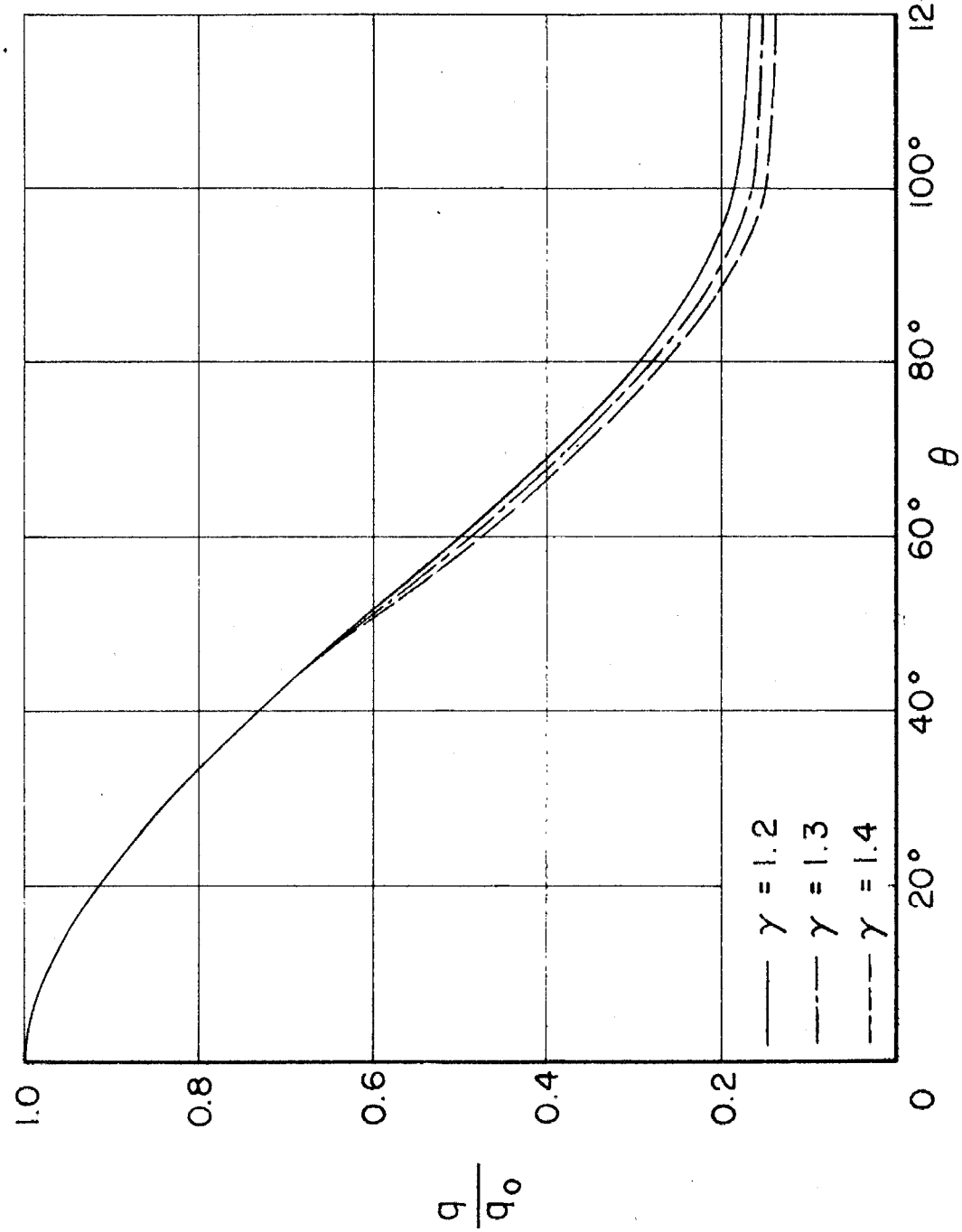

FIG. 35 - CALCULATED HEAT TRANSFER DISTRIBUTION BASED ON MEASURED PRESSURE DISTRIBUTION ON A CIRCULAR CYLINDER AT $M_2 = 1.85$, $T_1 = 298°K$.

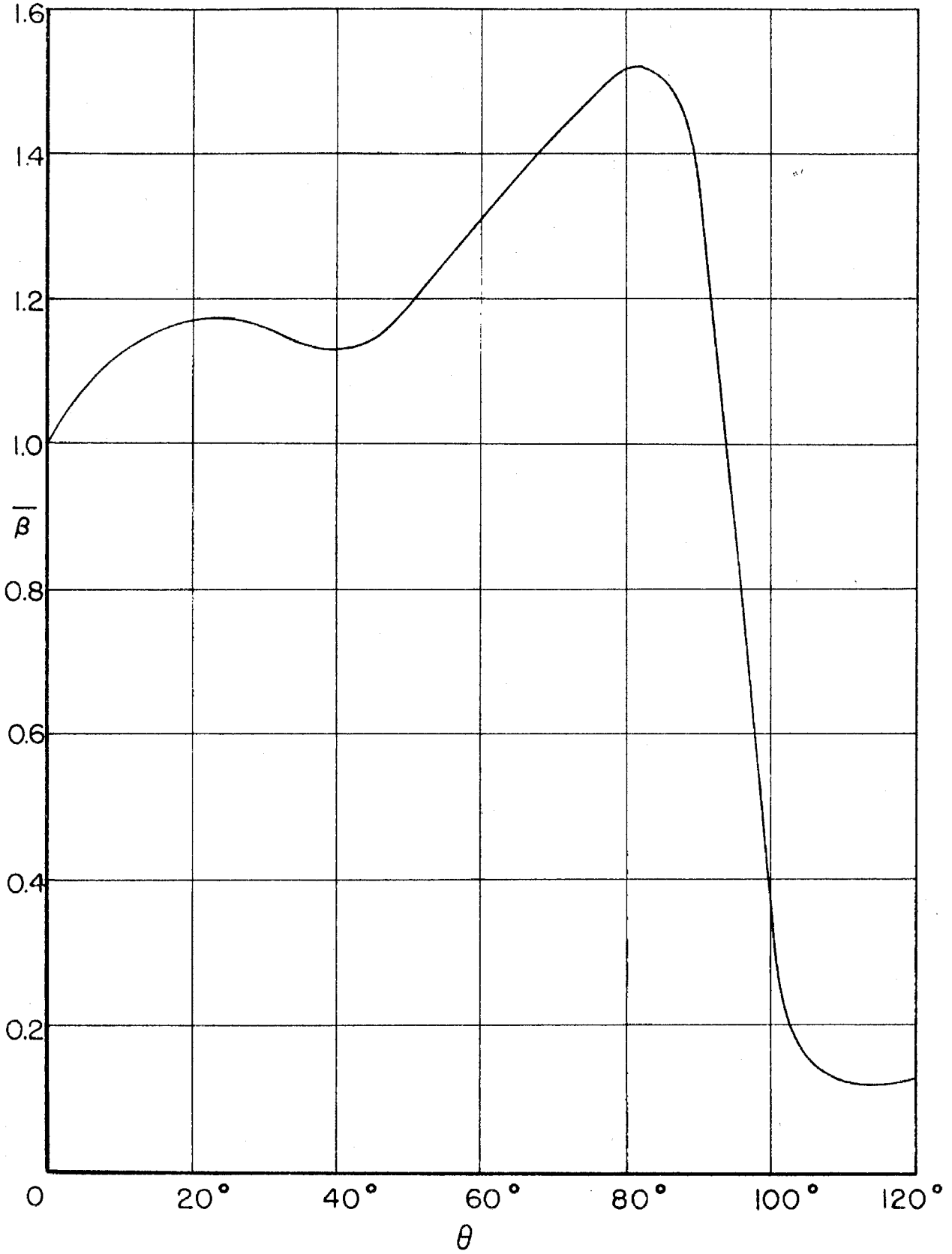

FIG. 36 - VARIATION OF THE PRESSURE GRADIENT PARAMETER $\overline{\beta}$ OVER A CIRCULAR CYLINDER

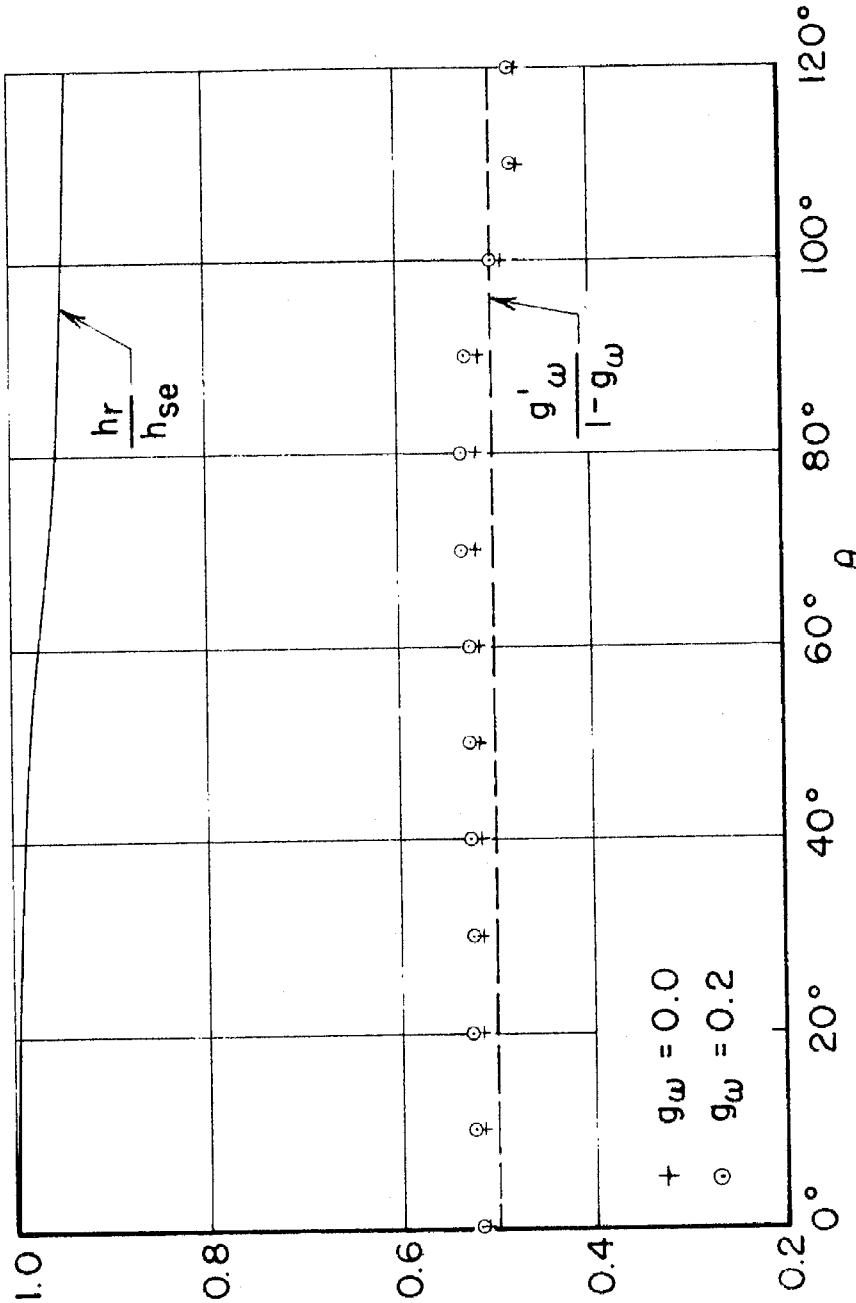

FIG. 37 - CORRECTIONS TO THE THEORY IN THE CALCULATIONS OF THE HEAT TRANSFER DISTRIBUTION ON A CIRCULAR CYLINDER

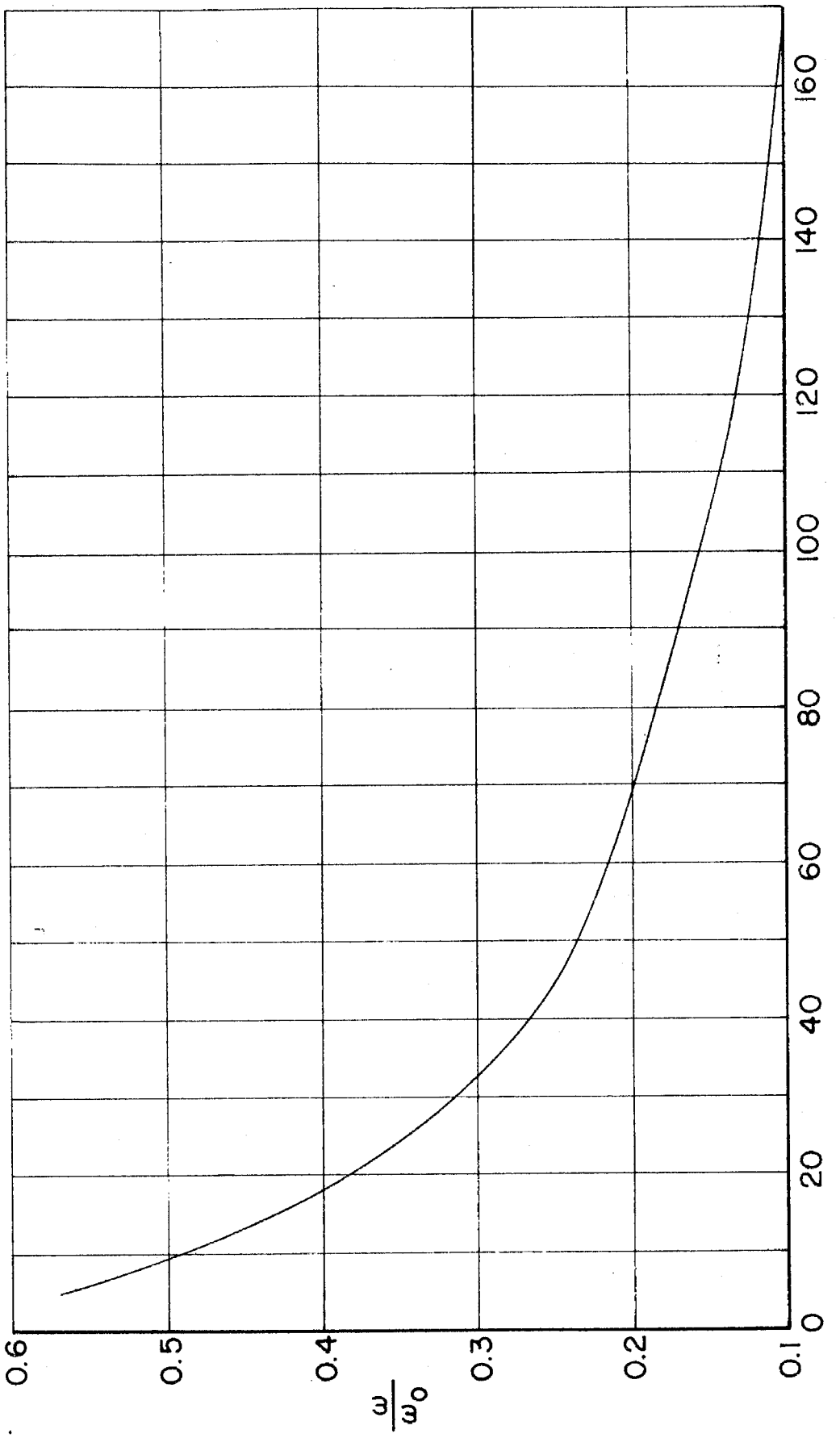

FIG. 38a- $\frac{\omega}{\omega_0}$ FUNCTION OF LOCAL ENTHALPY RATIO (REF. ENTHALPY AT $T_1 = 298°K$)

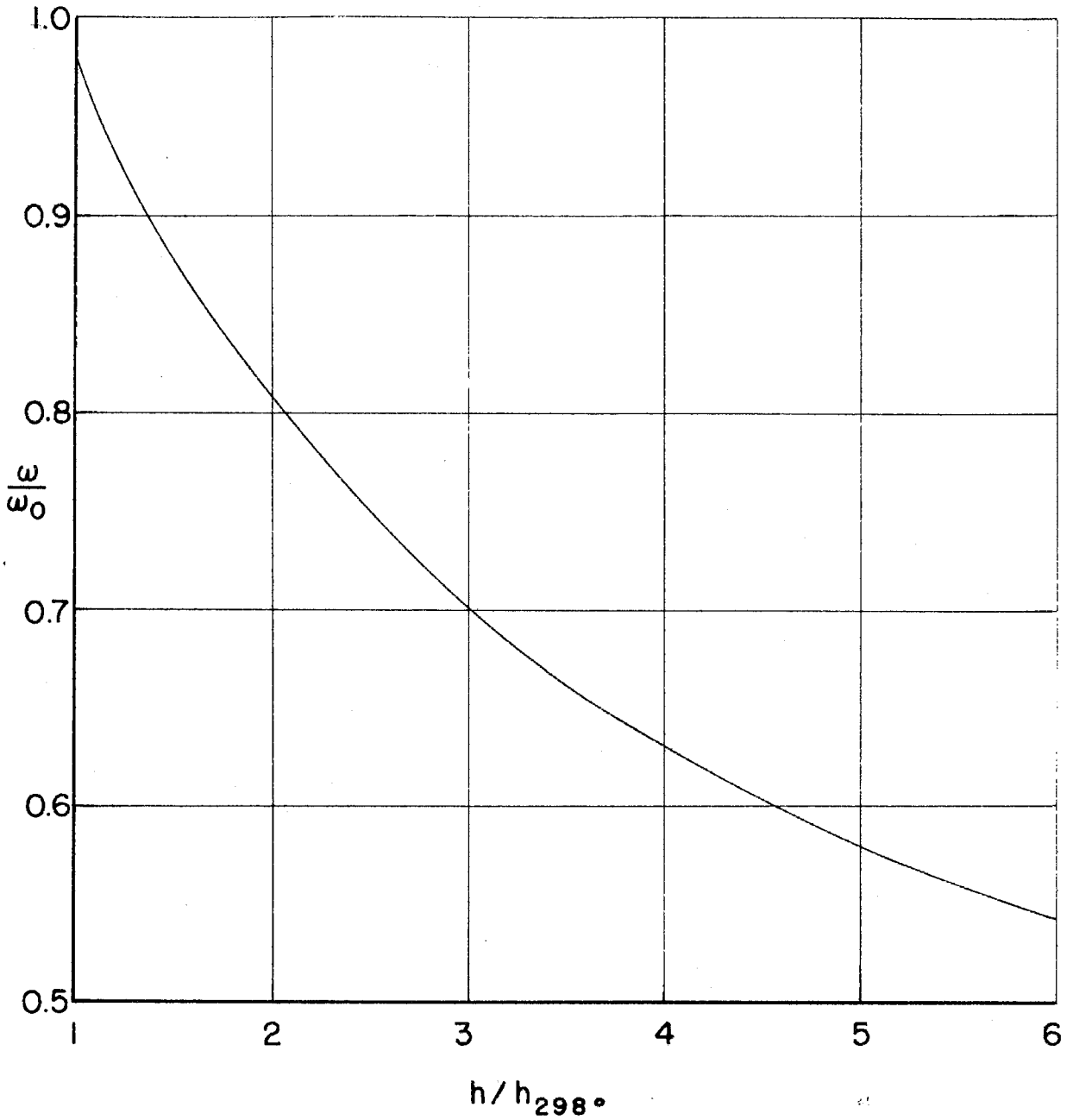

FIG. 38 b - $\frac{\omega}{\omega_o}$ FUNCTION OF LOCAL ENTHALPY RATIO

(REF. ENTHALPY AT $T_1 = 298°K$)

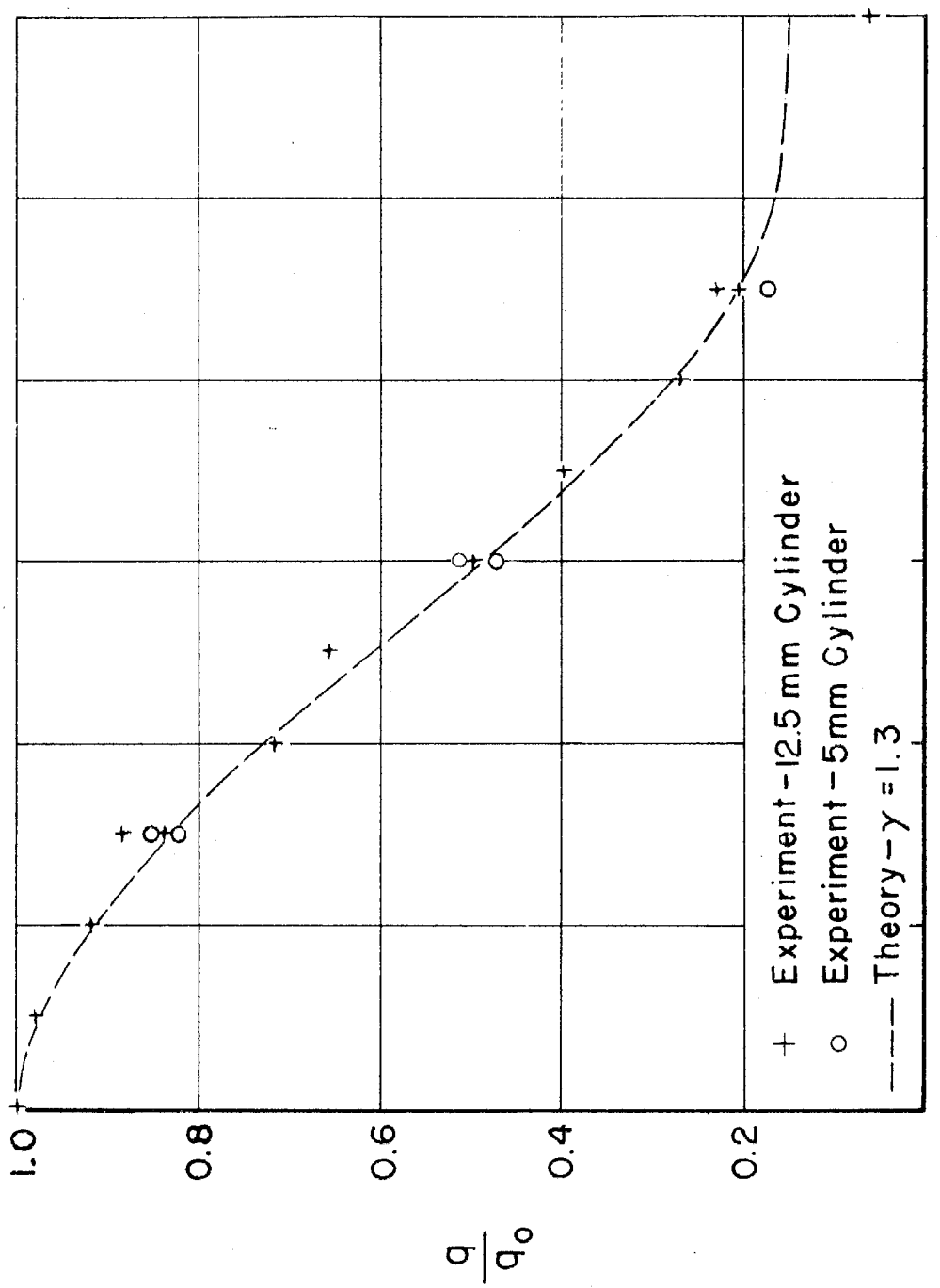

FIG. 39 - MEASURED HEAT TRANSFER DISTRIBUTION ON A CIRCULAR CYLINDER AT $M_2 = 1.85$, $T_1 = 298°$ K

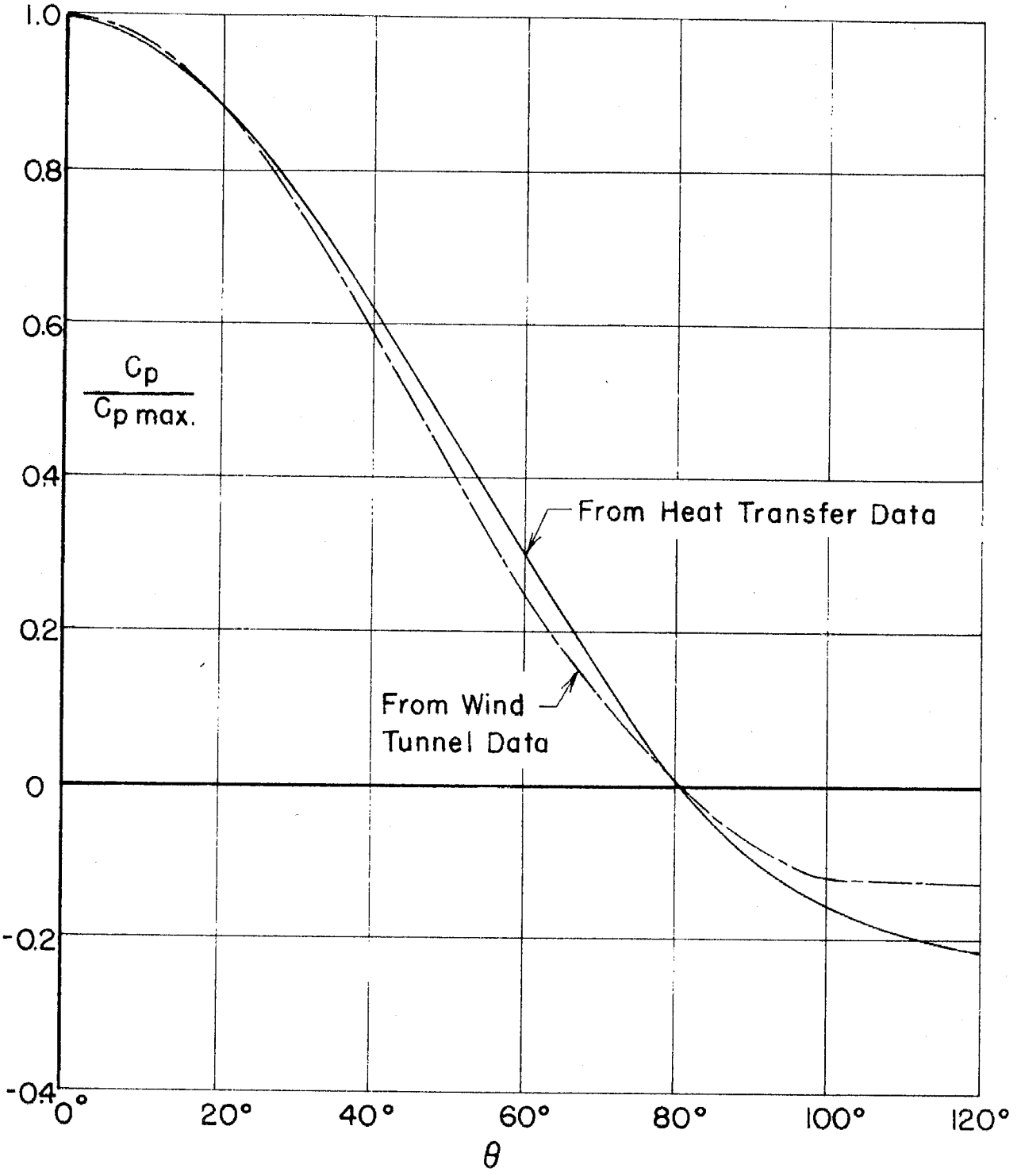

FIG. 40-COMPARISON OF CALCULATED PRESSURE DISTRIBUTION ON A CIRCULAR CYLINDER BASED ON HEAT TRANSFER DATA WITH PRESSURE DISTRIBUTION MEASURED IN WIND TUNNEL AT $M_2 = 1.85$

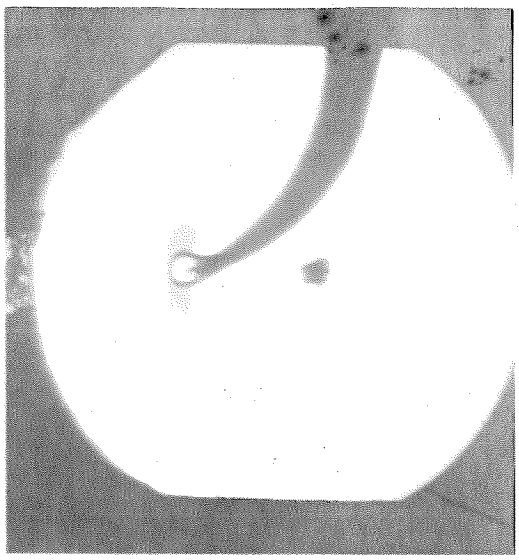

$M_s = 5.00$; $p_1 = 9.35$; $t = 1$

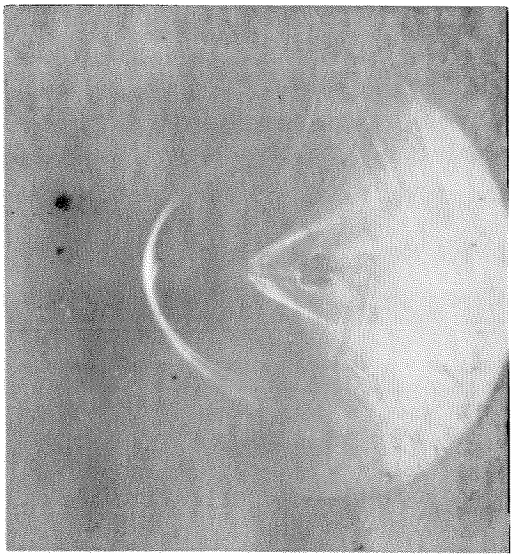

$M_s = 4.82$; $p_1 = 11.60$; $t = 3$

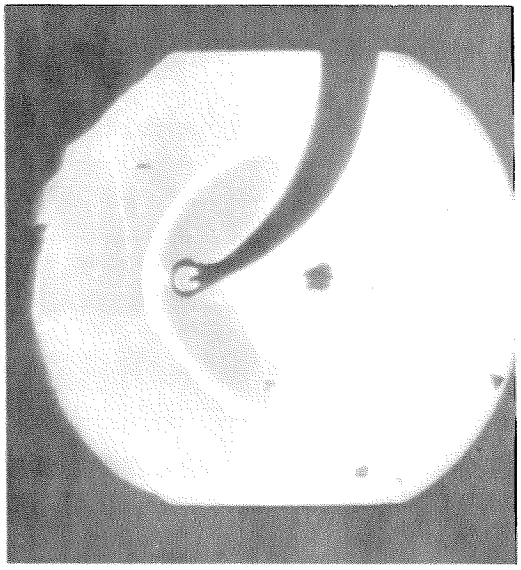

$M_s = 5.11$; $p_1 = 11.30$; $t = 5$

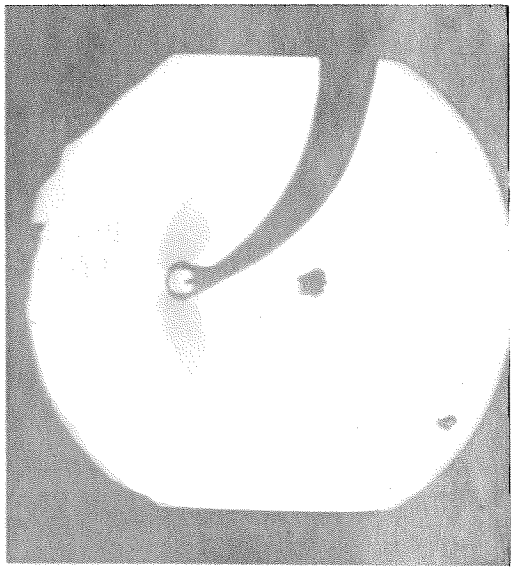

$M_s = 5.25$; $p_1 = 10.60$; $t = 14$

FIG. 41

FLOW ESTABLISHMENT ON A CIRCULAR CYLINDER

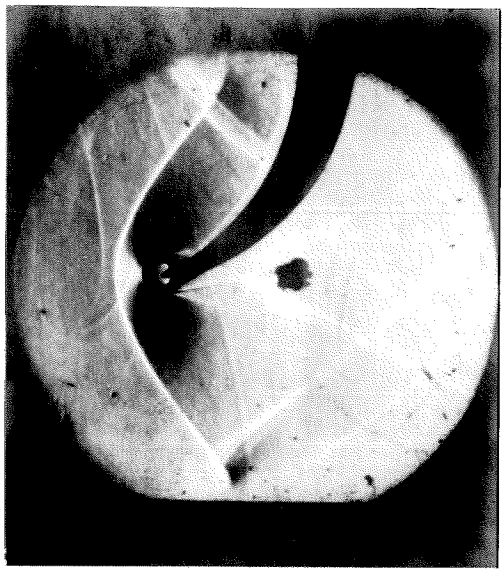

$M_s = 5.32$
$p_1 = 11.10$
$\Delta t = 183\,\mu$ sec

FIG. 42

FLOW ON A CIRCULAR CYLINDER IN THE SHOCK TUBE

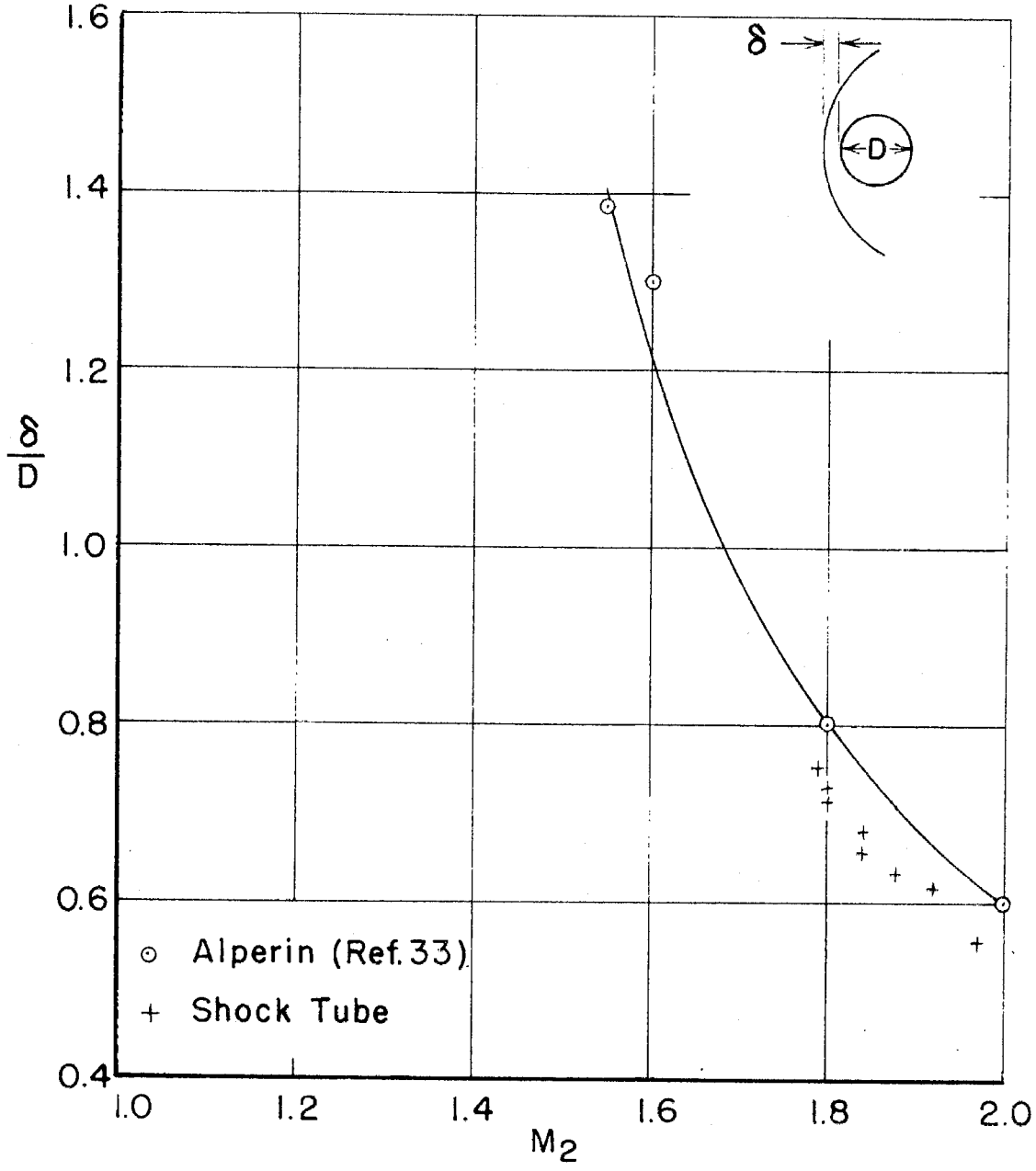

FIG. 43- COMPARISON OF SHOCK WAVE DETACHMENT DISTANCE IN FRONT OF A CIRCULAR CYLINDER MEASURED IN THE SHOCK TUBE AND IN THE WIND TUNNEL